Universidad de Valladolid

Escuela de Doctorado Universidad de Valladolid

PROGRAMA DE DOCTORADO EN INVESTIGACIÓN BIOMÉDICA

TESIS DOCTORAL:

Characterization of endogenous Kv1.3 channel isoforms in T cells.

Presentada por Julia Serna Pérez para optar al grado de

Doctor/a por la Universidad de Valladolid

Dirigida por:

Dr. Miguel Ángel de la Fuente García.

Dra. Teresa Pérez García

Funding

This thesis has been carried out under the supervision of Prof. Miguel Ángel de la Fuente García and Prof. Teresa Pérez García at the Instituto de Biología y Genética Molecular (Universidad de Valladolid-CSIC), Valladolid. It has been possible thanks to the following funding:

- **Project:** Canales iónicos y Fisiopatología Vascular: Historia de dos canales. (PID2020-118517RB-I00)
  Funding entity: Spanish Ministry of Science and Innovation
  From: 2021 To: 2024
- **Project:** Los canales iónicos del musculo liso como marcadores, dianas y efectores en el remodelado vascular. (BFU2016-75360-R)
  Funding entity: Spanish Ministry of Science and Innovation
  From: 2016 To: 2020
- **Project:** Nuevas terapias farmacológicas y génicas para la prevención y tratamiento de enfermedades vasculares oclusivas (VA114P17).
  Funding entity: Junta de Castilla y León (JCyL), Consejería de Educación
  From: 2017 to: 2019
- **Contrato predoctoral Universidad de Valladolid-Banco Santander**. From 2019 to 2023.
- **EMBO Scientific Exchange Grant** (number 9539) to conduct research in the lab of Dr. Claire Hivroz. The topic of the research project is "Kv1.3 role in the immunological synapse".

Some of the **original results** presented in this Thesis have been compiled in the following scientific publication:

- **Serna J**, Peraza DA, Moreno-Estar S, Saez JJ, Gobelli D, Simarro M, Hivroz C, López-López JR, Cidad P, de la Fuente MA, Pérez-García MT. Characterization of endogenous Kv1.3 channel isoforms in T cells. J Cell Physiol. 2023 May;238(5):976-991. doi: 10.1002/jcp.30984. Epub 2023 Feb 28. PMID: 36852591.

Additionally, within the framework of this Thesis, results were obtained for other projects that have resulted in the **participation of the doctoral student in the following publications**:

- Arévalo-Martínez M, Cidad P, García-Mateo N, Moreno-Estar S, **Serna J**, Fernández M, Swärd K, Simarro M, de la Fuente MA, López-López JR, Pérez-García MT. Myocardin-Dependent Kv1.5 Channel Expression Prevents Phenotypic Modulation of Human Vessels in Organ Culture. Arterioscler Thromb Vasc Biol. 2019 Dec;39(12):e273-e286. doi: 10.1161/ATVBAHA.119.313492. Epub 2019 Oct 10. PMID: 31597447.

- Bernardi A, Gobelli D, **Serna J**, Nawrocka P, March-Rosselló G, Orduña A, Kozlowski P, Simarro M, de la Fuente MA. Novel fluorescent-based reporter cell line engineered for monitoring homologous recombination events. PLoS One. 2021 Apr 30;16(4):e0237413. doi: 10.1371/journal.pone.0237413. PMID: 33930025; PMCID: PMC8087102.

- Perez-SanJose D, de la Fuente MA, **Serna J**, Simarro M, Eiros Bouza JM, Sanz-Muñoz I. CRISPR/CasRx Proof-of-Concept for RNA Degradation: A Future Tool against RNA Viruses? Pharmaceuticals (Basel). 2021 Dec 27;15(1):32. doi: 10.3390/ph15010032. PMID: 35056089; PMCID: PMC8778981.
-
- Gobelli D, Serrano-Lorenzo P, Esteban-Amo MJ, **Serna J**, Pérez-García MT, Orduña A, Jourdain AA, Martín-Casanueva MÁ, Á de la Fuente M, Simarro M. The mitochondrial succinate dehydrogenase complex controls the STAT3-IL-10 pathway in inflammatory macrophages. iScience. 2023 Jul 25;26(8):107473.

Communications have also been presented at the following **conferences**:

- **Reunión española de Canales Iónicos RECI VIII**

Characterization of novel endogenous Kv1.3 channels in T cells.

Julia Serna, Sara Moreno, Diego Peraza, Dino Gobelli, María Simarro, José R López-López, Pilar Cidad, Miguel A de la Fuente, and M. Teresa Pérez-García. 2022, 24-27 mayo, Alicante (España). Participación con póster.

- **66th Biophysical Society Annual Meeting,**

Characterization of endogenous Kv1.3 channel isoforms in t cells.

Julia Serna, Sara Moreno, Diego Peraza, Dino Gobelli, María Simarro, José R López-López, Pilar Cidad, Miguel A de la Fuente, and M. Teresa Pérez-García. 2022, 19-23 febrero, **San Francisco, California.** Participación con póster.

- **Reunión española de Canales Iónicos. RECI VII**

Mechanisms linking Kv1.3 to proliferation

P Cidad, MA de la Fuente, M Simarro; **J Serna** E Alonso; JR López-López, MT Pérez-García
2019/ 15-17 mayo, **Cáceres (España)** Participación con póster.

- **The Smooth Muscle Conference. FASEB**

Kv1.5 downregulation triggers phenotypic modulation in human vessels

Pérez-García MT; Arévalo-Martínez M; Moreno-Estar S; Alonso E; **Serna J**; de la Fuente MA; Cidad P; López-López JR
2019/ 14-19 julio, West Palm Beach, **Florida, United States of America**. Participación con póster.

Scientific Divulgation

- Universidad de Valladolid: Three-Minute Thesis contest 2021.
- Universidad de Valladolid: Three-Minute Thesis contest 2022. Finalist.
- Castilla y Leon inter-universities final: Three-Minute Thesis contest 2023.
- Invited speaker at Pint of Science Valladolid 2023.

Abstract

The voltage-gated potassium channel Kv1.3 plays a crucial role in T-cell activation and is considered a promising target for the treatment of autoimmune diseases. However, the lack of reliable antibodies has prevented its accurate detection and study under endogenous conditions, so that most published studies have been conducted in heterologous systems. To address this limitation, we engineered a Jurkat T-cell line expressing endogenous Kv1.3 channels tagged with a signal peptide to investigate the expression and localization of native Kv1.3 channels, and their role associated to T cell physiological responses. Using the CRISPR-Cas9 tool, we inserted a Flag-Myc peptide at the C terminus of the KCNA3 gene. Basal and activated channel expression were assessed through western blot analysis and imaging techniques. Surprisingly, besides the canonical Kv1.3 channel (54 KDa), we identified two additional isoforms with distinct N termini: a longer isoform (70 KDa) and a truncated isoform (43 KDa). All three isoforms showed upregulation after T-cell activation. Our focus was on characterizing the truncated isoform (short form, SF) as it had not been previously described and could be present in available Kv1.3-/- mouse models. Overexpressing SF in HEK cells generated Kv1.3-like currents with smaller amplitudes, which, unlike canonical Kv1.3, did not induce HEK proliferation. To explore the role of endogenous SF isoform in a native system, we generated both a knockout Jurkat clone and a clone expressing only the SF isoform. While the canonical isoform localized primarily at the plasma membrane, SF remained intracellular, accumulating perinuclearly. Consequently, SF Jurkat cells lacked Kv1.3 currents, exhibited depolarized resting membrane potential (E_M), reduced Ca^{2+} influx, and diminished increases in intracellular calcium ($[Ca^{2+}]_i$) upon stimulation. Functional characterization of these Kv1.3 channel isoforms revealed their differential contributions to signaling pathways involved in immunological synapse formation. In conclusion, alternative translation initiation generates at least three endogenous Kv1.3 channel isoforms in T cells with distinct functional roles. Importantly, some of these functions do not require the formation of functional plasma membrane channels by Kv1.3 proteins.

Abbreviations

AAV Adeno Associated Virus

APC Antigen-Presenting Cells

ATS Anti Sense

cDNA complementary DNA

CRAC Calcium Release-Activated Ca^{2+}

CRISPR Clustered Regularly Interspaced Short Palindromic Repeats

crRNA CRISPR RNA

DAG DiGiacylglycerol

DBS Double-Strand Break

DC Dendritic Cells

DMSO Dimethyl Sulfoxide

DNA Deoxyribonucleic Acid

eGFP enhance Green Fluorescence Protein

EM Resting membrane potential

ER Endoplasmic Reticulum

FBS Fetal Bovine Serum

FCS Fetal Calf Serum

HR Homologous Recombination

IP3 Inositol-1,4,5- trisphosphate

IS Immunological Synapse

ITR Inverted Terminal Repeat

KI Knock In

KO Knock Out

MHC Major Histocompatibility Complex

NHEJ Non-Homologous End Joining

PCR Polymerase Chain Reaction

PIP2 Phosphatidylinositol 4,5-bisphosphate

PLCγ1 Phospholipase Cγ1

PTK Protein Tyrosine Kinases

PVDF PolyVinylidene DiFluoride

qPCR Cuantitative PCR

RNA Ribonucleic Acid

RNP Ribonucleoprotein

SEE Staphylococcal Enterotoxin E

sgRNA single guide RNA

SOCE Store Operated Calcium Entry

TALE Transcription Activator-Like Effectors

TCR T Cell Receptor

TEM T cell Effector Memory

tracrRNA trans-activating RNA

TRP Transient Receptor Potential

ZFN Zinc Finger Nuclease

Index

Introduction

1.Introduction.

1.1 Voltage Gated Ion Channels.

1. 1.1 The origin of Voltage Gated Ion Channels.

Voltage-gated ion channels are essential proteins that support life in many forms. These channels are particularly fascinating, not only because of their important biological functions, but also because of the mechanisms by which they carry out these functions. Their most prominent role is in generating electrical activity in cells, which underpins many manifestations of life, including movement, sensation, and cognitive functions of the brain. Interestingly, some voltage-gated ion channels are also critical in non-excitable cells, performing functions unrelated to their ionic activity (1). The way these channels allow electrical events to occur is also intriguing, as they undergo rapid conformational changes that change their structure from impermeable to highly permeable to ions. In addition, although they are able to pass ions at nearly the diffusion rate, they are still able to selectively choose a specific class of ions while disregarding others at the opening of the pore.

While these channels are considered critical for animals, especially those with complex nervous systems, they are ancient proteins that are well represented in diverse prokaryotes. A plethora of channel types have evolved from a probably limited number of ancestors as a result of major genetic events such as gene duplications and numerous single base mutations (2). As our knowledge of ion channels and genomes has grown, so has our understanding of the evolutionary history of these important proteins. While voltage-gated ion channels are complex, the basic structure of all known ion channels is a simple protein consisting of two transmembrane segments (2-TM) separated by a pore-forming P-region loop. This basic motif is found in many prokaryotic channels and in the eukaryotic inward rectifier family[1], and it is thought to have undergone two rounds of gene duplication to form the early symporters (3). A symporter is an integral

[1] Inward rectifier: A channel that is "inwardly-rectifying" is one that passes current (positive charge) more easily in the inward direction (into the cell) than in the outward direction (out of the cell).

membrane protein that is involved in the transport of two (or more) different molecules across the cell membrane in the same direction.

The presence of over 200 potassium channel-related proteins in archaea and bacteria suggests that K^+ channels likely began to evolve from the moment that life emerged on Earth (4). The first crystallized channel, KcsA, was discovered in the bacterium *Streptomyces Lividans* (5). This channel is the one of the most broadly studied and it consists of four identical subunits that form a tetramer, each subunit containing 2TM domains linked by a pore region that houses the ion-selectivity filter. Specific amino acids in the pore region, including the signature sequence T/SXGXGX, contribute to the exceptional K^+ selectivity of this type of ion channel (6) (Figure I1).

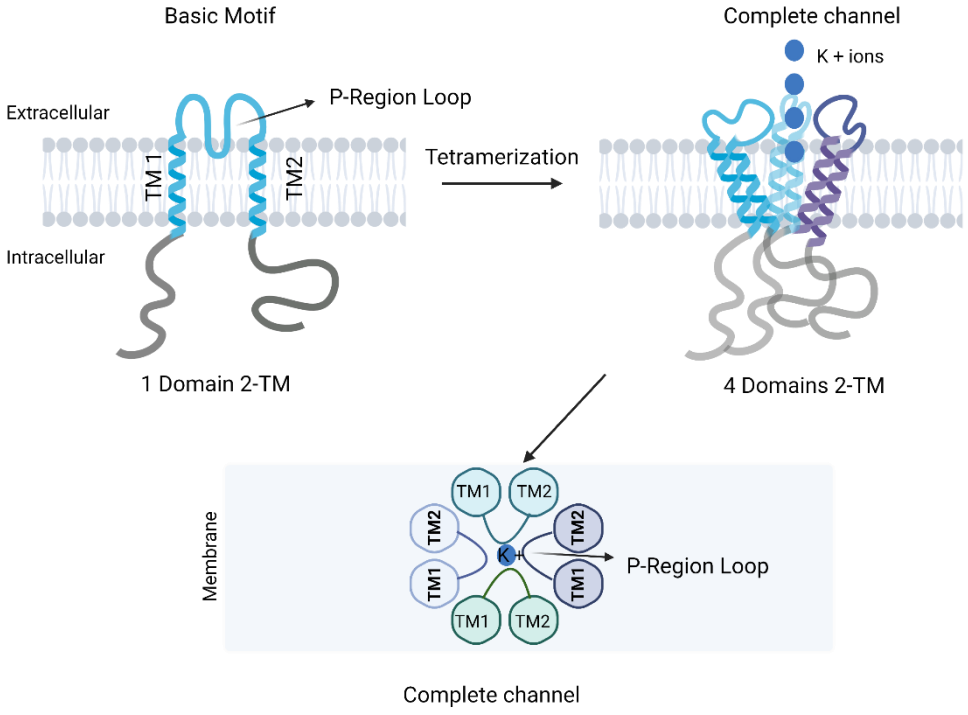

Figure I 1 The basic subunit of 2TM helix tetramerize with three other subunits to form a complete ion channel with the pore in the center. This structure is shared by many prokaryotic channels (as the KcsA) and in the eukaryotic inward rectifier family.

In most eukaryotic channels and some prokaryotic channels, the 2-TM basic motif has been expanded with the addition of four additional transmembrane segments, resulting in the six transmembrane segment (6-TM) protein (4). These 6TM proteins likely evolved through the fusion of a voltage-gating module (4TM) with a 2-TM pore module, as both modules exist as independent functional units

such as voltage-gated phosphatases (7) and voltage-gated proton channels (8), both of which lack a pore-module (Figure I2). The 6-transmembrane (6-TM) motif serves as the basic structure for eukaryotic voltage-gated ion channels, including potassium (K), calcium (Ca), and sodium (Na) channels. The voltage sensor is located in the positively charged residues of transmembrane segment 4 (S4), while the P region is responsible for ion selectivity (9).

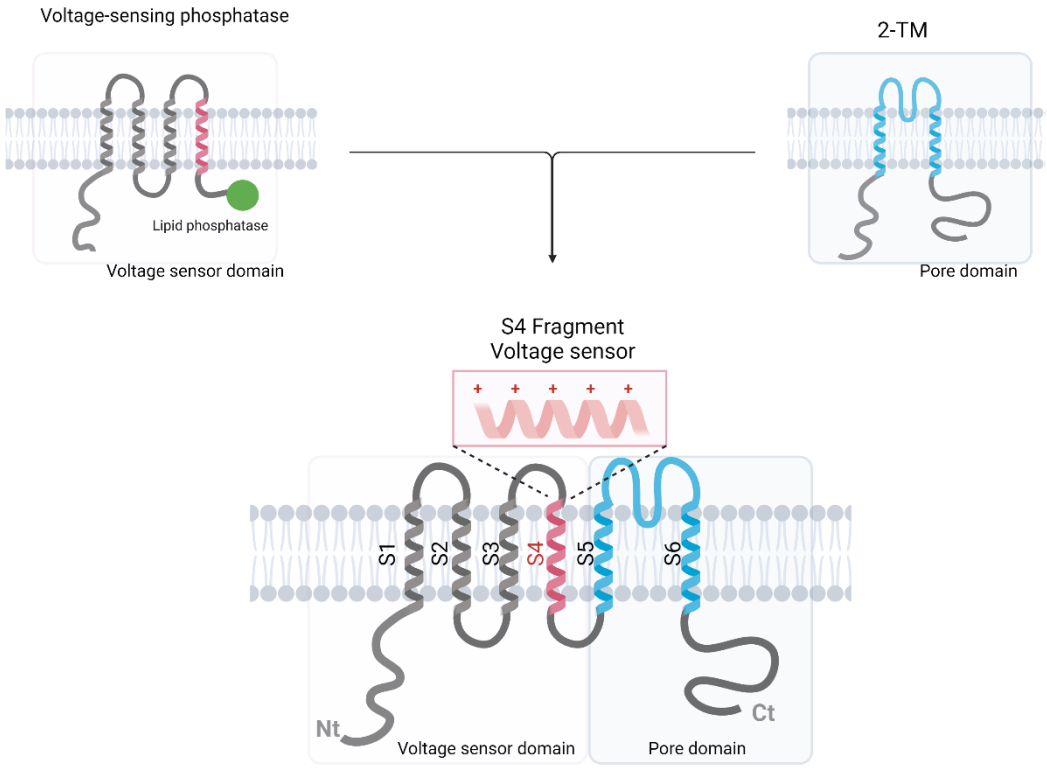

Figure I 2 Basic structure of voltage-gated ion channels. Each subunit consists of six transmembrane helices connected by intracellular and extracellular domains. Two distinct functional domains have been identified, the voltage sensor domain is composed of the helix from S1 to S4 and controls the gating of the protein. The pore domain is formed by the S5-P loop -S6 and forms the pore of the channel after tetramerisation with other subunits. The 6TM proteins likely evolved through the fusion of a voltage-gating module (4TM) with a 2-TM pore module, as both modules exist as independent functional units such as voltage-gated phosphatases (7).

Voltage Gated Potassium channels (Kv) are the most diverse in terms of both structure and function among voltage-gated channels. The basic unit of Kv channels is the 6-TM subunit, and four of these subunits come together in the membrane to form a functional K channel. Initially, the Kv channel family was identified to have four original members, namely Kv1, Kv2, Kv3, and Kv4, which were found in Drosophila, corresponding to shaker, shab, shaw, and shal channels, respectively (10,11). Later, additional variants of K channels were discovered in mammals including Kv5, Kv6, Kv7, Kv8, and Kv9. Moreover, there

are several members in many Kv families, such as Kv1.1 to Kv1.6, Kv2.1 to Kv2.2, Kv3.1 to Kv3.4, Kv4.1 to Kv4.3, and Kv9.1 to Kv9.2. Each member of these families exhibits slightly different functional properties, which can often be attributed to structural differences. Additionally, other forms of K channels resulting from post-translational modifications and splice variants have also been identified. As the functional tetrameric K^+ channel can be formed by four subunits that are not necessarily identical but can be closely related subunits or splice variants, the possible number of structural combinations is vast (9). A detailed discussion of voltage-dependent K channels is provided in section 1.3 of this thesis.

All known 6-TM channels possess pore-forming units comprising four subunits, which can be identical or highly homologous. K^+ channels have separate proteins for each domain, whereas Na^+ and Ca^{2+} channels have a single protein that covers all four domains (12). This evidence suggests that Na^+ and Ca^{2+} channels evolved from K^+ channels. The theory is reinforced by the observation that domains I and III of Na^+ channels are more similar to each other than to domains II and IV, which share greater similarity with each other. This indicates that the four-domain precursor protein that led to the development of Na^+ and Ca^{2+} channels was created through two gene duplication events from a single-domain 6-TM channel. Initially, the single domain transformed into a two-domain protein, which then duplicated entirely to generate the four-domain channel (13) (Figure I3).

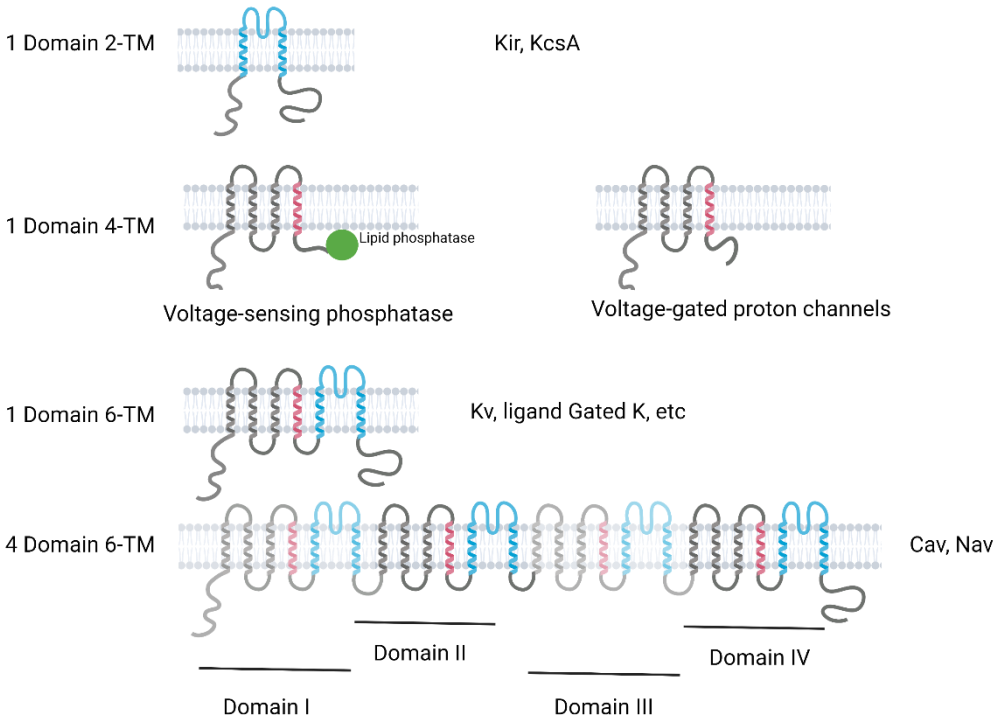

Figure I 3 Comparison of the structure of the different ion channels suggests an evolutionary process, with the 2-TM being the oldest and the 4-domain 6-TM being the most recent.

Similar to K^+ channels, **Voltage-gated Calcium Channels** also exhibit great structural and functional variation. The extensive diversity of Ca^{2+} channels was evident from early studies of Ca^{2+} currents, which identified three broad categories: L-type (long-lasting), T-type (transient), and N-type (Neuronal) currents (14). Many of these currents can be present in the same organism and in the same cell. L- and N-type currents necessitate significant depolarization for activation and were classified as high voltage-activated currents. T-currents, on the other hand, require only minor depolarizations and were identified as low voltage-activated currents (14). The analysis of the effects of peptide toxins revealed three additional Ca^{2+} current types, the P-type, the Q-type and the R-type Ca^{2+} currents (15). While L-type and T-type currents are observed in a wide variety of cell types, N-, P-, Q-, and R-type are most prevalent in neurons (15,16). As molecular cloning techniques were employed in Ca^{2+} channel studies, it became apparent that the functional diversity of Ca^{2+} currents correlate with significant structural differences. To date, ten families of voltage gated Ca^{2+} channels have been described.

Voltage-dependent sodium channels exhibit relatively low variability among them. They are activated by changes in membrane potential, allowing for the rapid influx of sodium ions into the cell, ultimately resulting in membrane depolarization and the initiation of an action potential (12). While 11 genes of these channels have been identified in mammals, the characteristics of the recorded currents are highly similar across all of them. The primary dissimilarities between different Na currents are pharmacological properties (17).

1.1.2 Types of Potassium channels.

All known K^+ channels, from fungi and protozoans to metazoans, share a conserved 2TM pore structure like that found in KcsA channels. However, while the pore structure has remained stable, other regions of the channel sequence have undergone significant structural diversity. As a result, K^+ channels are classified into three distinct structural categories (Figure I4).

1. The Kir family, also known as the inward rectifier family, shares the same structural design as the KcsA channel, with subunits composed of **2TM segments** on either side of the pore-forming domain and arranged as tetramers (18). The functions of Kir channels vary greatly depending on their type and location. In mammals, Kir channels are produced by 15 distinct genes that fall into seven subfamilies, named Kir1.x to Kir7.x. The seven Kir subfamilies can be grouped into four functional categories. Classical Kir channels, represented by Kir2.x, that are inherently active, G protein-gated Kir channels which include Kir3.x, which are modulated by G protein-coupled receptors (19,20). Kir6.x channels that are associated with cellular metabolism and are sensitive to ATP levels (21). Finally, the K^+ transport channels, comprising Kir1.x, Kir4.x, Kir5.x, and Kir7.x, are involved in the transportation of K^+ ions influenced by intracellular pH (22).
2. The second category of K^+ channels is the **two-pore 4TM segments** K^+ channels (K2P) family, whose subunits assemble as dimers, unlike the other families (23). In mammals, 15 distinct genes have been identified in this family that are classified into six subfamilies based on both their amino acid sequence and functional characteristics. Despite the lack of a

canonical voltage sensor domain, K2P channels can be modulated by various stimuli, such as mechanical force, polyunsaturated fatty acids like arachidonic acid, volatile anesthetics, pH/acidity, pharmacological agents, heat, and signaling processes such as protein-protein interactions and phosphorylation(24,25).

3. The third category of K^+ channels is composed by **the 6TM (S1-S6) segments** with a single pore domain (S5-P-S6). This family encompasses the Voltage-Gated potassium channels, the Calcium Activated potassium channels and the Sodium Activated potassium channels.

   3.A **Voltage-Gated channels**: Includes members from Kv1.x to Kv12.x. **Kv1.x to Kv4.x** (Shaker, Shab, Shaw, and Shal channels in Drosophila), as well as the KCNQ (**Kv7.x**), ether-a-go-go (**Kv10.x**; gated by voltage and cyclic nucleotides), erg (**Kv11.x**), and elk (**Kv12.X**) subfamilies form functional channels that conduct K ions across the plasma membrane. While **Kv5, Kv6, Kv8,** and **Kv9** share the same overall structure as other members of the Kv family, they do not form functional channels and are thus referred to as silent (KvS) subunits (26). Nevertheless, by combining with **Kv2** and **Kv3** α-subunits to create heterotetrametric channels, they regulate the biophysical properties and repress the expression of these outward rectifier channels (27,28)).

   3.B **Calcium Activated Potassium channels** (KCa). There are three main types of KCa channels: the **small-conductance (SK) channels**, the **intermediate-conductance (IK) channels** (29), and the **large-conductance (BK) channels** (30). SK and IK channels are voltage independent and gated by submicromolar levels of intracellular Ca^{2+} that bind to the obligatory channel subunit calmodulin. On the other hand, BK channels are now well-established to have seven transmembrane segments, these channels contain an additional transmembrane segment, S0, which results in the N-terminal of the protein being oriented towards the outer side of the membrane (31). Within the S4 segment of BK channels, there are numerous arginine residues. These residues render the channels sensitive to changes in voltage and lead to activation at elevated levels of calcium through direct interaction between calcium ions and the C-terminal domain (32). KCa channels play important roles in a

variety of physiological processes, including regulation of neuronal excitability, smooth muscle tone, and cardiac function. Dysfunction of these channels has been implicated in several diseases, including epilepsy (33) or hypertension (34).

3.C **Sodium Activated Potassium Channels** (KNa). Currently, there are two identified genes responsible for encoding KNa channels, which have been designated as Slack and Slick (35). They represent a distinct subgroup of ion channels characterized by sensing intracellular changes in Na ion concentrations (36,37). KNa channels are very widely expressed in the central nervous system but also found cardiac cells (38). The significance of these channels extends beyond basic excitability control, as human mutations in Slack genes produce extremely severe defects in learning and development, suggesting that KNa channels play a central role in neuronal plasticity and intellectual function (39,40).

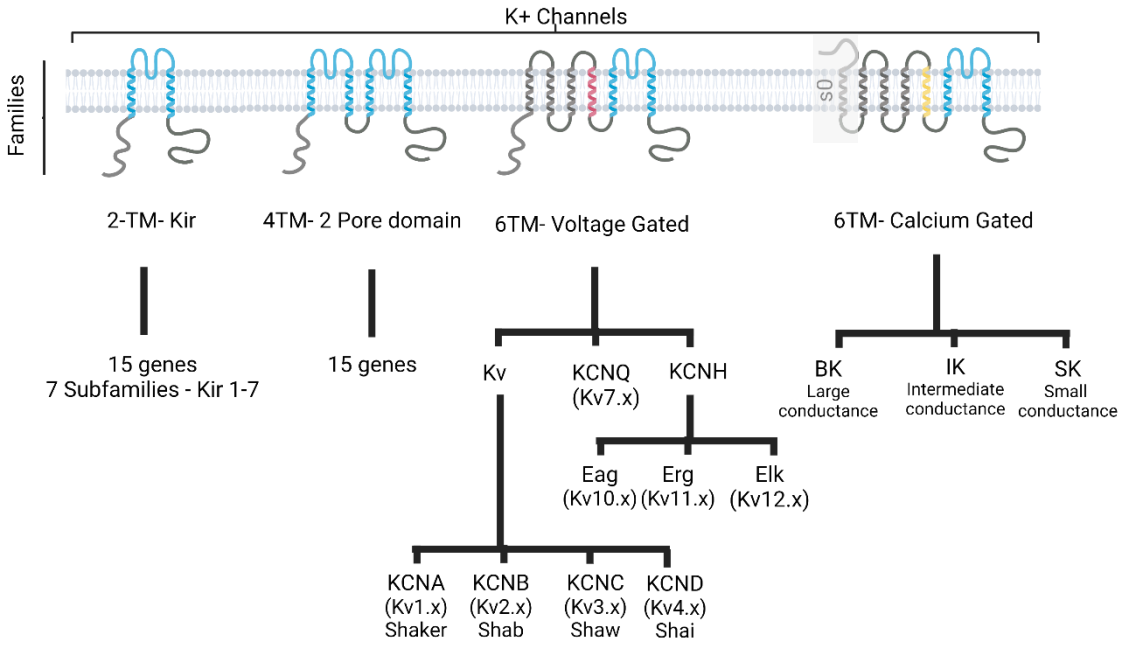

Figure I 4 Classification of potassium channels according its structure. The different families of potassium channels depicted in the figure include 2-TM (Two-Transmembrane), 4TM 2 pore domains, 6TM voltage gated, and 6TM calcium gated potassium channels. While IK and SK Calcium Gated Channels contain a classic 6TM structure, BK Channels contain an additional transmembrane domain known as S0.

1.1.3 Voltage Gated Potassium channels. The Kv1.3 channel.

The idea that the repolarization of action potentials is attributed to the outward potassium currents was first proposed by the classic electrophysiological studies conducted by Hodgkin and Huxley. They suggested that depolarization of a membrane causes a delayed activation of outward currents, which serve to repolarize the membrane (41). These channels are selective for potassium ions, which permeate the channel pore much more efficiently than calcium or sodium ions. Hence, these channels were termed delayed rectifier or voltage-gated potassium channels (Kv). To operate effectively, Kv channels necessitate a tetrameric organization with a minimum of four-fold symmetry, where the ion conduction pore is located along the axis. The hydrophobic segments of all Kv α-subunits display commonalities in their primary sequence, including the presence of a voltage-sensing domain that is made up of TM segments S1 to S4, and a pore domain that comprises S5 to S6 (9) (Figure I5).

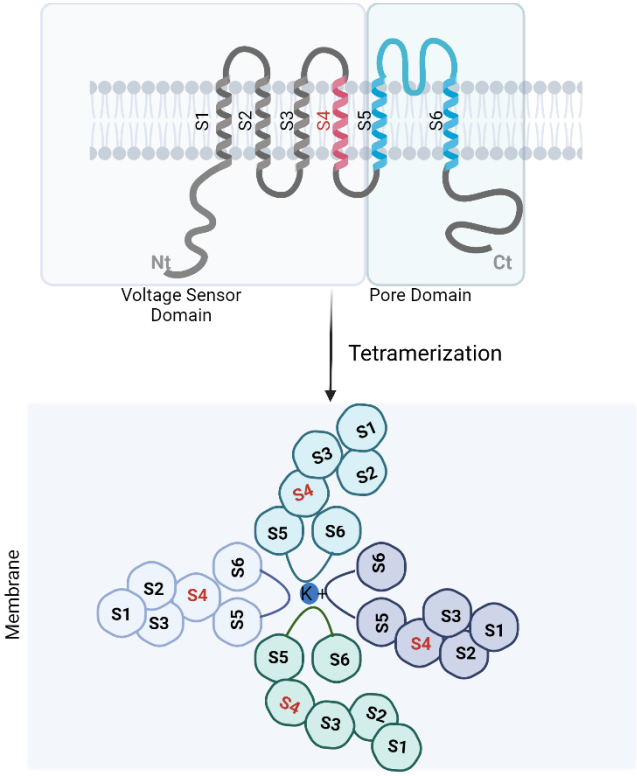

Figure I 5 Basic subunit of voltage-gated potassium channels. Each subunit consists of six transmembrane helices connected by intracellular and extracellular domains. Two distinct functional domains have been identified, the voltage sensor domain is composed of the helix from S1 to S4 and controls the gating of the protein. The pore domain is formed by the S5-P loop -S6 and forms the pore of the channel after tetramerisation with other subunits.

Kv channel expression patterns can be very diverse at different cell types from the expression of different combinations of Kv channels. This diversity is further amplified through several mechanisms:

- Heteromultimerization with subunits of the same family. Kv1, Kv7, and Kv10 families, form heterotetramers with novel functional properties not seen in the homotetramers (42).
- Heteromultimerization with silent subunit families. For example, Kv2 family-form heterotetramers with Kv5, Kv6, and Kv8 (26,43).
- Multimerization of Kvα tetramers with accessory β-subunits. For example, Kv1.1, Kv1.2, Kv1.3, and Kv1.5 (44,45).
- Alternative splicing: Kv3, Kv4, Kv6, Kv7, Kv9 Kv10, and Kv11 present alternative splicing (46,47).
- Posttranslational modifications such as phosphorylation, palmitoylation, ubiquitinylation, etc (48–50)

1.1.4 Voltage dependent Kv 1.3 channel.

Kv1.3 (KCNA3) is a voltage-gated potassium channel that belongs to the Shaker-related (Kv1, KCNA) subfamily. It has a typical Kv channel structure which is conserved in all Kv1 family members, consisting of tetramers of pore-forming subunits, each with six transmembrane helices (S1-S6) connected by intra- and extracellular loops. The voltage sensor domain is present in the S1-S4 transmembrane helices, while the K^+ selective pore is formed by S5 and S6 helices and their linker. The selectivity filter of the pore contains a motif of five amino acids (TVGYG) and forms the narrowest part of the channel (6). The four subunits arrange symmetrically around the conduction pathway. The S4 segment is a key player in the channel's gating mechanism, as it contains a positively charged amino acid every third position that contributes to its voltage sensitivity. When the membrane is depolarized, the S4 segment undergoes a conformational change, causing the S4-S5 linker to move and thus altering the opening or closing state of the conduction pathway (51). The intracellular NH2- and COOH-terminal

domains participate in channel assembly and association with auxiliary subunits, as well as the regulation of inactivation and trafficking (52). Tetramerization of Kv1.3 subunits involves a conserved NH2-terminal domain (the T1 domain) (51,53). Additionally, Kv subunits can assemble with ancillary Kv subunits through this T1 domain, increasing functional diversity. Recent studies suggest that these cytoplasmic domains may also play a role in cell signaling through protein-protein interactions (54).

Kv1.3 kinetic properties: The Kv1.3 channel activation and inactivation are voltage-dependent, with an activation threshold occurring between -60 and -50 mV. Kv1.3 activation time course is fast, taking a few milliseconds, while the inactivation time constant is much larger, about 200 ms at 50 mV. Kv1.3 channels inactivate with slow C-type inactivation, caused by the rearrangement of the outer mouth of the channel which blocks the ion conduction pathway (55).

Kv1.3 selective blockers: There are two primary structural categories of molecules that inhibit Kv1.3 channels: venom-derived peptides and organic small molecules.

- **Venom-derived peptides** (56), which typically consist of 18-60 residues, can block the ion-conducting pore of Kv1.3 channels from either the external or internal side. Examples of venom-derived peptides include Charybdotoxin (IC50 2.6nM)., Margatoxin (IC50 50pM), and Stichodactyla helianthus Neurotoxin (ShK) (IC50 0.6nM).
- Many blockers of Kv1.3 channels are **organic small molecules** that can access the channel pore. These blockers often have a similar structural motif, which allows them to bind to a specific site within the channel pore. The binding site typically involves interactions with amino acid residues lining the pore, such as aromatic residues or amino acids with positively charged side chains. The binding of blockers to Kv1.3 channels can involve various mechanisms, including electrostatic interactions, hydrogen bonding, and hydrophobic interactions. These interactions can either physically block the channel pore or modify the channel's conformation, preventing the passage of potassium ions and thus inhibiting the channel's activity. Additionally, some blockers may exhibit additional interactions

with regions outside the pore-forming region, further influencing their binding and functional effects on the channel (57). 4-aminopyridine (4-AP) (IC50 150µM) and TEA were among the first small molecules used to identify Kv channels pharmacologically. 5-Methoxypsoralen (5-MOP) (IC50 1.6 µM), a compound used to treat psoriasis, was identified as the primary K^+ channel-blocking principle of *R. Graveolens*. Afterward, derivatives with higher potency and selectivity for Kv1.3 channels, such as phenoxyalkoxypsoralen-1 (PAP-1) (IC50 10nm), were developed (58,59).

Kv1.3 functional role(s): Kv1.3 is expressed in various tissues and cell types, including excitable cells (neurons in the central nervous system, mostly in the inferior colliculus, olfactory bulb, and pons) (60,61), and non-exitable cells in the immune system (B and T lymphocytes, macrophages, and microglia) (62,63), thymus, spleen and testis.

The primary role of Kv1.3 in these cells is to regulate membrane potential and control K^+ efflux through the pore, which can lead to Ca^{2+} influx. However, Kv1.3 has also been shown to be involved in various signaling pathways through its intracellular domains, controlling the function of enzymes, transcription factors, and cell cycle regulation in multiple cell types. Three different models have been proposed to explain the role of Kv1.3 channels in cell proliferation, which are not exclusive and may vary across different cells and tissues (55) (Figure I6).

- The "membrane potential model" suggests that Kv1.3 activation leads to membrane hyperpolarization, providing the driving force for Ca^{2+} influx required to activate Ca^{2+}-dependent transcription. This model explains most of the data obtained from various immune system cells and will be discussed in detail in section 2.2.
- The "voltage sensor model" proposes that Kv1.3 channels mainly serve as sensors that transduce electrical signals into biochemical cascades, independently of their effect on membrane potential. This model may explain Kv1.3-dependent proliferation of vascular smooth muscle cells (VSMCs).

- The "channelosome balance model" suggests that the Kv1.3 to Kv1.5 ratio may act as a master switch determining proliferation, as observed in glial cells and VSMCs.

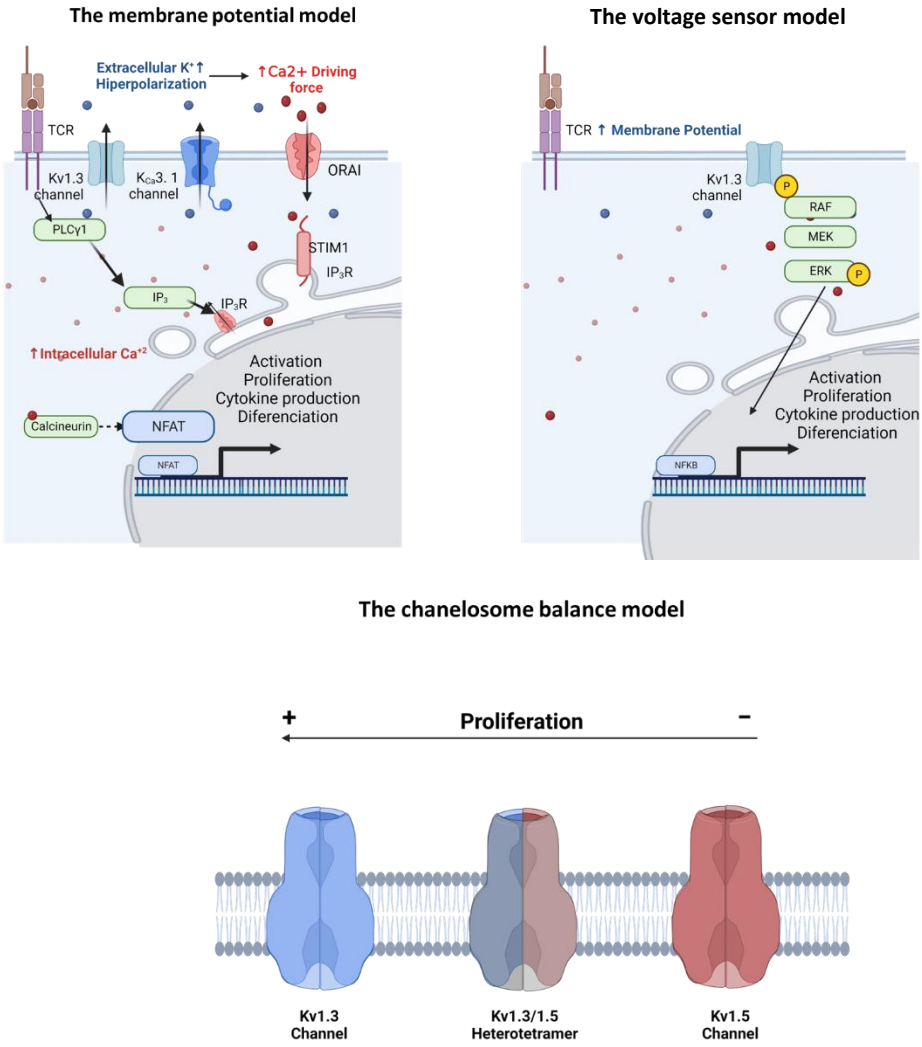

Figure I 6 Proposed models illustrating the involvement of Kv1.3 channels in cellular proliferation control (55). ***(A)*** *The Membrane Potential Model suggests that Kv1.3-mediated potassium efflux repolarizes the membrane potential, creating a calcium driving force that promotes downstream signaling pathways involved in cell proliferation.* ***(B)*** *The Voltage Sensor Model suggests that Kv1.3 channels interact with other proteins or signaling molecules, directly modulating cellular processes associated with proliferation.* ***(C)*** *The chanelosome balance model suggest that the ratio of Kv1.3/Kv1.5 may act as a master switch determining proliferation. These models provide insights into the multifaceted mechanisms by which Kv1.3 channels contribute to the regulation of cellular proliferation.*

It is well-established that Kv1.3 is predominantly localized in the plasma membrane. Several studies have explored the trafficking and assembly of Kv1.3 in the membrane. During translation of the channel mRNA, the nascent polypeptide chain is inserted into the endoplasmic reticulum (ER) membrane, and

the rate of retrograde and anterograde transport determines the expression level in the plasma membrane (64). Unlike many membrane proteins that have a cleavable signaling sequence for targeting to the plasma membrane, Kv1.3 channels lack this motif. Instead, the S2 segment of the channel serves as a recognition site for membrane targeting (51). Studies have shown that Kv1.3 is guided to the plasma membrane by two acidic glutamate (E) residues located at the C-terminus of the channel. Removal of these amino acids through C-terminal deletion or mutation to isoleucine leads to the loss of ionic current and plasma membrane expression(52,65).

Kv1.3 location and trafficking: Kv1.3 is primarily located in the plasma membrane; however, it has also been found in other organelles, such as mitochondria (66), the nucleus (67), and the Golgi Apparatus (68) although the trafficking route for Kv1.3 to these organelles is not completely well understood it has been proposed that Kv1.3 uses the TIM23 complex to translocate to the inner mitochondrial membrane (69). While the role of Kv1.3 in the nucleus or the Golgi Apparatus is not completely clear, the presence of Kv1.3 in mitochondria has been widely studied. Several studies have reported that Kv1.3 in the inner mitochondrial membrane is closely related to apoptosis. It has been shown that during apoptosis, Bax (a member of the Bcl-2 family) binds to and inhibits Kv1.3 located on the inner mitochondrial membrane. This inhibition leads to hyperpolarization, increased production of reactive oxygen species, and cytochrome c release, which triggers Bax-dependent apoptosis (70). Kv1.3 located in mitochondria has been reported in numerous cancer cell types and inhibiting mitochondrial Kv1.3 has been suggested as a potential target in cancer treatment. Application of mitochondrial Kv1.3 channel inhibitors (derived from PAP-1) can induce glioblastoma cell apoptosis and reduce tumor volume up to 90% in vivo in an orthotopic mouse model (71–73).

Several types of cancer cells and human brain tissues have been reported to contain Kv1.3 channels localized in the nucleus. It was described that nuclear Kv1.3 can regulate nuclear membrane potential and activate transcription factors such as phosphorylated CREB and c-Fos (67).

1.2 The Immune system

1.2.1 Cellular components of the Immune System. T cells.

The human immune system has two major components: innate (natural) and adaptive (specific) immunity. Together, they work to protect the host from disease-causing agents. Innate immunity is the first and rapid responder against pathogens, recognizing common molecular patterns present in microorganisms. Its function is nonspecific. The adaptive immune system, on the other hand, reacts specifically to each antigen, making it slower to respond (days to weeks) after infection. Both types of immune responses involve defense effector mechanisms that can either involve the elaboration of soluble products acting systemically (humoral immunity) or require direct cell-to-cell contact or the activity of cytokines and chemokines in the cellular microenvironment (cell-mediated immunity). Most immune responses involve participation of both modes of response (74).

The major cellular constituents of both innate and adaptive immunity originate in the bone marrow, where they differentiate from multipotent hematopoietic stem cells along several pathways to become granulocytes, lymphocytes, and antigen-presenting cells. The elements of innate immunity are diverse, including physical barriers to pathogen invasion, such as skin or mucous membranes, as well as an array of cell types that can be activated by cell-surface motifs of the pathogen. Activation of innate immunity induces an inflammatory response using mechanisms that are broadly shared with those of the specific immune system. These include natural killer (NK) cell-mediated cytotoxicity, activation of granulocytes and other phagocytes, the secretion of inflammatory cytokines and chemokines, and the interactions of the many participants in the complement cascade (75) (See Figure I7).

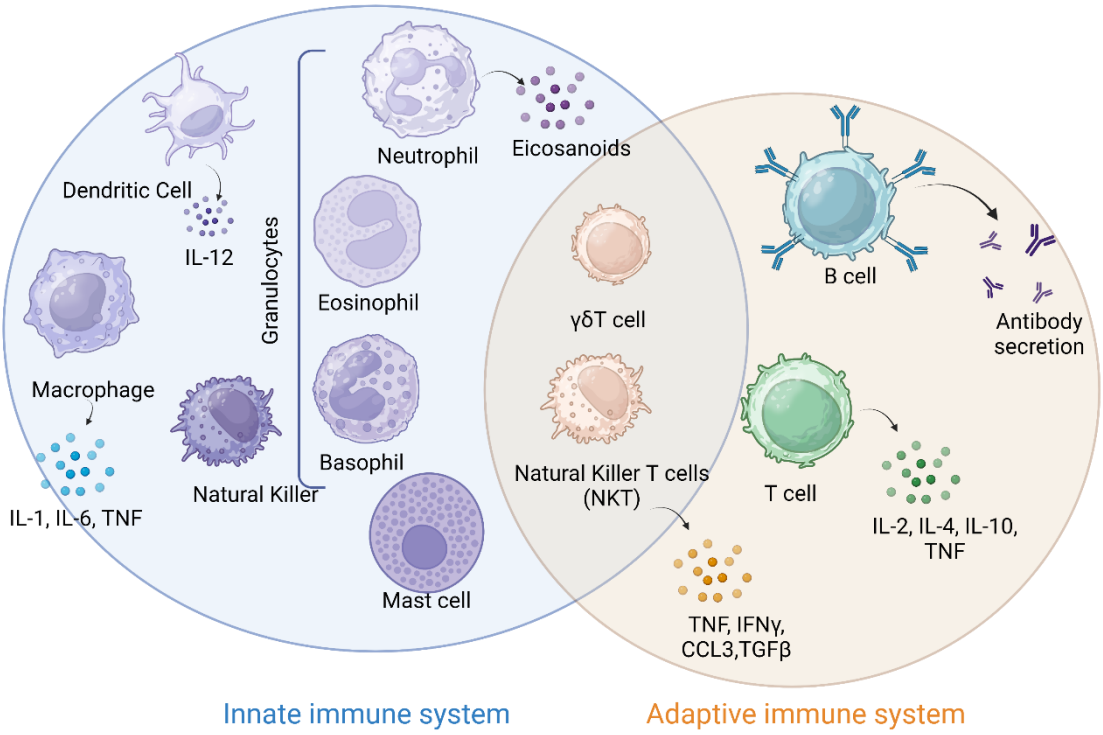

Figure I 7 Overview of key immune cells of the innate and adaptive immune systems and their major secreted soluble mediators. ***Innate immune cells****, including macrophages, granulocytes, natural killer (NK) cells, and dendritic cells, release a variety of soluble mediators such as cytokines (interferons, tumor necrosis factor), chemokines (CCL3, CCL4), and antimicrobial peptides.* ***Adaptive immune cells****, such as T cells and B cells, secrete soluble mediators like cytokines (interleukins), antibodies (immunoglobulins), and cytotoxic granules (granzymes and perforins). The coordinated release of these soluble mediators enables effective immune responses against pathogens and aberrant cells, contributing to immune surveillance and homeostasis.*

The adaptive immune system can be divided into two types: humoral and cellular immunity, both of which work together to defend the host against a wide range of infectious agents(76). In humoral immunity antibody molecules are secreted by B lymphocytes. These antibodies can neutralize toxins and specifically recognize microbes, flagging them for phagocytosis by phagocytic cells. Cellular immunity is mainly conducted by T lymphocytes (T cells) against intracellular pathogens, which cannot be accessed by antibodies (77). In this situation, T cells function to kill infected cells directly with the help of cytotoxic T cells or indirectly by activating macrophages and neutrophils to stop the spread of infection.

T cells are key elements of the adaptive immune system, they express the T cell receptor (TCR) on the surface of the plasma membrane which allow them to recognize antigens specifically. TCR molecules have a great diversity, which enables the adaptive immune system to recognize 10^7 to 10^9 different antigens (77).

T lymphocytes are divided into two main groups based on their surface markers: helper (CD4+) and cytotoxic (CD8+) cells. CD4+ T cells are twice as frequent as CD8+ T cells in humans and mainly assist B cells while producing phagocytosis-stimulating cytokines. CD8+ T cells have the major role in defense against intracellular and tumoral antigens. Regulatory T cells (Tregs) are a subtype of CD4+T cells involved in immune response suppression. NKT cells and mucosa-associated invariant T (MAIT) cells are a smaller group of T cells that carry receptors with limited diversity. NKT cells exhibit both NK-like cytotoxicity and antigen-specific T-cell responsiveness.

Prior maturation in the primary lymphoid organs, T cells are functionally inactive and called **naïve T cells**. After maturation, they migrate to secondary lymphoid tissues, where they recognize their specific antigens by antigen-presenting cells (APC). T cell activation is initiated when APC presents the antigen through the major histocompatibility complex (MHC) to the TCR. To achieve full activation, T cells require a second signal, which is provided by co-stimulatory molecules expressed on a APCs. CD80 and CD86 are the most well-known co-stimulatory molecules present on activated APCs, and they interact with CD28 on T cells to provide the second signal (Figure I8A). After receiving the first and second signals (TCR and CD28 signaling), PI3 and Akt kinases are activated, as well as PLC and MAP kinases. Ultimately, this leads to T cell survival, proliferation, cytokine production, and differentiation into **effector** and **memory cells.** Effector and memory cells are less reliant on the second signal, and thus, they can activate with other APCs (74).

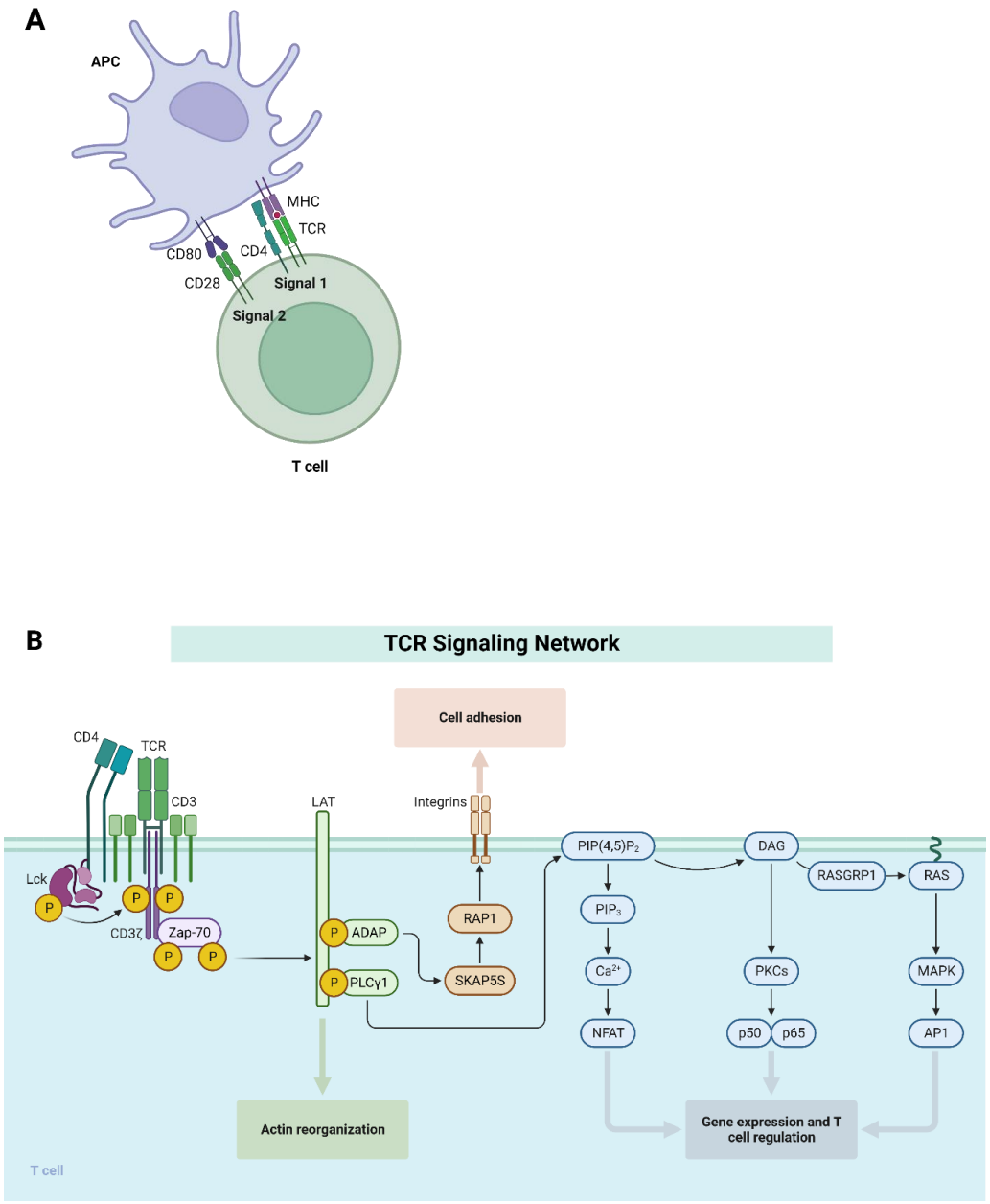

Figure I 8 A. To achieve full activation, T cells require two different signals. The antigen recognition through the MHC to the TCR and a second signal provided by co-stimulatory molecules expressed on a APCs. I B. Representation of TCR Signaling initiated after T cell activation.

After T cell activation, the expression of CD69 and CD25 on the cell surface is upregulated (78). **CD69** induction results in a decrease in sphingosine 1-phosphate receptor, which facilitates the release of T cells from lymphoid organs. The upregulation of **CD25** allows T cells to respond to IL-2, which is the primary T cell growth, differentiation, and survival factor. Along with adhesion molecules such as integrins and selectins, other cytokine receptors also upregulate during T cell activation to facilitate T cell effector functions and migration to different

tissues. The transcription of the IL-2 gene and expression of its receptor are also induced after T cell activation, resulting in the promotion of cell cycle progression and antiapoptotic proteins production (79). **Effector T cells** produce other cytokines that influence B cells and macrophages during the immune response. The formation of **memory T cells**, which provide long-term immunity against an antigen, is a crucial part of T cell activation. Memory T cells have the ability to self-renew in the absence of antigens and rapidly migrate to infectious tissues upon reinfection. IL-7 is a critical cytokine for memory cell survival, and memory T cells express CD127 (IL-7 receptor). CD45RO and CD27 are additional markers of memory T cells. The memory cell population can be divided into **central memory (TCM)** and **effector memory (TEM)** based on location and their function. TCM are located at the lymph nodes because they maintain a reservoir of the memory cells. Their effector function is low and they express the markers CCR7 and CD62L (Figure I9). TEMs do not express specific markers, and they act as the memory cells that rapidly turn into effector T cells in the tissues that produce cytokines like IFN-γ.

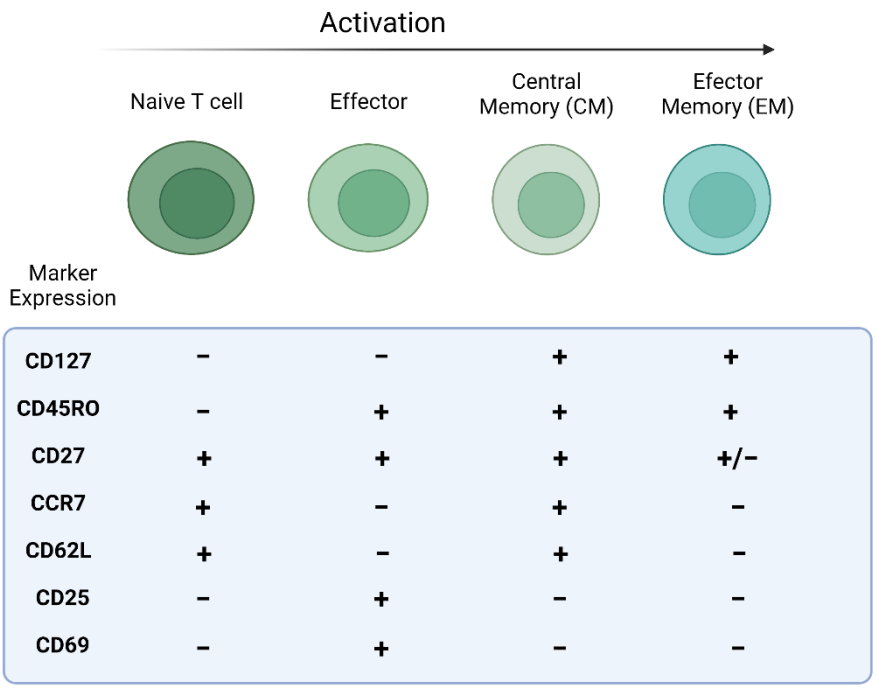

Figure I 9 Characterization of T cell subsets: Naive, effector, central memory, and effector memory T cells and their associated markers. Naive T cells, marked by CD27, CCR7 and CD62L expression, represent antigen-inexperienced T cells. Effector T cells, characterized by high expression of activation markers such as CD25 and CD69, exhibit immediate effector functions. Central memory T cells, identified by the presence of CCR7 and CD45RO, possess a high proliferative

capacity and can migrate to lymphoid tissues. Effector memory T cells, lacking CCR7 expression but expressing CD45RO, are specialized for rapid responses in peripheral tissues.

After the elimination of antigens, T cell activation is declined, and immune response is attenuated. This is result of the lack of stimuli, which leads to less IL-2 production, and the downregulation of antiapoptotic proteins. Consequently, the activated cells die, and the immune response is abolished.

1.2.2 Ion Channels in T cells.

To generate an effective T cell immune response, two critical components are necessary: sustained calcium influx and the creation of a stable immunological synapse (IS) with the APC. To achieve this, ion channels play a pivotal role in forming a functional network at various levels. Lymphocytes have been found to have many different types of ionic currents, including several calcium currents (Orai1+/STIM1, IP3Receptor, adenosine triphosphate responsive purinergic P2 receptors (P2XR) and TRP currents), two potassium currents (Kv1.3, KCa3.1), and one chloride current (Cl swell) (80,81). At the individual cell level, ion channels regulate global calcium signaling, which, through a balance of calcium influx and potassium efflux, leads to changes in gene expression and motility. Additionally, cell volume is regulated by balancing chloride efflux and potassium efflux.

To trigger a T cell response, APCs like B cells, dendritic cells (DCs), or macrophages must present antigens to the T cells. This interaction prompts the T-cell receptor/CD3 complex (TCR/CD3) to bind with the antigens, which then activates phospholipase Cγ1 (PLCγ1) through protein tyrosine kinases (PTKs). PLCγ1 separates phosphatidylinositol 4,5-bisphosphate (PIP_2) from plasma membrane phospholipids, which produces diacylglycerol (DAG) and inositol-1,4,5- trisphosphate (IP3). IP3 synthesis induces a biphasic increase in intracellular Ca^{2+} concentration by liberating Ca^{2+} from intracellular storages (like the ER) and by initiating a continued Ca^{2+} influx through calcium release activated Ca^{2+} channels (CRAC). These CRAC channels become activated in response to

Ca^{2+} store depletion. The genes responsible for this calcium entry pathway in T cells are ORAI1 and STIM1(82).

In addition to CRAC channels, other calcium channels have been implicated in TCR-mediated calcium signaling. These channels include the transient receptor potential (TRP) channels that can be activated by DAG and SOCE (83–85) or purinergic P2 (P2X) receptors that respond to adenosine triphosphate (86). The cumulative effect of these channels results in an elevation of intracellular calcium, which activates the calmodulin-calcineurin pathway. This pathway triggers the nuclear translocation of NFAT and the transcription of target genes, ultimately directing T cell homeostasis, activation, proliferation, differentiation, apoptosis, and survival.

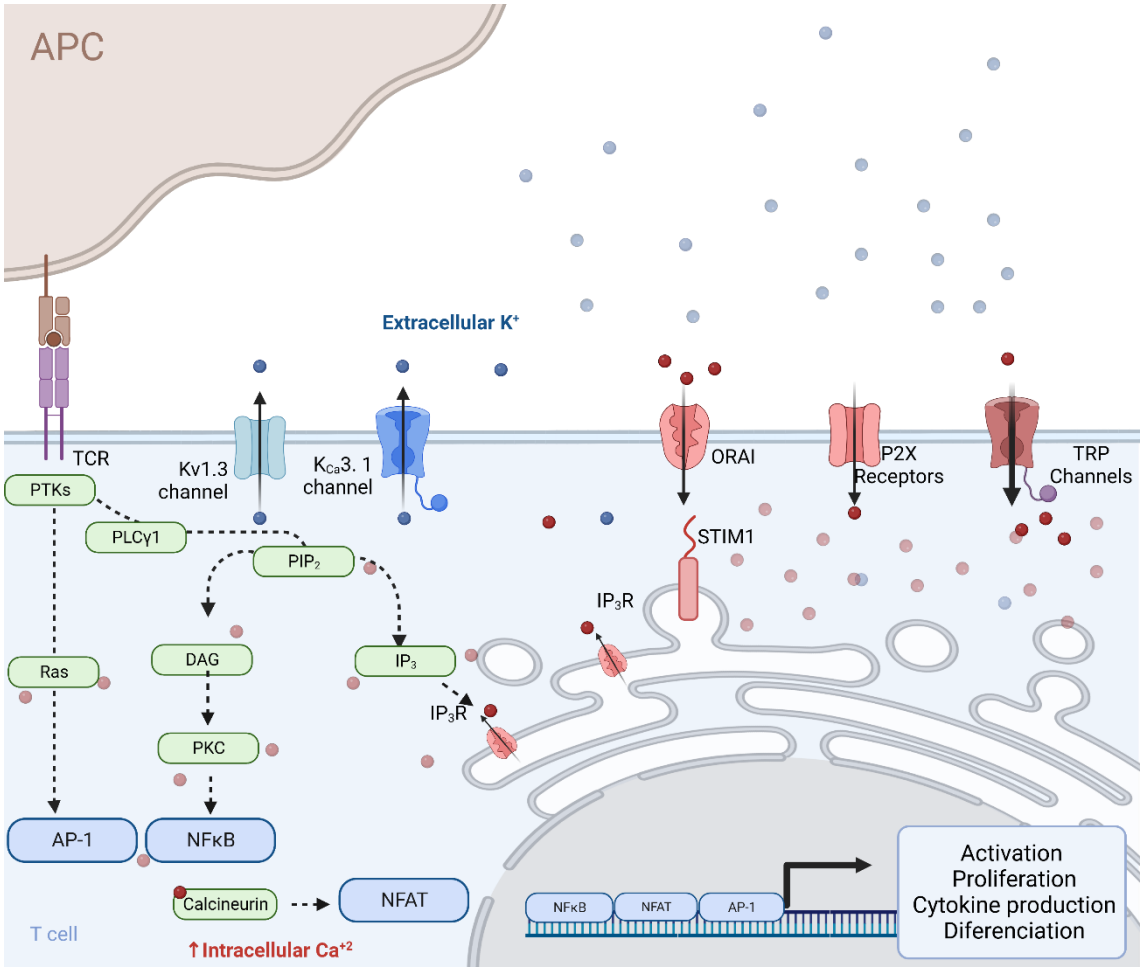

Figure I 10 To trigger a T cell response, APCs must present antigens to the T cells. This interaction prompts the TCR-MHC binding which activates PLCγ1. PLCγ1 promote the formation of DAG and IP3. IP3 synthesis induces a biphasic increase in intracellular Ca^{2+} concentration by liberating Ca^{2+} from ER and by initiating a continued Ca^{2+} influx through CRAC channels. DAG promotes the activation of NFkB pathway. The rise in intracellular Ca^{2+} activates the NFAT pathway which induce genes involved in T cell activation such as IL2.

The elevation of cytosolic calcium also promotes membrane depolarization, which, in turn, activates potassium channels. In T cells, Kv1.3 channels and intermediate conductance Ca^{2+}-activated K^+ channels (KCa3.1 channels) are the primary K^+ channels. Activation of these channels, either through membrane depolarization (Kv1.3) or increased intracellular Ca^{2+} (KCa3.1), results in membrane hyperpolarization, amplifying the driving force for calcium (87). These channels determine the resting membrane potential of T cells, thereby regulating the intensity of the calcium signal necessary for gene transcription and cell proliferation. In essence, Kv1.3 channels, with their sigmoid voltage dependence, protect against membrane potential depolarization, ensuring that the lymphocyte's membrane potential does not significantly depolarize, even when calcium enters the cell.

As previously mentioned, TCR engagement induces the activation of PLC-γ, which hydrolyzes phosphatidylinositol-4,5-bisphosphate to generate IP3 and DAG. This results in the activation of two primary signaling cascades in T cells. The first is the Calcium-calcineurin-NFAT pathway, which is stimulated by the binding of free cytosolic calcium to the phosphatase calcineurin. Activated calcineurin dephosphorylates NFAT proteins, promoting their nuclear translocation and inducing NFAT-mediated gene transcription of T-cell-activation-induced proteins such as IL2 genes (88). The second pathway initiated after TCR engagement is the Ras/MAPK pathway. DAG activates PKC, which phosphorylates and activates several transcription factors, including NF-κB. Moreover, Kv1.3, KCa3.1, and CRAC channels are recruited to the immunological synapse (IS) during antigen presentation, which likely provides additional signaling functions (89,90). The IS is a highly organized structure that forms at the point of contact between a T cell and an APC. Correct IS formation is essential for the proper development of signaling events (91). CRAC channels are recruited to the synapse to produce a high localized Ca^{2+} nanodomains close to the APC, which can trigger activation of calcium dependent-enzymes or other signaling proteins (82). Kv1.3 and KCa3.1 channels are also described to be accumulated at the synapse to facilitate the clustering and to modulate the Ca^{2+} response (90). The disruption of this process was described to promote alterations of downstream Ca^{2+}-dependent signaling events (89).

The expression pattern of potassium channels in T cells can vary widely depending on the T cell subtype, activation state, and secondary differentiation. Upon activation, KCa3.1 expression is upregulated in Naïve cells and in Central Memory cells, while Kv1.3 expression is upregulated in Effector Memory cells. As Effector Memory T cells play a key role in autoimmune diseases, blocking Kv1.3 channels presents a promising therapeutic opportunity as they rely heavily on these channels for Ca^{2+} signaling and cytokine production. Selective Kv1.3 blockers have been shown to hinder Effector Memory T cell migration, proliferation, and cytokine secretion (92,93) (Figure I 11).

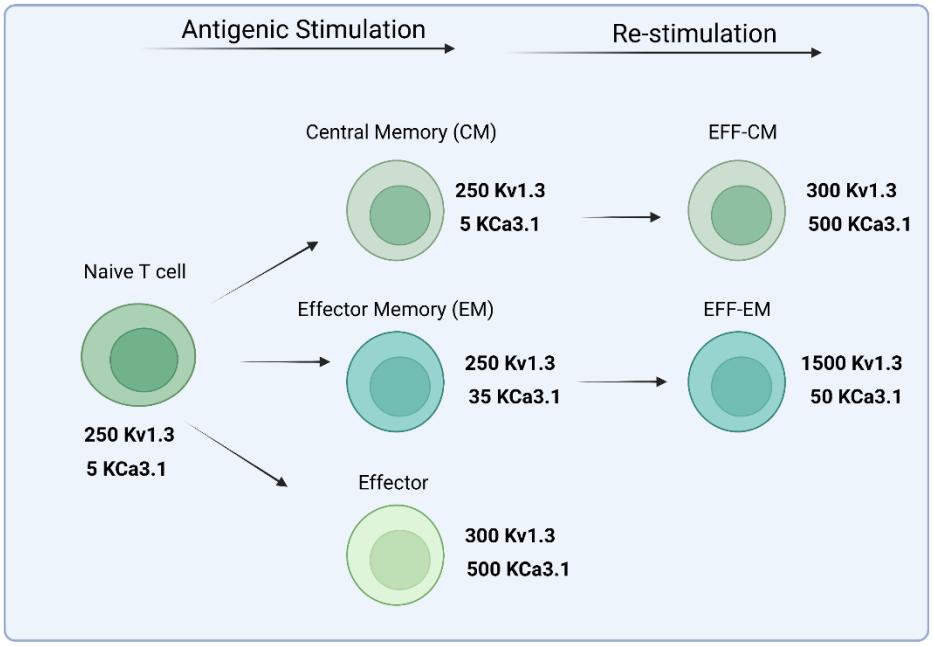

Figure I 11 The number of Kv1.3 and KCa3.1 channels expressed in T cells varies through the T cell subset. Numbers represent the number of potassium channels expressed in each cell according to Ueyama A. et al.

In addition to changes in K^+ channel expression during the activation of naive T cells, the mRNA levels of the CRAC channel components STIM1 and Orai1, as well as Orai2 and Orai3, are upregulated in T-cell blasts within a day of TCR engagement (82). These changes occur in tandem with the upregulation of functional KCa3.1 and Kv1.3 channels, indicating that all three main channel types involved in Ca^{2+} signaling in T cells are upregulated following TCR engagement. Upregulation of Orai1 and STIM1 likely contributes to enhanced store-operated Ca^{2+} influx in activated T cells, which is crucial for the regulation

of gene expression, clonal expansion, and differentiation in T cells during an immune response (94).

1.2.3 Kv1.3 in T cells.

The best characterized role of Kv1.3 resides in the immune system. Kv1.3 is the unique voltage dependent potassium channel expressed in T cells. Therefore, the link between Kv1.3 and immune physiology is unsurprising. Pharmacological inhibition of Kv1.3 has been shown to reduce proliferation and cytokine production in pathogenic TEM cells while preserving other lymphocyte subsets (58). Consequently, Kv1.3 blockers have emerged as promising treatments for autoimmune diseases. Therapies based on Kv1.3 blocking are advantageous because unlike other Kv channels, Kv1.3 has minor implications in heart physiology which is one of the most limiting factors in ion channel drug development (95).

Kv1.3 knockout animal models are viable, with gene deletion having a minimal impact on the immune system, likely due to a compensatory increase in Cl- currents in lymphocytes (96). Kv1.3 deficiency decreases the severity of autoimmune diseases and decreases the prevalence of tissue-specific TEM cells while promoting the proliferation of T lymphocytes with suppressive properties instead of TEM (75). These findings correlate with in vivo studies showing that Kv1.3 genetic ablation or pharmacological inhibition significantly reduces the production of proinflammatory cytokines(97). Importantly, pharmacological blockade of Kv1.3 channels selectively inhibits clonally expanded TEM cell-mediated autoimmune responses while leaving naive and TCM immunity intact (59). Kv1.3 blockers have also been shown to be effective in rodent models of various autoimmune diseases such as Multiple Sclerosis, Rheumatoid Arthritis, Contact Dermatitis, type 1 Diabetes Mellitus, and Psoriasis(93,98,99).

However, mouse models may not be the ideal choice for studying this channel for several reasons. Although a comprehensive comparison between both channels has not been extensively studied, it is known that, firstly, the compensatory Cl current described in the knockout (KO) does not exist in human cells (96). Secondly, the protein sequence of the channel differs between the two

species, with the human channel containing an additional 54 amino acids in its amino-terminal end, which could have implications for its regulation. Thirdly, mouse T cells are markedly distinct from human T cells regarding ion channels, differing both in the number of expressed channels and the types of channels present limiting their utility as a model for evaluating pharmacological inhibitors (80). In resting cells, mouse T cells express various K^+ channels such as Kv1.1, Kv1.3, Kv1.6, and Kv3.1 (100). Moreover, there is a distinct persistence of high KCa3.1 expression in chronically activated effector memory T (TEM) cells in mice. As a result, mouse TEM cells can evade the inhibition of Kv1.3 since they still maintain KCa3.1 expression, which counterbalances Ca^{2+} influx through CRAC channels(101). Notably, while KCa3.1 blockade proves effective in experimental autoimmune encephalitis (EAE) in mice (102), it does not yield similar outcomes in rats or humans.

Given that a significant portion of the studies on Kv1.3 have been conducted in mice, we deem **it crucial to enhance our understanding of the role of the Kv1.3 channel in human models of T lymphocytes**.

1.3 Genome editing.

1.3.1 Genome editing techniques.

The ability to modify a specific gene in eukaryotic organisms is of enormous importance not only in molecular biology, but also in the fields of medicine and biotechnology. Indeed, the goal of introducing desired changes into genomes has long been a goal of molecular biology. The discovery of restriction enzymes in 1970 marked a turning point, ushering in the era of recombinant DNA technology. These enzymes were produced by bacteria to protect themselves from phages by cutting DNA sequences at sequence-specific sites (103). This discovery gave scientists the ability to manipulate DNA in the laboratory for the first time. A few years later, in the 1980s, the second breakthrough in genetic modification came with the description of the process of homologous recombination (104,105). This was the first description of how eukaryotic cells could insert an exogenous DNA sequence at a specific site in the genome if the exogenous sequence was flanked by regions complementary to the insertion site. Targeted gene integration into the genome offered a remarkable advantage for studying the functional roles of different genes in model organisms. However, this approach had certain limitations: the spontaneous integration rate of an exogenous DNA copy was extremely low (from 1 in 10^3 to 10^9 cells) and it was not suitable for all cell types.

Researchers sought alternative strategies to increase the efficiency of homologous recombination, leading to the discovery that introducing a double-strand break (DSB) into the DNA at a target site significantly increases the frequency of targeted gene integration by several orders of magnitude. They discovered that two different repair mechanisms can occur following the creation of a DSB at the gene of interest: homologous recombination (HR), in which the cell machinery uses exogenous DNA as a template to repair the break, and non-homologous end joining (NHEJ), in which the cell machinery rejoins broken ends without a template (106). NHEJ often results in localized gene mutations that render a gene inactive, leading to loss of function (107) (See Figure I12). HR was suitable for introducing mutations or generating a knock-in gene, while NHEJ was very efficient for generating knock-out models. This discovery led to the

development of various methods to create specific DSBs, including high-precision nucleases.

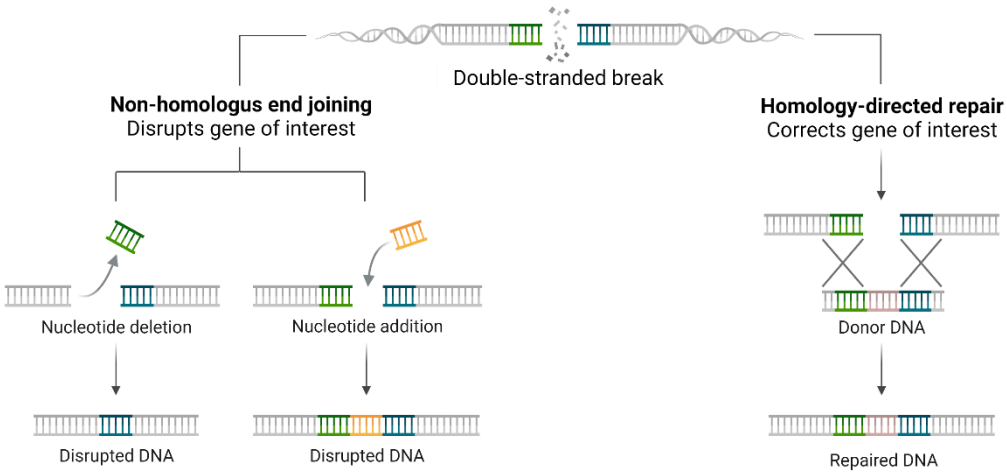

Figure I 12 Two different repair mechanisms can occur following the creation of a DSB at the gene of interest: non-homologous end joining (NHEJ), in which the cell machinery rejoins broken ends without a template. NHEJ often results in localized gene mutations (insertions or deletions) that render a gene inactive, leading to loss of function and homologous recombination (HR), in which the cell machinery uses exogenous DNA as a template to repair the DBS.

The first widely used programmable nuclease proteins were created by fusing zinc finger proteins, a DNA-binding domain that is made up of multiple zinc finger motifs, with the DNA cleavage domain of the Fok I endonuclease (108). The DNA-binding domain of zinc finger endonucleases was designed to recognize a specific DNA sequence through the specific interactions of the amino acid residues in the zinc finger motifs with the DNA bases. After the target DNA sequence recognition by the zinc finger domain, the endonuclease domain cleaved the DNA at the specific location within or adjacent to the zinc finger recognition sequence, creating a double-stranded DNA break. These proteins significantly increasing targeted homologous recombination and were used to generate specific mutations in model organisms and human cells (109).

Although Zinc Finger Nucleases (ZFNs) were effective in generating DSBs in mammalian cells, their design and optimization processes were laborious and had some limitations. TALENs (from transcription activator-like effectors nucleases), on the other hand, were developed by fusing a DNA-binding domain derived from transcription activator-like effectors (TALEs) with a DNA cleavage

domain from FOKI (110). TALEs are proteins found in certain bacteria that bind to specific DNA sequences, and each TALE contains similar repeat domains, each of which recognizes a single nucleotide in the DNA sequence. By changing the amino acids in the repeat domains, the sequence specificity of TALEs can be easily programmed (111) . TALENs offered several advantages over ZFNs, including ease of design and assembly, high specificity and the ability to recognize single nucleotides in the DNA sequence. Although ZFNs and TALENs increased the efficiency of genome editing, the discovery of the CRISPR-Cas9 system in 2012 ushered in a new era of genome editing (112). This system provided a more robust and efficient tool for genome editing that was also easier and more flexible to use, making it widely adopted by the scientific community (FIGURE I13).

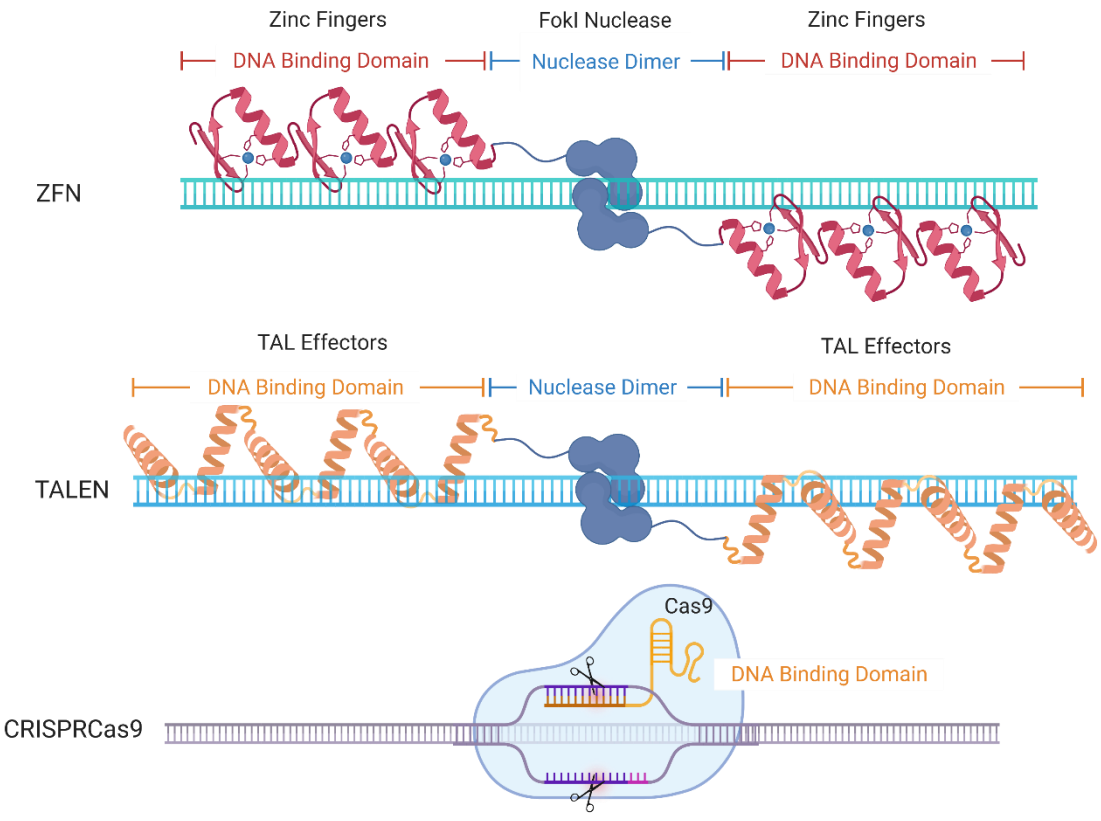

Figure I 13 Comparison between the structure of the most used nucleases for genome editing.

1.3.2 The CRISPR Cas9 System

CRISPR (Clustered Regularly Interspaced Short Palindromic Repeats) is a type of DNA sequence found in bacteria and archaea. It was originally discovered as part of the bacterial immune system, which uses CRISPR to fight off viral infections (113). The CRISPR sequence consists of short, repeated DNA sequences separated by unique 'spacer' sequences. These spacer sequences are derived from viruses or other foreign DNA that the bacterium has encountered in the past. The CRISPR elements are adjacent to several well-conserved genes called CRISPR-associated (Cas) genes. After a viral infection, bacteria use a Cas enzyme (CRISPR-associated protein) to cut the viral DNA and insert a piece of it into the CRISPR sequence as a new spacer into their genome (114). More importantly, the CRISPR spacer sequences dictate the targeting specificity of the Cas enzymes, which provide a defense against the phage in future reinfections. (See figure I14)

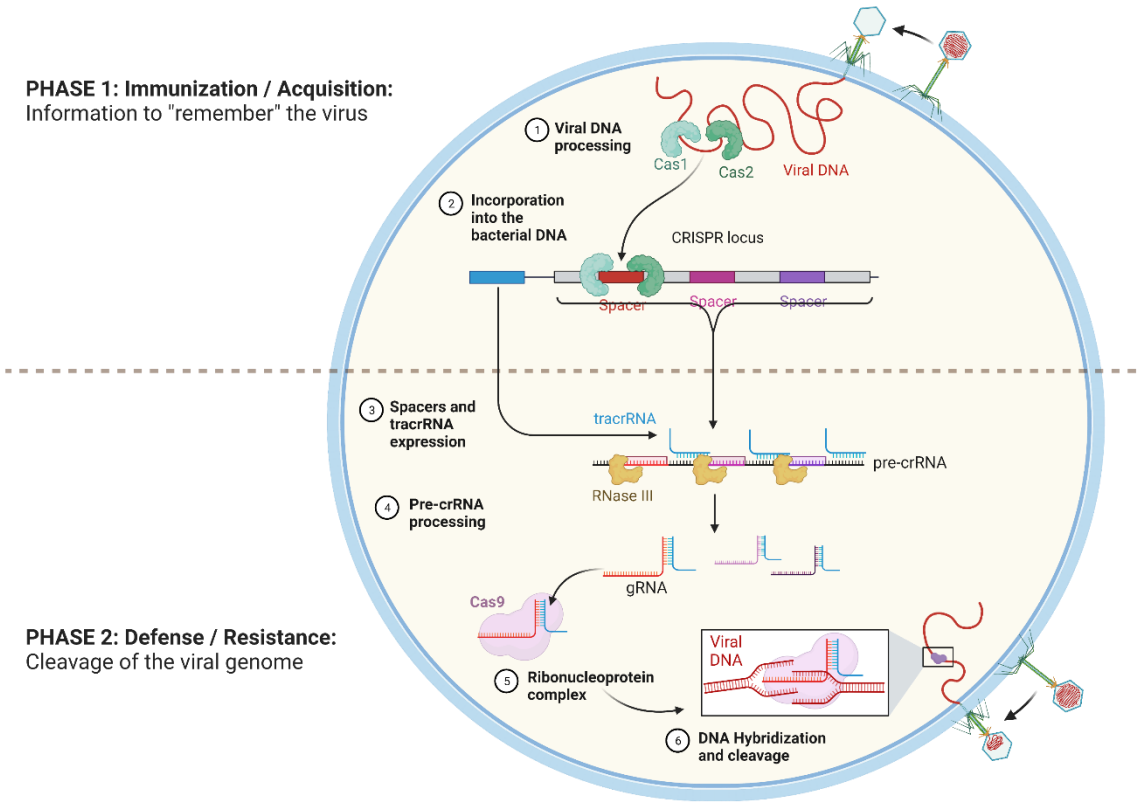

Figure I 14 Mechanism of action of the CRISPR system in bacteria. The CRISPR system serves as a bacterial adaptive immune system that enables the recognition and targeting of foreign genetic elements, such as viral DNA or plasmids.

The figure showcases the two key steps of CRISPR functioning: acquisition and defense. In the acquisition step, the bacteria incorporate fragments of foreign DNA into their own genome as "spacers" between repeated DNA sequences known as CRISPR arrays. During the defense step, the CRISPR array is transcribed and processed into small CRISPR RNAs (crRNAs) that guide the system. crRNAs, in complex with Cas proteins, recognize and bind complementary sequences on foreign genetic elements, leading to their degradation or inactivation.

The discovery of CRISPR led to the development of the CRISPR-Cas9 system, a powerful gene-editing tool. The Cas9 enzyme can be directed by a short RNA called a guide RNA (gRNA) to target a specific DNA sequence. This allows scientists to cut and modify specific genes with a high degree of precision. The Cas9 protein requires two short RNAs: the mature CRISPR RNA (crRNA) and a trans-activating RNA (tracrRNA). Both crRNA and tracrRNA are required to form the Cas9 protein-RNA complex, which cleaves DNA with DSBs at target sites. However, a chimeric RNA formed by the fusion of tracrRNA and crRNA, called a single guide RNA (sgRNA), can also guide CRISPR-Cas9, simplifying the system.

CRISPR-Cas9 technology has been adapted for in vivo genome editing in eukaryotic cells, making it a versatile tool that can be easily directed to almost any location in the genome by designing a short sgRNA. Its high efficiency and ease of use have made CRISPR technology the method of choice for various genome-targeting purposes, from the generation of animal models to the application of human therapeutics.

Hypothesis

2. Hypothesis.

According to the published literature, Kv1.3 channels play a critical role in modulating T-cell activation, proliferation, cytokine production, immunological synapse formation, and migration. However, most of the published work on Kv1.3 so far has been performed in mouse models or in heterologous systems. We consider essential to validate and elucidate the relevance of these findings in native human systems. Understanding the specific functions and regulatory mechanisms of Kv1.3 channels in human T cells is essential for developing therapeutic strategies targeting autoimmune diseases and immune-related disorders.

Hypothesis 1: These novel tools for gene editing could be used to generate edited Kv1.3 channels with tagged molecules in native systems, which will allow the study of the expression, trafficking and regulation of endogenous channels avoiding the use of unreliable antibodies. This approach will also allow us to directly investigate their reported expression in intracellular compartments other than the plasma membrane, such as mitochondria or the endoplasmic reticulum, and their physiological functions there.

Hypothesis 2: The specific functional role(s) of Kv1.3 channels in native human systems can be explored using these tools to generate edited human T-cell lines expressing channel variants, or complete channel KO.

Hypothesis 3: Non-conducting functions of Kv1.3 proteins could still be present in the partial Kv1.3 KO mice (which is the only presently available KO model). We will use gene editing to generate a full Kv1.3 KO mice model to elucidate potential differences with the partial deletion of the Kv1.3 protein.

Objectives

3. Objectives

While heterologous models and mouse models have provided valuable insights into Kv1.3 function and regulation, it is essential to validate and elucidate the relevance of these findings in human systems. Human T cells play a pivotal role in immune responses and can exhibit unique characteristics and responses compared to their murine counterparts. Therefore, investigating the involvement of Kv1.3 in human T cells holds great potential for uncovering novel therapeutic targets and strategies for immune-related disorders. This study aims to bridge the gap in our knowledge by investigating the functional properties, regulation, and potential therapeutic implications of Kv1.3 in human T lymphocytes.

To this end, the main goal of this thesis is to **explore the role of Kv1.3 in human T cells** in a native system.

The specific objectives of the work will be:

1. To generate a Jurkat T-cell line expressing endogenous Kv1.3 channels tagged with a signal peptide at the C terminus and a Jurkat cell line Kv1.3 KO using the CRISPR-Cas9 system.

2. To investigate the changes in the expression and the functional contribution of Kv1.3 to the T cell physiology including the process of activation, cytokine secretion, apoptosis, calcium signaling and immune synapsis formation comparing our Jurkat-Kv1.3-3F2M cell line and the Jurkat-Kv1.3-KO cell line. The result will be validated with the use of specific Kv1.3 blockers (PAP-1 and/or MargaToxin) in human derived primary T cell cultures.

3. To explore the presence and possible role of Kv1.3 in intracellular organelles in which has been described in literature such as mitochondria under endogenous conditions.

4. To generate a full Kv1.3 KO animal model to compare its phenotype with the phenotype of the partial Kv1.3 KO mice available.

Materials and Methods

4. Materials and Methods

4.1 Cell lines

In this thesis, we used four different immortalized cell lines.

Jurkat cell line (ATCC, TIB-152) is a human T lymphocyte cell line established from the peripheral blood of a 14-year-old, male, acute T-cell leukemia patient. This cell line has been broadly used in immunology and immuno-oncology research. It express human CD3 at the plasma membrane and it can produce large amounts of IL-2 after stimulation with phorbol esters or monoclonal antibodies against the T3 antigen (115). We chose Jurkat cell line as our model because Kv1.3 is the only voltage-dependent potassium channel expressed in this cell line (116). Jurkat cells were cultured at 37 ◦C 10% CO2 in High Glucose DMEM (11965092, Gibco) supplemented with 10% Fetal Bovine Serum (FBS) (10100147, Gibco) 100 units/ml of penicillin-streptomycin (15140148, Gibco, UK), 1mM sodium pyruvate (11360070, Gibco), and 2 mM l-glutamine (25030081, Gibco) and were passed every 2–3 days at ~0.5 × 10^6 cells/mL.

HEK-293 (Human embryonic kidney) cell line was used as a heterologous expression system for the overexpression of our plasmids of interest. HEK-293 is a cell line isolated from the kidney of a human embryo that exhibits epithelial morphology. It is a good transfection host.

293FT cell line (R70007, Invitrogen), a HEK-293 derived cell line optimized for the packaging of viral particle was used for AAV6 generation. The 293FT Cell Line is highly transfectable clonal isolate derived from HEK-293 cells transformed with the SV40 large T antigen (from pCMVSPORT6TAg.neo plasmid) which increase viral DNA replication. Both cell lines were cultured at 37 ◦C 10% CO2 in High Glucose DMEM (11965092, Gibco) supplemented with 10% FBS , 100 units/ml of penicillin-streptomycin (15140148, Gibco), 1mM sodium pyruvate (11360070, Gibco, UK), and 2 mM l-glutamine (25030081, Gibco) and handled according to each manufacturer's recommendations. 293FT cells were supplemented with 500 µg/mL Geneticin (10131035, Gibco).

Raji B cells (ATCC, CCL-86) is a human B lymphocyte cell line established from a Burkitt's lymphoma of an 11-year-old Black male. Raji B cells were cultured at 37 ◦C 5% CO2 in RPMI 1640 Glutamax (61870-010, Gibco) supplemented with 10%FBS, and were passed every 2–3 days at ~0.5 × 106 cells/mL.

Primary CD4+ T cells. Mononuclear cells were extracted from the peripheral blood of healthy donors using a ficoll density gradient. T cells were then purified using human total CD4+ isolation kits (Miltenyi Biotech, 130-096-533). Soluble anti-CD28/CD3 magnetic beads were added at 2.5 µg/mL final concentration, along with recombinant human IL-2 (20 U/mL) in RPMI culture medium (Life Technologies) with 10% fetal calf serum (FCS) and cells were incubated at 37ºC 5%$C0_2$. Fresh medium containing human recombinant IL-2 (20 U/mL) was added every 3 days and lymphoblasts were used from day 6.

4.2 Plasmid Generation.

4.2.1 General protocol:

The generation of a plasmid requires six different steps from designing the primers to clone and amplify the plasmids that are graphically summarize in Figure M1.

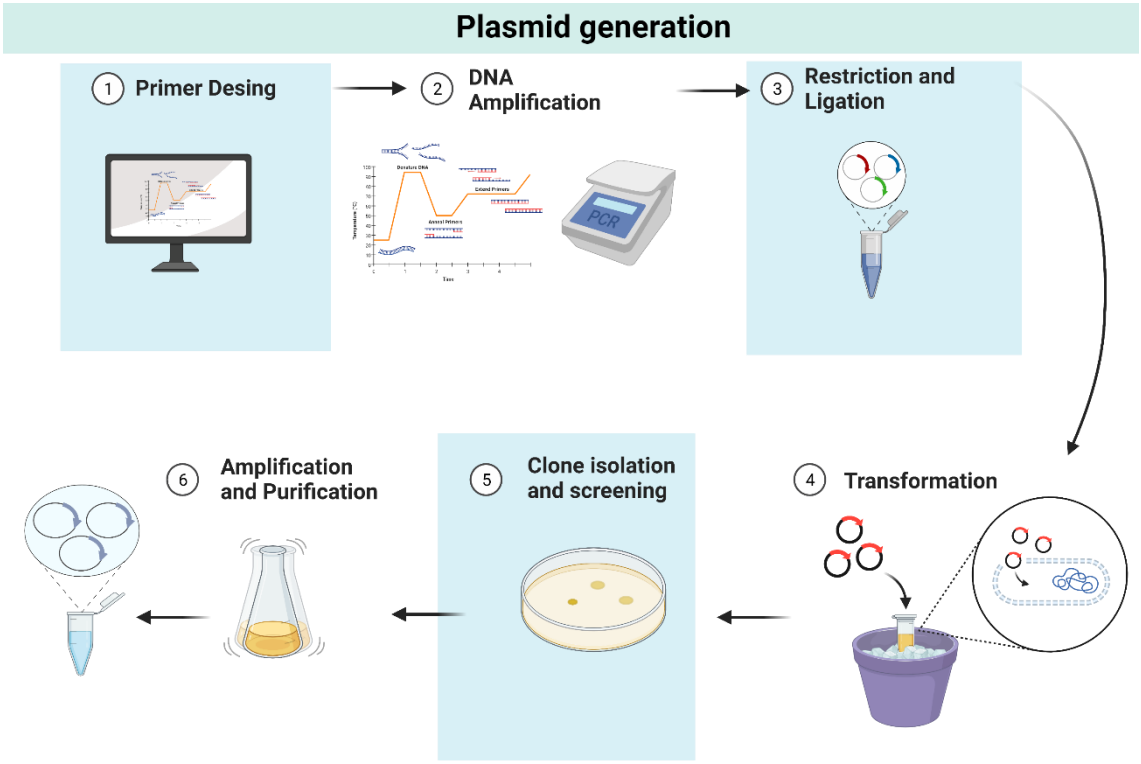

Figure M 1 Step-by-Step scheme for the construction of a Plasmid, from primer design to amplification and purification. The diagram highlights the essential stages and techniques utilized in each step to achieve the desired plasmid construct.1. Primer Design: Design specific primers targeting the desired DNA sequence within the plasmid.2. Polymerase Chain Reaction (PCR): Perform PCR to amplify the target DNA region using the designed primers. 3. Plasmid Insertion: Ligate the amplified DNA fragment into a plasmid vector. 4. Transformation: Introduce the ligation mixture into competent host cells through transformation. 5. Clone isolation using antibiotics and screening. 6 Bacterial Culture and Amplification: Culture transformed cells to amplify the plasmid-bearing cells and Plasmid Purification: Purify the plasmid DNA from the bacterial culture to obtain a pure product.

A. Primer design.

The first step was to design a set of PCR (Polymerase Chain Reaction) primers that amplify the DNA fragment of interest. The primers were designed to anneal to the ends of the DNA fragment using the Primer Designing Tool from NCBI (https://www.ncbi.nlm.nih.gov/tools/primer-blast/). The sequences of the primers used in this thesis are shown in **Table 1**. According to their utility, we could classify all our primers into three groups showed in Figure M2:

a. Screening primers: Screening primers are unmodified primers that contain the same sequence as the region of interest and were obtained from the Primer Designing Tool with a theoretical Melting Temperature of 60-62ºC. They were primarily used for screening purposes based on PCR.
b. Cloning primers: The primers designed for cloning contain the same sequence as the region of interest, but with the addition of a restriction site of interest at the 5' end. The restriction site allows for the creation of sticky ends that are compatible between two fragments, facilitating their ligation. These primers were designed manually and are used for fragment cloning into plasmids.
c. Mutagenic primers: These primers carry a small mutation and are designed tail-to-head in opposite orientations, so that the entire plasmid of interest is amplified. This plasmid will now incorporate the mutation introduced in the primer (Figure M2.C). These primers are used to introduce small mutations into plasmids.

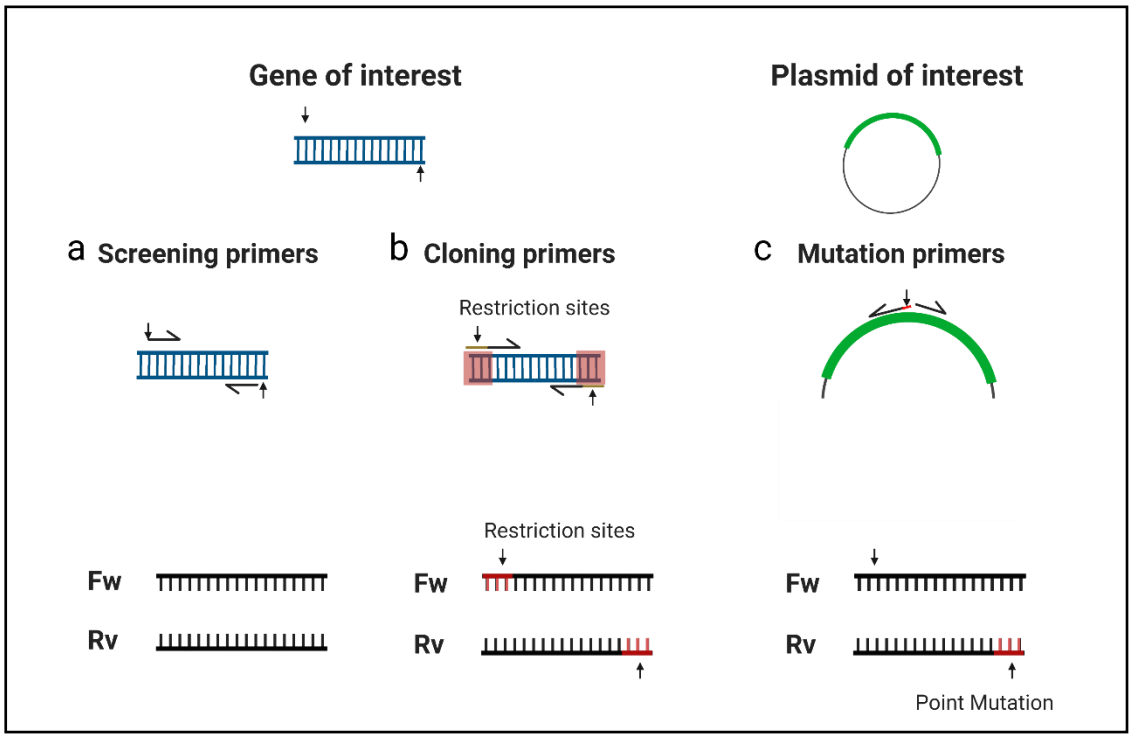

Figure M 2 Classification of primers generated in this thesis. A. Screening primers: Used to amplify a region of interest. B. Cloning primers: Designed to amplify regions to be cloned into a plasmid. C. Mutation primers: Used to introduce a point mutation into a plasmid of interest.

Table 1: Primers used for generation of constructs or cell lines.

Ref	Description	Sequence 5-3
F1	Left Arm MluI	acgcgtggtggagacgctgtgcat
R1	Left Arm SalI	agcattagactaacagattcctgtcgac
F2	Blasticidin SalI	gtcgacaatcccgggtctccgcg
R2	Blasticidin EcoRI	ggcgcgcccccagatcggaatt
F3	Right Arm EcoRI	gaattcatatgtcccagccccaacaac
R3	Right Arm RsrII	ccacaataaggcatgatctggaaccgaccg
R4	3xFLAG peptide	catcaaaaagatattcaccgatgactataaggaccacgacggagactacaag
F4	3xFLAG peptide	ggatcatgatattgattacaaagacgatgacgattaatatgtgatacaagtgacatgctgtg
F5	NheI site	gctagcgactataaggaccacgacggag
R5	NheI site	caacatcaaaaagatattcaccgat
F6	MYC peptide	ctagcgagcagaaactcatctcagaagaggatctgg
R6	MYC peptide	ctagccagatcctcttctgagatgagtttctgctcg
F7	NeonGreen NheI	taagctagcgtgagcaagggcgaggagg
R7	NeonGreen NheI	taagctagcttgtacagctcgtccatgcc
F8	Long Form EcoRI	attgaattcccgacatgaccgt
R8	Long Form AgeI	ggtggcgaccggtggatcc
F9	short form ecori	aatgaattcgaggccatggagaagttccg
R9	short form agei	ggtggcgaccggtggatcc
F10	long form ecori	acgcgtggtggagacgctgtgcat
R10	long form xhoi	agcattagactaacagattcctgtcgac
F11	mut hkv1.3 m0	gcggacgagcgcctcagccttct
R11	mut hkv1.3 m0	gcggcggggaagaggcggc
R12	mut hkv1.3 m1	gcggacgagcgcctcagccttct
F12	mut hkv1.3 m1	gcggcggggaagaggcggc
F13	mut hkv1.3 m137	gcgaggtacttcgacccgctccgc

R13	mut hkv1.3 m137	gcgccgcttggggtcgccca
R14	mut hkv1.3 m2	gcggagaagttccgcgaggacgag
F14	mut hkv1.3 m2	ggcctcctcgcccagctggt
F15	gRNA KI	taatacgactcactatagttgtatcacatattaaac
R15	gRNA KI	ttctagctctaaaacgtttaatatgtgatacaa
F16	gRNA total KO 1	taatacgactcactataggctggtgaaccacggctacg
R16	gRNA total KO 1	ttctagctctaaaacctatagtgagtcgtatta
F17	gRNA total KO 2	taatacgactcactataggaagtacctcatgcgccgct
R17	gRNA total KO 2	ttctagctctaaaacagcggcgcatgaggtacttc
F18	gRNA short KO	taatacgactcactatagtaccgagctggccgaacgac
R18	gRNA short KO	ttctagctctaaaacgtcgttcggccagctcggta
F19	mitocherry	agatctgccatcatgtccgtcctgac
R19	mitocherry	cggtatcggcaacgaatggatcttgg

B. PCR amplification.

Next, the DNA fragment was amplified by PCR using the designed primers and a template DNA. The source of template DNA was different in each experiment:

Genomic DNA: Genomic DNA was used as a template DNA for amplification of specific genes or regions of interest. The extraction of genomic DNA was performed as follows: First, 1x 10^6 Jurkat cells were collected and resuspended in 300µL of lysis buffer containing 50 mM Tris-HCl (pH 8.0), 10 mM EDTA, 1% SDS, 200µg/mL proteinase K and 500mM NaCl. Sample was incubated for 1 hour at 56ºC. After lysis, the DNA was precipitated using 500 mM de NaCl and absolute ethanol. Once the DNA was precipitated, it was pelleted by centrifugation and washed with 70% ethanol to remove any remaining contaminants and salt. The purified DNA was resuspended in TE buffer, and its concentration and purity were measured using a Nanodrop spectrophotometer reading at 260 nm.

cDNA: cDNA (complementary DNA) is synthesized from mRNA using reverse transcription and was used as a template DNA for amplification of transcripts. To synthetize cDNA, first RNA was extracted from Jurkat cells using Trizol. Briefly, 1x 10^6 Jurkat cells were collected and resuspended in Trizol and chloroform. The homogenate was incubated at room temperature to allow the Trizol to lyse the cells and denature the proteins. After incubation, the sample was centrifuged at a 21500g for 10 minutes to separate the phases. The aqueous phase, which contains the RNA, was transferred to a new tube and mixed with 0.5 mL of absolute ethanol per mL of Tizol used. The RNA was then purified by isopropanol precipitation and quantified using a spectophotometer. When RNA was extracted, 500ng of RNA were treated with a DNase enzyme (ThermoFisher, EN0525) to remove any contaminating genomic DNA. Reverse Transcription was performed using a mixture of reverse transcriptase enzyme (First Strand cDNA Synthesis Kit, ThemoFisher, K1612), oligo(dT) primers, and dNTPs. The reaction mixture was incubated at 42°C for 1-2 hours to allow for cDNA synthesis. After cDNA

synthesis was complete, the reverse transcriptase enzyme was inactivated by heating the reaction mixture to 70-80°C for 10 minutes.

Plasmid DNA: The plasmid DNA served as the template for amplifying particular genes or regions of interest, which had been previously cloned into the plasmid, as well as for creating mutants.

The PCR conditions to amplify the DNA were optimized to each experiment, but the general protocol was performed as follows: First, a reaction mix was prepared in a sterile microcentrifuge tube, with the final concentration of each component being: Hot Start II High-Fidelity DNA Polymerase (F537S, Thermo Scientific) at 1 unit, PCR buffer at 1X, forward and reverse primers at 0.5 µM each, template DNA at 10-100 ng, dNTPs at 200 µM each, and sterile distilled water added to a final volume of 25 µL. The reaction components were then mixed by gently pipetting up and down and placed into the Thermo Cycler (Biorad, 563BR1538) with the following program: an initial denaturation step at 98ºC for 1 minute, 40 cycles of denaturation at 95°C for 30 seconds, annealing at 60-65°C for 30 seconds (depending on the Tm of the primers) and extension at 72°C for 1 minute/kb of DNA to be amplified, a final extension step at 72°C for 5 minutes. Once the PCR was complete, the PCR product was analyzed to confirm the correct size of the amplified DNA fragment by running a 1% agarose electrophoresis gel. When the correct size was confirmed, PCR product was extracted from the gel using a scalper and purification was performed using the Wizard SV Gel and PCR Clean-Up System kit (A9281, Promega).

C. Digestion and ligation.

The purified PCR product was then cloned into a suitable vector using restriction enzymes and DNA ligase (Figure M3). Plasmid DNA and PCR DNA were digested with the appropriate enzymes to generate the desired fragments. To identify the correct buffer for double digestions we used the Thermo Fisher software “Double Digest Calculator”. The mixture was incubated at 37ºC for at least one hour. After incubation, PCR product was purified using the column-based PCR Clean-Up System kit (A9281, Promega) and the plasmid DNA was

loaded in a 1% agarose electrophoresis gel. The desired plasmid band was confirmed by its molecular weight and extracted from the gel as previously described. Then, we determined the concentration and purity of the DNA fragments using a spectrophotometer. After purification, we prepared the ligation reaction mixture in a microcentrifuge tube, which contained the purified DNA fragments, T4 DNA ligase (Thermo Scientific, EL0014) ligase buffer, and nuclease-free water. The quantity of DNA fragments was calculated according to its molecular weight using the software “NEBioCalculator” at a molar ration vector insert 1:3. The reaction mixture was incubated at room temperature for 15 minutes to allow for the ligation of the DNA fragments.

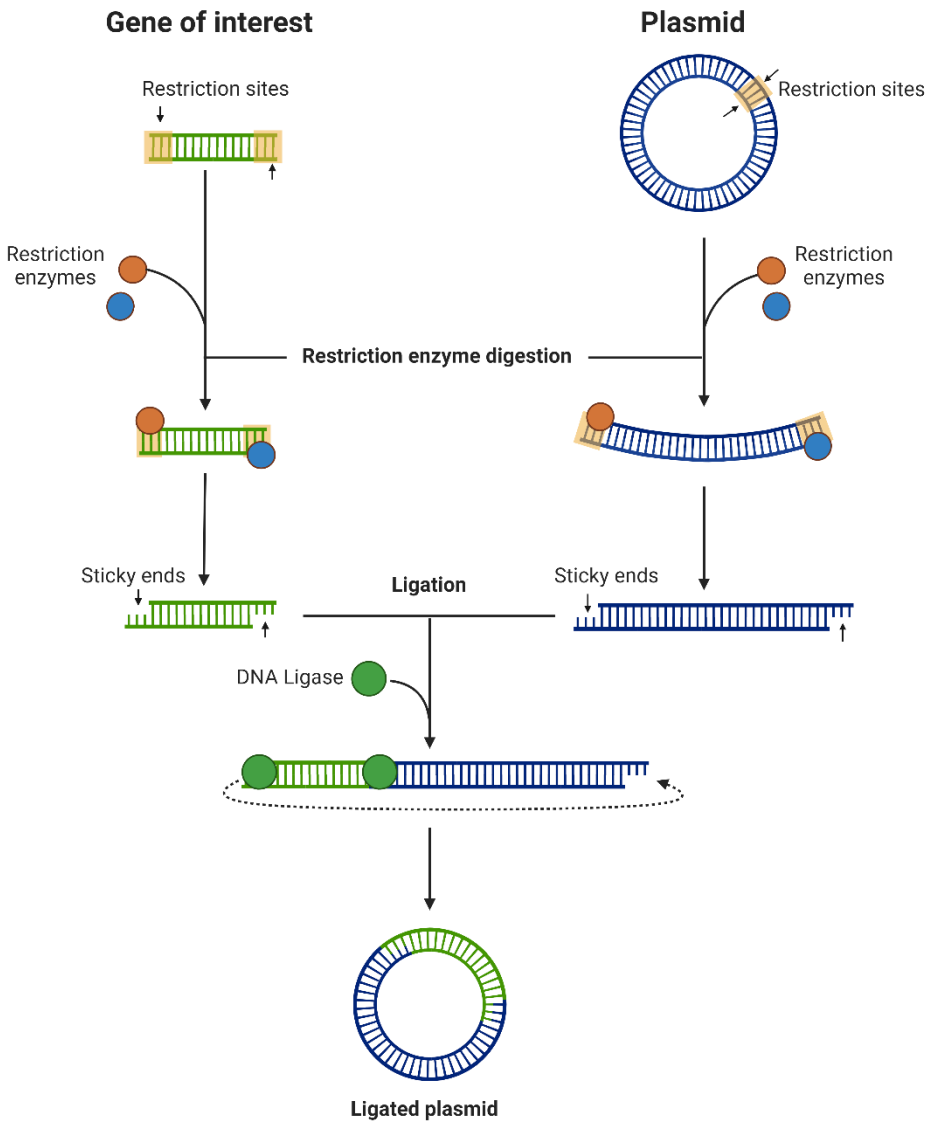

Figure M 3 Workflow of plasmid ligation process following restriction enzyme digestion, where the cut ends of the plasmid DNA are ligated together using DNA ligase, resulting in a recombined plasmid molecule.

D. Transformation.

After ligation, we transformed the ligated DNA into a competent Escherichia Coli DH10α strain by heat shock. 100 ng of plasmid DNA was added to the competent bacteria and gently mixed by pipetting up and down. The mixture was incubated on ice for 30 minutes. After incubation, sample was subjected to a heat shock by placing the tube in a 42°C water bath for 30 seconds. The tube was then immediately transferred back to ice and allowed to cool for 2 minutes. After cooling, 500 µl of LB broth was added to the tube and incubated with shaking at

37°C for 1 hour. Finally, transformed bacteria were plated on selective agar plates with the desired antibiotic resistance and incubated overnight at 37ºC colony formation. (Figure M4)

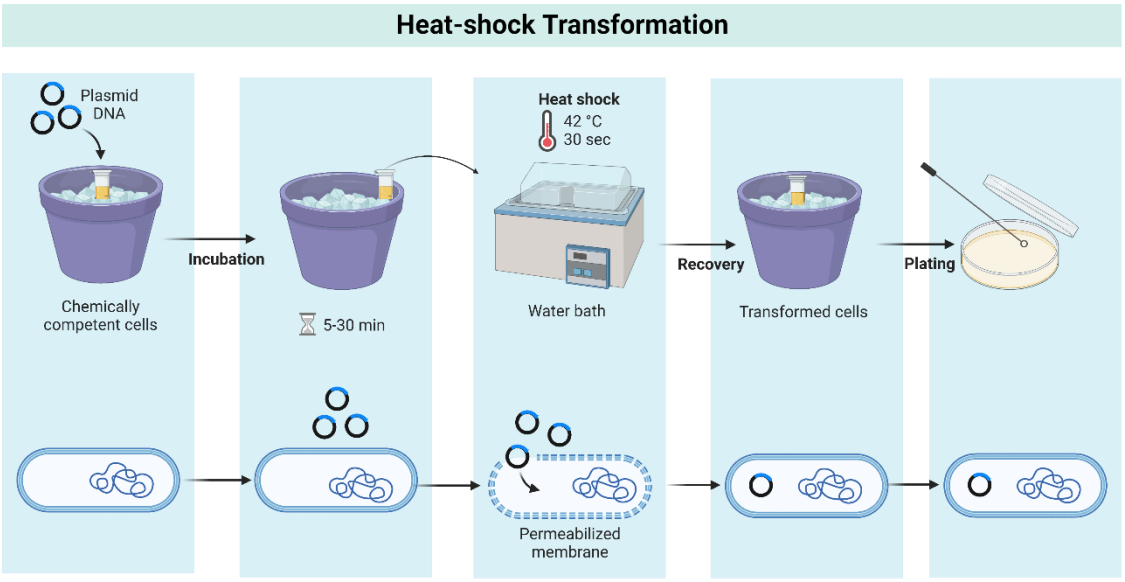

Figure M 4 Graphical protocol for bacterial transformation using heat shock method.

Generation of competent bacteria.

Competent bacteria for transformation were generated as follows: To begin, a single colony of the bacteria was inoculated into 5 ml of LB broth and incubated at 37°C overnight. The next day, 2mL of the overnight culture was added in 100 ml of fresh LB broth and incubated at 37°C until the culture reached an optical density of 0.5 - 0.6 at 600 nm (About 2 hours). Once the culture reached the desired optical density, it was centrifuged at 4°C for 5 minutes at 4,000 x g. The supernatant was removed, and the bacterial pellet was resuspended in 30ml of ice-cold GMP buffer (50 mM $CaCl_2$, 50 mM $MgCl_2$) and incubated for 15 minutes. This step was repeated twice. Then, 500 µl of DMSO were added to the bacterial suspension and incubated on ice for 5 minutes. After incubation, the bacterial suspension was aliquoted stored at -80°C until needed.

E. Clone isolation and screening.

After transforming the ligation product, the plates were incubated at 37°C for 12 hours to allow the colonies to appear. If successful, bacterial colonies were visible as small, circular, and opaque dots on the surface of the agar. We picked a several single bacterial colonies using a sterile pipette tip and transferred them to a sterile centrifuge tube containing 2 ml of LB broth with the desired antibiotic resistance each. The tube was incubated overnight at 37°C with shaking to grow a culture of bacteria. The following day, plasmid was extracted from the bacteria culture using PureLink™ HiPure miniprep Kit (Invitrogen, k210003) following manufacturer's instructions. Briefly, 1mL of bacteria were pelleted by centrifugation at 5000 x g for 10 minutes at room temperature. The pellet was resuspended in 100 µl of resuspension buffer. 100µl of lysis buffer was added to the bacterial suspension and incubated for 10 minutes at 37ºC. After incubation, 100µl of neutralization buffer from the plasmid isolation kit were added. After neutralization, the bacterial lysate was centrifugated and the supernatant was transferred into a fresh tube. 500 µl of isopropanol were added to the supernatant, the sample was incubated at room temperature for 10-15 minutes. After incubation, the mixture was centrifuged at 13,000 x g for 15 minutes at room temperature. The resultant pellet was washed with 70% ethanol. Finally, pellet was air-dried for 10 minutes and resuspended in 50µl of sterile water. (Figure M5)

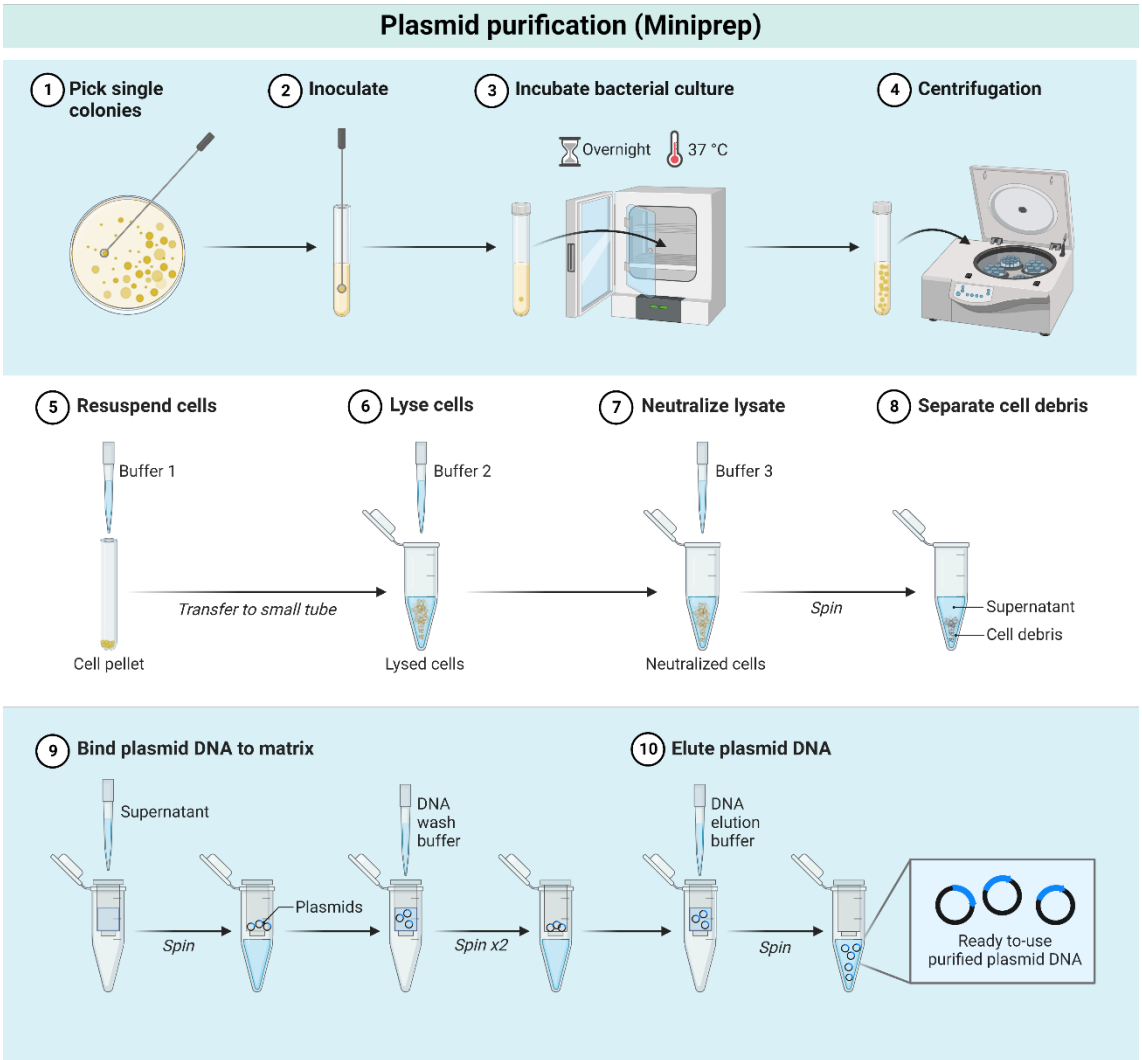

Figure M 5 Workflow for plasmid purification from a bacterial culture.

After the plasmid isolation, the screening to identify the corrected ligated plasmids was performed using restriction enzymes. When corrected plasmid was identified, 1 mL of the bacteria culture was transferred to Erlenmeyer containing 200 ml of LB broth with the desired antibiotic resistance each. The culture was incubated overnight at 37ºC with shaking to expand the bacteria culture.

F. Amplification and purification.

Finally, the generated plasmid was extracted and purified from the bacteria culture using the Midiprep HiPure PureLink Kit (ThermoFisher, K210005) following manufacturer's instructions. Briefly, the culture was centrifugated at 4000 x g for 30 minutes at 4ºC. The pellet was resuspended in 10 mL of

resuspension buffer. Next, 10mL of lysis buffer were added to the bacterial suspension and incubated for 10 minutes at 37ºC. After incubation, 10mL of neutralization buffer were added. After neutralization, the bacterial lysate was filtered to eliminate cellular debris and 3.5 mL of isopropanol were added to the resultant sample. The mixture was centrifugated and the resultant pellet was washed with 70% ethanol. Finally, pellet was air-dried for 10 minutes and resuspended in 100µl of sterile water. Purified plasmid was sequenced by Sanger Sequencing (External facility) to confirm the correct ligation.

4.2.2 Plasmids encoding donor DNA for the in vivo tagging of the KCNA3 gene in Jurkat Cells.

The pAAV-HomologyArms-TAG plasmid used as DNA Donor to generate the *KCNA3*-tagged Jurkat cell line was obtained through the following steps.
Firstly, a 1516 bp fragment containing the *KCNA3* gene was amplified using primers F1 and R1 and cloned into the AAV-MCS (from AAV Helper-Free System kit, 240071) vector with the enzymes MluI and SalI to create the Left Homology Arm Secondly, a blasticidin cassette containing the promoter, the blasticidin resistance gene and a polyadenylation signal was amplified from a pBluescript II based plasmid previously generated in our lab with the primers F2 and R2 inserted after the Arm A using the enzymes SalI and EcoRI. Thirdly, a 500bp fragment containing the downstream sequence of KCNA3 was amplified from genomic Jurkat DNA and cloned into the vector using F3 and R3 to create the Right Homology Arm. Next, a triple FLAG sequence was introduced right before the KCNA3 stop codon by a directed mutation with primers F4 and R4. Lastly, a NheI restriction site was introduced before the triple FLAG sequence using a directed mutation with primers F5 and R5. The tag sequences of double Myc (F6/R6) and NeonGreen (F7/R7) protein were cloned using this NheI restriction site.

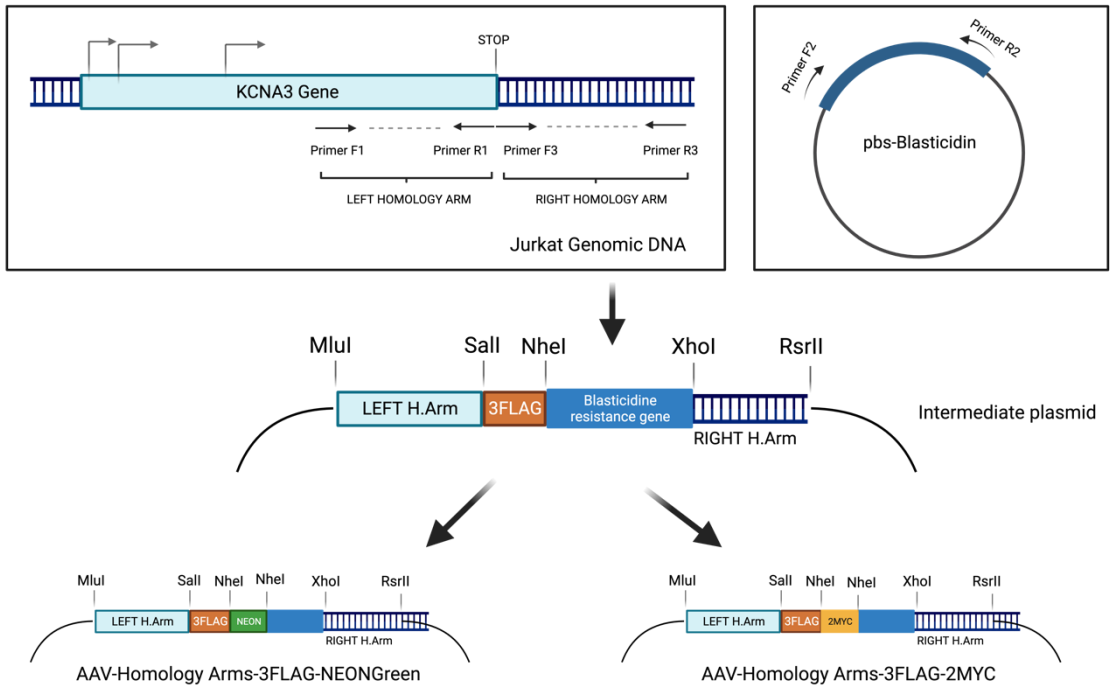

Figure M 6 Schematic representation of AAV-homologyArms plasmid generation. Primer sequences are indicated in Table 1.

4.2.3 Plasmids encoding KCNA3 gene for HEK heterologous expression.

EGFP/mCherry: Plasmids encoding Short Form or Long Form of KCNA3 gene EGFP/mCherry tagged at the N-termini was generated by PCR from Jurkat genomic DNA using primers F8/R8 (Long Form) and F9/R9 (Short Form) and cloned into EcoR1/Age1 digested EGFP-N1 vector (6085-1,Clontech) or mCherry vector (20956, Clontech)

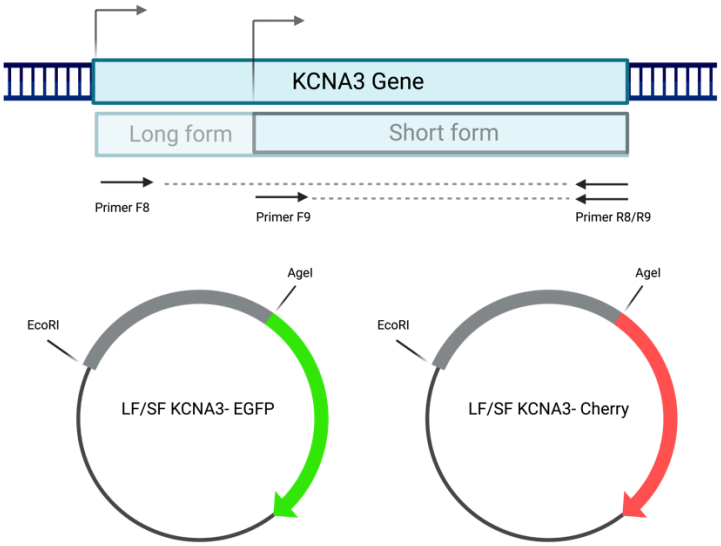

Figure M 7 Schematic representation of LF or SF KCNA3 EGFP/mCherry plasmids.

pCDNA3: Plasmid encoding KCNA3 gene Flag-tagged at the C-terminus was generated by PCR from Jurkat-3Flag Tagged genomic DNA using primers F10 and R10 and cloned into mammalian expression vector pcDNA3 (V79020, Invitrogen) digested with EcoR1/XhoI. Point mutations of ATG>CGG were introduced on the methionines of interest by a directed mutation with the primers F11/R11 for M0, F12/R12 for M1, F13/R13 for M2' and F14/R14 for M2.

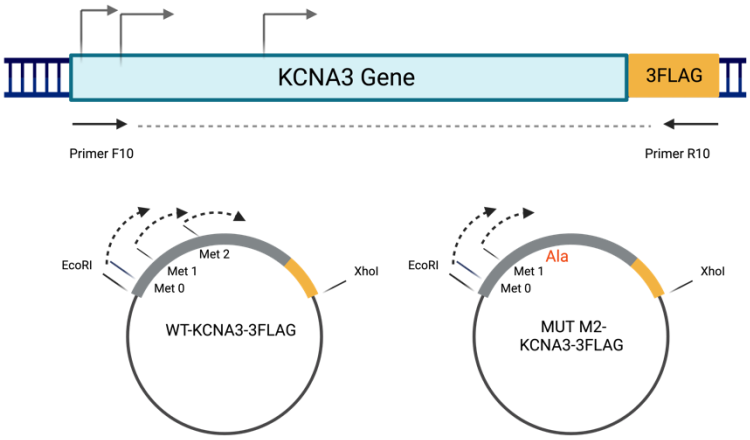

Figure M 8 Schematic representation of Mutants of KCNA3-3xFLAG plasmids.

4.3 Jurkat T cell Knock-In generation.

In this thesis, we have generated a Jurkat cell Knock-In that endogenously expresses the Kv1.3 protein tagged with a 3xFLAG-2MYC peptide or a NeonGreen fluorescence protein.

To this end, we performed a targeted gene edition at the *KCNA3* loci. To generate a KCNA3 knock-in in Jurkat cells, we used the CRISPR/Cas9 tool. In summary, we used a ribonucleoprotein (RNP) composed of Cas9 and an RNA guide that we transfected into the target cell along with an adeno-associated virus of serotype 6 (AAV6). The RNP's function is to locate and cleave the double-stranded DNA, facilitating the homologous recombination mechanism that allows for modification of the locus using an AAV virus as the donor, which carries homology fragments of the target gene and incorporates the desired mutation. DNA donor contained two homology arms from the KCNA3 gene flanking the exogenous TAG sequence (3FLAG-2MYC or 3FLAG-NeonGreen) and a blasticidin resistance gene. Edited cells were isolated by blasticidin selection. (Figure M9)

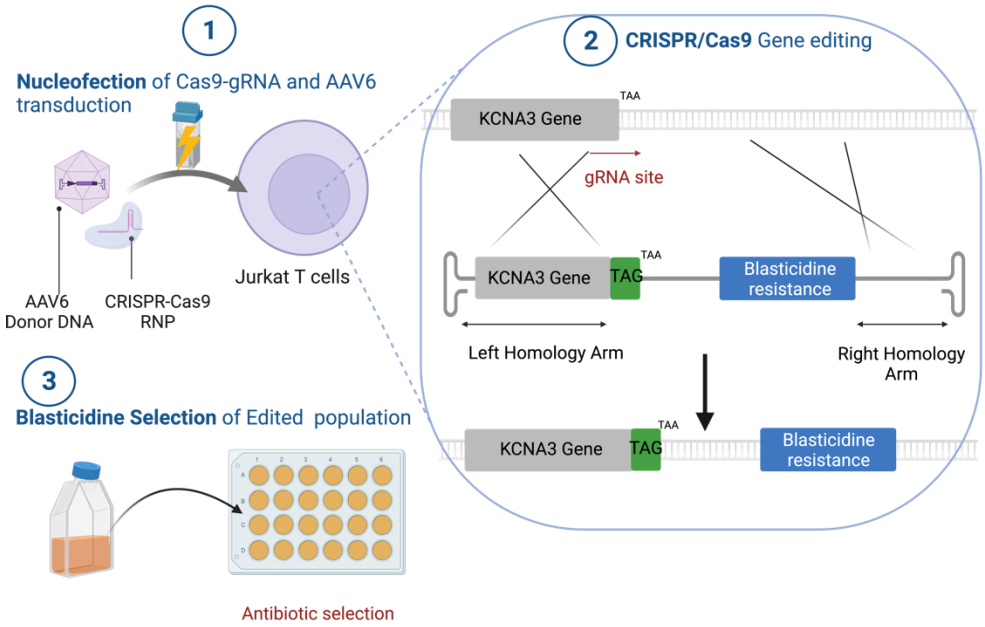

Figure M 9 Strategy for the generation of Jurkat Kv1.3-TAG Knock-In.

Vector donor for gene edition. Adeno Associated Virus (AAV) production.

AAV (Adeno-associated virus) is commonly used as a transduction vector for delivering an exogenous gene to a cell. AAV is an attractive vector because it can efficiently transduce a wide range of cell types (dividing and non-dividing), has low immunogenicity, and can persist long-term in cells without causing disease. AAV particles are used for transduction following several steps that are shown in Figure M10:

1. Design of the Donor DNA: Donor DNA is designed to provide a functional copy of a defective gene or to introduce a new gene that can treat or prevent a disease. The selected DNA Donor is cloned into the AAV vector, and the vector is purified to remove any contaminants.
2. Production of the AAV particles: AAV particles are produced by using helper plasmids to provide the genes required for AAV replication and packaging. AAV-DNA Donor plasmid and Helper plasmids are co-transfected into HEK cells to produce AAV particles. Three to four days after HEK transfection AAV particles are extracted and purified from the cells.
3. Transduction and gene expression: The purified AAV particles can be introduced into the target cells by direct transduction. The AAV vector enters the target cells and delivers the DNA Donor to the nucleus. In the nucleus, the Crispr-Cas9 machinery breaks the DNA at the site of interest and the DNA Donor is recombined to introduce the desired mutation at the specific locus.

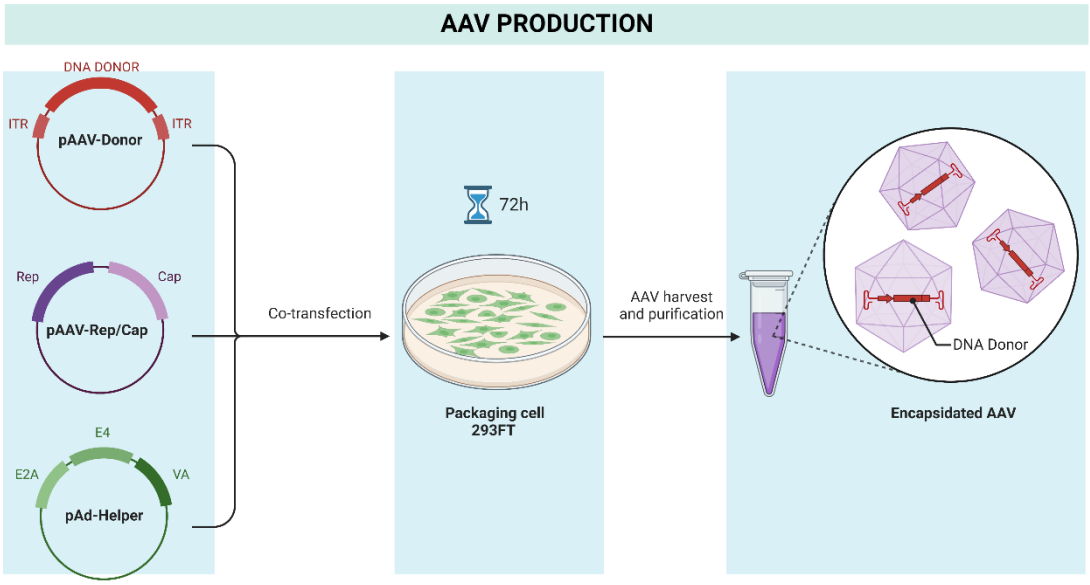

Figure M 10 Workflow illustrating the production of viral particles through triple transfection of HEK cells, where plasmids encoding viral structural proteins, viral genome, and packaging vectors are introduced into the cells, leading to the assembly and release of viral particles.

There are several serotypes of AAV (Adeno-associated virus) that have been identified and characterized, each with its own unique characteristics. AAV6 (Adeno-associated virus serotype 6) is the preferred AAV vector to transduce Jurkat cells because it has been shown the maximal efficiency to transduce this type of cells.

To produce our AAV6-HomologyArms-TAG particles, 8×10^6 293FT cells were seeded on 75cm flasks and transfected using the pDGM6 plasmid and the previously generated pAAV-HomologyArms-TAG plasmid at a molar ratio of 2:1. pDGM6 was a gift from David Russell (Addgene plasmid # 110660) and it contained the AAV6 cap genes, AAV2 rep genes, and adenovirus helper genes. Cells were transfected using Polyethylenimine 2mg/mL (Sigma Aldrich, 408727) at ratio 3:1 PEI: DNA. After 24 h of transfection, medium was replaced for fresh culture medium. Cells were harvested after 72h post transfection. The pellet was resuspended in 0.5mL of fresh medium before undergoing 5 freeze-thaw cycles of 10 minutes each, followed by centrifugation to harvest the cell debris. After

centrifugation, supernatant containing AAV6 particles was recovered and stored at –20°C or –80°C for long-term preservation.

AAV titration was performed to determine the number of viral particles in our sample. Titration is an important step in AAV vector production and is used to ensure the quality. Quantitative PCR (qPCR) is a highly sensitive method that can be used to detect and quantify the presence of AAV genomes in a vector preparation. This method is based on the amplification of a specific sequence of the AAV genome using PCR and the detection of the amplified product using fluorescent probes. The number of AAV genomes in the sample is determined by comparison to a standard curve generated using known amounts of a plasmid containing the same AAV sequence.

Titration was performed by qPCR using Power SYBR® Green Master Mix (ThermoFisher Scientific) and primers targeting the ITRs regions (117): FW-ITR primer: 5´-GGAACCCCTAGTGATGGAGTT-3´ and REV-ITR primer: 5´-CGGCCTCAGTGAGCGA-3´ (117). The qPCR reaction was carried out in a Light Cycle 480 (Roche) thermocycler with the following protocol: 15 min at 95 ºC followed of 40 cycles of 95 ºC 15s - 60 ºC 20s - 72 ºC 20s. A standard curve was generated by serially dilution of the pAAV-MCS vector (1:102, 1:103, 1:104, 1:105) to estimate the titer of the virus sample.

gRNA designing and RNP production.

gRNA directed to the 3 end of the KCNA3 gene was designing using the CRISPOR software and it is detailed in Table 1 (primers F11/R11). CRISPOR is an online tool used for designing and evaluating guide RNAs (gRNAs) for the CRISPR/Cas9 gene editing system. To this end, CRISPOR uses an algorithm to design potential gRNAs that target the input sequence by considering several factors, including the location of the target site, the presence of potential off-target sites, and the efficiency of the gRNA. The most appropriate gRNA sequence for our experiment was selected and gRNA was synthesized using GeneArt Precision gRNA Synthesis Kit (A29377, Invitrogen, EEUU) according to manufacturer instructions. Briefly, target oligonucleotide was used as a template for PCR amplification using the provided primers and PCR reagents. PCR was

performed following the protocol 5 min at 98 ºC followed of 32 cycles of 98 ºC 10s - 55 ºC 15s - 72 ºC 60s. After PCR amplification, in vitro transcription reaction was performed from PCR assembly as a template for gRNA using 25 mM NTP mix, 1X TranscriptAid™ Reaction Buffer and TranscriptAid Enzyme. Sample was incubated at 37°C for 4 hours. DNase I was added into the reaction mix after the transcription reaction. Finally, gRNA was purified using a column-based DNA purification included in the kit and resultant gRNA was stored at -80ºC until further use.

Knock-In generation and selection.

CRISPR-Cas9 tool was used to generate a Double Strand Break (DSB) at the 3' end of the *KCNA3* gene before the STOP codon. To this end, Jurkat cells were nucleofected using Neon Electroporation System (MPK10096, ThermoFisher, EEUU) according to manufacturer instructions. Briefly, 10^6 Jurkat cells were mixed with 5 µg of Cas9 (TrueCut Cas9 Protein v2, ThermoFisher) and 1µg of previously generated gRNA and resuspended in 100µL of Buffer R (Thermo Fisher). One pulse of 1700V/20 ms was applied to deliver CRISPR components into the cells. Following electroporation, Jurkat cells were seeded in a 24 well plate and transduced with 10^6 AAV6-HomologyArms-TAG particles. Next day, media was replaced with fresh media containing 10ng/mL of blasticidin to isolate edited cells. Following selection with blasticidin (3-4 days), a limiting dilution was performed. A limiting dilution is a technique used to establish individual clones by serially diluting the cells until individual cells are present in some of the dilutions (Figure M11). To this end, we prepared a range of dilutions of our Jurkat cell suspension between 1:3 to 1:162. Dilutions were plated in 96-well plate with fresh media containing 10ng/mL of blasticidin. Plates were incubated for several weeks until we observed the presence of cell growth. Individual clones were identified from plates where growth was observed in less than one-third of the wells. The isolated clones underwent PCR and sequencing analyses to verify the in-frame insertion of the signal tag in the KCNA3 gene.

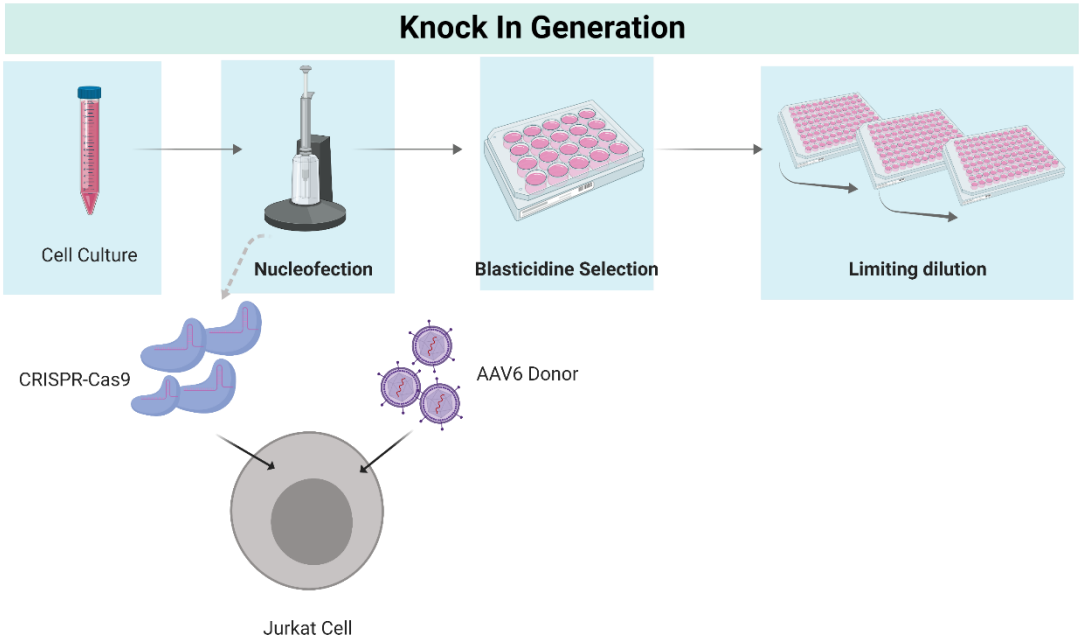

Figure M 11 Strategy for Knock In generation in Jurkat T cells.

4.4 Jurkat T cell Knock-Out generation.

After the identification of the Kv1.3 isoforms we decided to generate two Jurkat Knock-Out models, first a Jurkat cell line that lacked the expression of the Long forms of Kv1.3 (only expressing the Short Form) and a second cell line that did not express any of the Kv1.3 forms (total KO) (Figure M12).

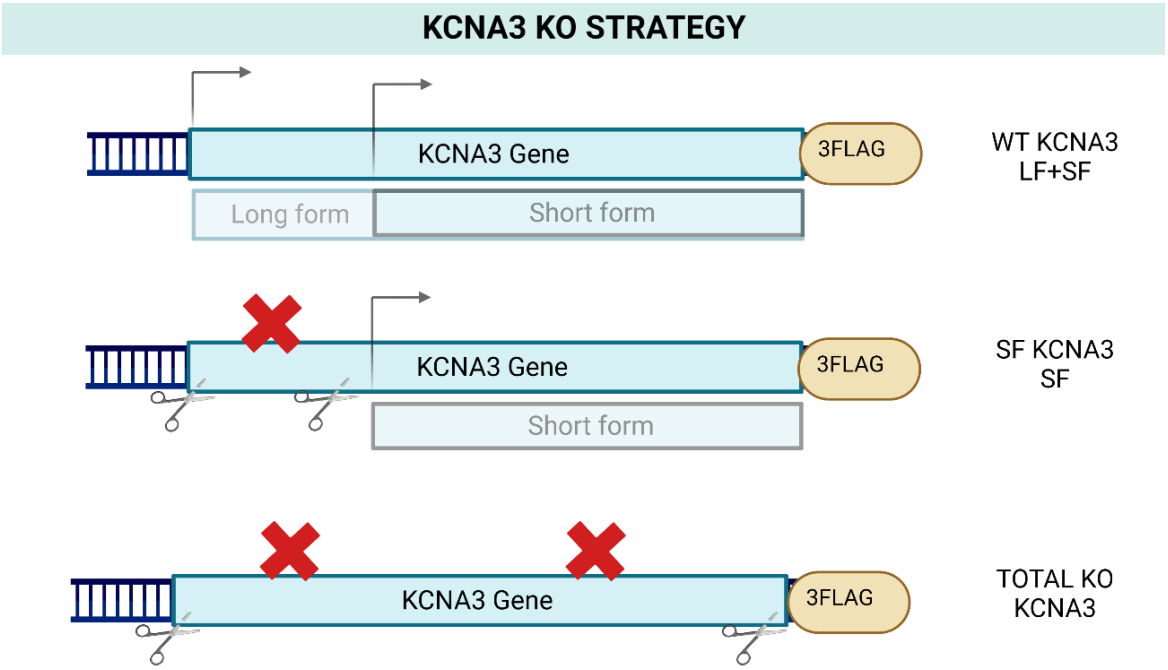

Figure M 12 Strategy performed to generate a Jurkat KO and a Jurkat cell expressing only the Short Form of Kv1.3. The strategy was performed on the Jurkat 3flag2myc tagged cells.

CRISPR-Cas9 tool was used to generate the Jurkat KO cells. gRNA were designed using the CRISPOR software and are detailed in Table 1. To generate a total KO two gRNA located at the beginning and at the end of the KCNA3 were selected to eliminate the complete exon. The clone expressing only the short form was generated by choosing two gRNAs located both at the 5P end of the KCNA3 gene. gRNA was generated using GeneArt Precision Synthesis Kit (A29377, Invitrogen) as previously described.

Jurkat cells were Nucleofected using Neon System (ThermoFisher). Briefly, 10^6 Jurkat-3F2M cells were mixed with 5 µg of Cas9 (ThermoFisher) and 500ng of each gRNA and resuspended in 100µL of Buffer R (Thermo Fisher). One pulse of 1700V/20 ms was applied to deliver CRISPR components into the cells. Following electroporation, cells were seeded in fresh media. Next day, a limiting dilution was performed to establish individual clones as previously described. Isolated clones were analyzed by Western Blot to confirm the correct elimination of the KCNA3 gene.

4.5 Protein determinations.

Protein expression studies were performed by Western Blot, Immunoprecipitation and immunofluorescence assays.

4.5.1 Western Blot

Western blotting was used to detect proteins previously separated by SDS PAGE gel electrophoresis and transferred to a polyvinylidene difluoride (PVDF) membrane.
This technique was applied in different assays.

Kv1.3 detection in Jurkat cells.

To extract total protein from Jurkat T cells, 2×10^6 cells were washed with cold PBS and incubated on ice for 20 min in 50 µL lysis buffer (20 mM Tris pH 7.4, 150 mM NaCl, 1mM EDTA, 0.1%SDS, 1% sodium deoxycolate, 1% Nonidet P-40,) supplemented with a protease inhibitor cocktail (11873580001, Sigma-Aldrich, USA). SDS Sample Buffer (200 mM Tris pH 6.8, 8%SDS, 40% Glycerol, 4% Bromophenol Blue, 100 mM DTT) was added and samples were heated at 95 °C for 5 min and kept at −20 °C before immunoblotting assays. When activating or pro-apoptotic stimuli was required, the compound was added to the culture prior to lysis step at the concentration and time indicated in Table 2. Protein lysates were quantified using Bradford Protein Assay (23236, Thermo Fisher). 50µg of protein lysates were loaded into SDS-PAGE 10% homemade gel, after gel resolution proteins were transferred into a PVDF membrane and blocked with 5% milk plus 5% BSA in TTBS for one hour. Membrane was incubated overnight at 4ºC with 1:2000 α-FLAG M2 primary antibody (Sigma Aldrich, A8592). Next day, membrane was washed with TTBS and incubated with 1:3000 anti-mouse HRP secondary antibody for 1 hour at Room Temperature. Finally, membrane was washed with TTBS 1X and protein detected using chemiluminescent detection kit (32106, Thermo Fischer). The relative amount of protein was quantified by densitometric analysis of the bands obtained using Image J software.

Treatment	Concentration	Time
Phorbol-12-myristate-13-acetate (PMA)	100ng/ml	16h
Ionomycin	1µM	16h
Phytohemagglutinin (PHA)	2 µg/ml	16h
Thapsigarguin	0.2µM	Experiment dependent
Dexamethasone,	1µM	4h
2-Deoxyglucose	10 mM	4h
Staurosporin	1µM	4h

Table 2 Treatments used to Jurkat stimulation, all of them are from Sigma.

Phospho-ERK detection in Jurkat cells.

Detecting ERK phosphorylation in Jurkat cells after TCR stimulation was carried out through a time-dependent assay. 25 × 10^6 cells were washed with cold PBS and resuspended in 500 µL of complete media supplemented with 0,5% FBS. 2 µL of αCD3 and αCD28 (4 µg/mL) antibodies were added into the cells and incubated on ice for 15 min. After incubation, cells were centrifuged at 4000g for 5 min and resuspended in 250µL of Complete Media supplemented with 0,5% FBS. The sample was then separated in 5 different Eppendorf (50 µL each) and 100 µL of media containing 2 µL of goat αmouse (4 µg/mL) antibody was added to the samples. Samples were incubated at 37ºC to start stimulation according to their stimulation time (0, 1, 3, 5 or 15 minutes). After stimulation, cells were washed with cold PBS and resuspended in 50 µL of lysis buffer (20 mM Tris pH 7.4, 150 mM NaCl, 1mM EDTA, 0.1% SDS, 1% sodium deoxycholate, 1% Nonidet P-40,) supplemented with a protease inhibitor cocktail. SDS Sample Buffer (200 mM Tris pH 6.8, 8%SDS, 40% Glycerol, 4% Bromophenol Blue, 100

mM DTT) was added and samples were heated at 95 °C for 5 min and kept at −20 °C before immunoblotting assays (Figure M13).

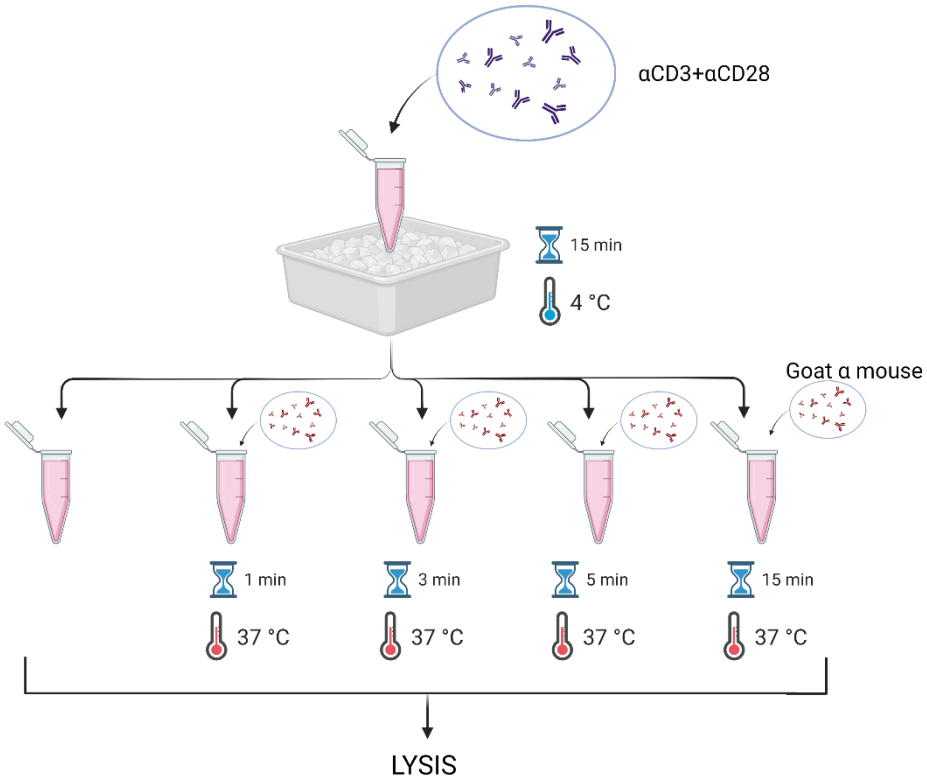

Figure M 13 Schematic protocol for P-ERK determination assay in Jurkat T cells.

Protein lysates were quantified using Bradford Protein Assay (23236, Thermo Fisher). 20µg of protein lysates were loaded into SDS-PAGE 10% homemade gel, after gel resolution proteins were transferred into a PVDF membrane and blocked with 5% BSA TTBS for one hour. Membrane was incubated overnight at 4ºC with 1:3000 α-p-ERK primary antibody (9101, Cell Signaling). Next day, membrane was washed with TTBS and incubated with 1:3000 anti-rabbit HRP secondary antibody for 1 hour at Room Temperature. Finally, membrane was washed with TTBS 1X and protein was detected using chemiluminescent detection kit (32106, Thermo Fischer) following manufacturer instructions. The relative amount of protein was quantified by densitometric analysis of the bands obtained using Image J software and normalized against Total ERK protein (118). To quantify total ERK protein, the membrane was stripped to remove the previous antibodies. Membrane was incubated twice in 0.2 M NaOH for 10 min. After incubation, membrane wash washed with water and blocked in 5% BSA TTBS for 1hour. Membrane was incubated overnight at 4ºC with 1:3000 α-total -

ERK primary antibody (9102, Cell Signaling). Next day, membrane was incubated with secondary antibody and protein detected following same protocol described for p-ERK protein.

Phospho-proteins detection in Jurkat cells.

The degree of phosphorylation of proteins after TCR stimulation was studied in our clones. To this end, a flat bottom 96 well plate was coated with 10µ /mL of mouse anti-human CD3 and 10□g/mL of mouse anti-human CD28 overnight. Next day, $3x10^5$ Jurkat T cells per well were seeded on the coated 96 well plate and incubated at 37°C for 10 min to activate the cells. The activation was stopped by directly at the plate adding 10x lysis buffer and incubating the plate for 15 minutes on ice. Lysates were centrifugated at 21500g for 10 minutes at 4°C, SDS Sample Buffer was added, and samples were heated at 95 °C for 5 min and kept at −20 °C before immunoblotting assays. 20µg of protein lysates were loaded into SDS-PAGE 10% homemade gel, after gel resolution proteins were transferred into a PVDF membrane and blocked with 5% BSA TTBS for one hour. After blocking, membrane was divided in several pieces according to different protein sizes expected. Membrane was incubated overnight at 4ºC with primary antibodies resumed in Table 3. Next day, membrane was washed with TTBS and incubated with specific HRP secondary antibody (Table 3) for 1 hour at Room Temperature. Finally, membrane was washed with TTBS 1X and protein was detected using chemiluminescent detection kit (32106, Thermo Fischer, USA) following manufacturer instructions. The relative amount of protein was quantified by densitometric analysis of the bands obtained using Image J software and normalized against GP96 protein. When needed, the membrane was stripped to remove the previous antibodies. Membrane was incubated twice in 0.2 M NaOH for 10 min. After incubation, membrane was washed with water and blocked in 5% BSA TTBS for 1hour and incubated with specific antibodies following previous indications.

Antibody	**Working concentration**	**Supplier**
Mouse anti-FLAG-M2 (F1804)	1:2000 (WB)	Sigma
Mouse anti-MYC (9B11)	1:2000 (WB)	Cell Signaling

Rabbit anti-ERK (137f5)	1:1000 (WB)	Cell Signaling
Rabbit anti-pERK (20611)	1:1000 (WB)	Cell Signaling
Rabbit anti-pLAT (07278)	1:1000 (WB)	Merck
Rabbit anti-pSLP76 (92711s)	1:1000 (WB)	Cell Signaling
Rabbit anti-pZAP70 (2701)	1:1000 (WB)	Cell Signaling
Mouse-anti-pCD3 (558402)	1:1000 (WB)	BD Biosciences
Rat anti-GP96 (ADI-SPA-850-F)	1:1000 (WB)	Enzo Life sciences
Rabbit anti-pPLCγ1 (2821)	1:1000 (WB)	Cell Signaling
Mouse anti-CD3 (OKT3)	10µg/mL	BioLegend
Mouse anti-CD28 (CD28.2)	10µg/mL	Biolegend
Goat IgG (H+L) F (ab') 2	5µg/mL	ThermoFisher

Table 3 Antibodies used in this thesis.

4.5.2 Immunoprecipitation of Kv1.3-FLAG in Jurkat cells.

Immunoprecipitation assay was performed to purify and enrich Kv1.3-Flag protein from Jurkat-3F2M in resting conditions. In this method, total protein of Jurkat-3F2M was incubated with the α-FLAG antibody to bind the protein in solution. The antibody/antigen complex was then pulled out of the sample using protein G-coupled agarose beads. This step isolates the Kv1.3-3F2M from the rest of the sample. The sample obtained was then separated by SDS-PAGE for western blot analysis (Figure M14).

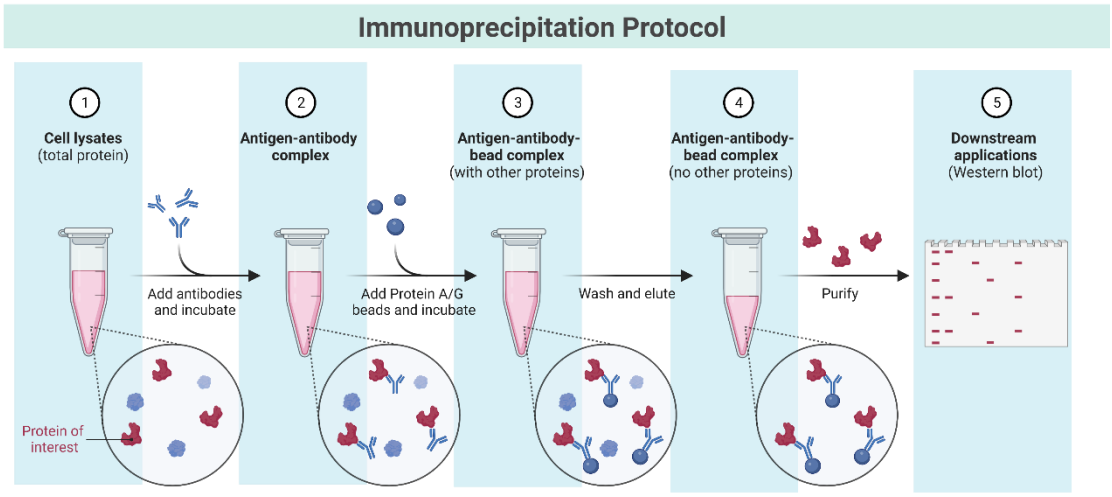

Figure M 14 Graphical resume of our immunoprecipitation protocol.

20 × 10^6 Jurkat cells were washed with cold PBS and resuspended in 500 µL of lysis buffer (20 mM Tris pH 7.4, 150 mM NaCl, 1mM EDTA, 0.1%SDS, 1% sodium

deoxycolate, 1% Nonidet P-40,) supplemented with a protease inhibitor cocktail (11873580001, Sigma-Aldrich, USA) for 15 min at 4ºC. Then, samples were centrifugated at 21500g for 5 minutes and supernatant was recovered. 1mL of protein G-coupled agarose beads were washed twice in lysis buffer. Lysates were precleared to reduce non-specific binding, to this end, 100 µL of Bead slurry was added to the lysates and incubated for 30 minutes at 4ºC with gentle agitation. After incubation, sample was centrifugated at 4000g for 5 minutes and the supernatant was recovered. This step was repeated twice. When preclearance was completed, supernatant was divided in three different Eppendorf to perform three different conditions. Negative control (without αFLAG antibody), experimental sample (with αFLAG antibody) and experimental sample treated with N-Glycosylase (With αFLAG antibody and treated with N-glycosylase). 300 µL of lysis buffer was added to the three tubes, 1 µg of α-FLAG antibody was added to the tubes 2 and 3. Samples were incubated for 1h at 4º with gentle agitation. After 1 hour, 40 µL bead slurry was added to each tube and incubated for 4h at 4º with agitation. After incubation, Samples were centrifuged and supernatant discarded. The beads were washed with lysis buffer three times to remove non-specific binding. Finally, lysis buffer was removed from tubes 1 and 2 and proteins were eluted from beads by adding 40 µL of SDS Sample Buffer, samples were heated at 95 °C for 5 min and kept at −20 °C before immunoblotting assays.

Tube 3 was treated with 2,5 units of N-Glycosidase enzyme (11365169001, Roche) and incubated overnight at 37ºC. Next day, 20 µL of SDS Sample Buffer was added and sample was heated at 95 °C for 5 min and kept at −20 °C (Figure M15).

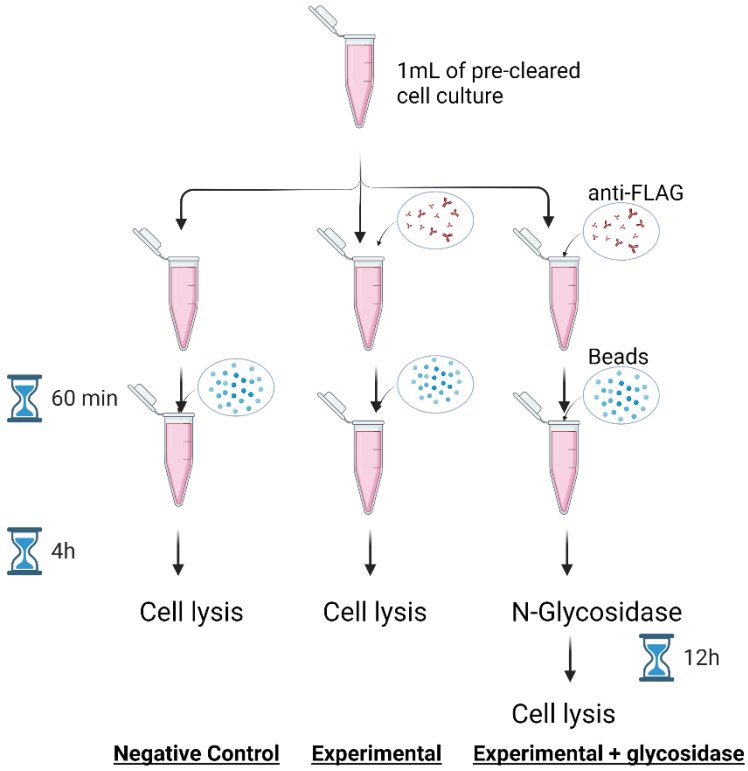

Figure M 15 Overview of the process of immunoprecipitation.

20µL of protein lysates were loaded into SDS-PAGE 10% homemade gel, after gel resolution proteins were transferred into a PVDF membrane and blocked with 5% milk plus 5% BSA TTBS for one hour. Membrane was incubated overnight at 4ºC with 1:2000 α-FLAG M2 primary antibody (Sigma Aldrich, A8592). Next day, membrane was washed with TTBS and incubated with 1:3000 anti-mouse HRP secondary antibody for 1 hour at Room Temperature. Finally, membrane was washed with TTBS 1X and protein was detected using chemiluminescent detection kit (Thermo Fischer, 32106) following manufacturer instructions.

4.5.3 Immunocytochemistry

Immunocytochemistry was used for Kv1.3-3F2M protein detection in our Jurkat clones. Jurkat T cells were seeded into poly-l-lysine coated coverslips placed in 12 mm wells. Next day, cells were fixed with 4% paraformaldehyde and blocked in PBS with 2% of BSA using a permeabilizing blocking solution. Cells were incubated with the sigma anti-Flag M2 primary antibody (1: 200) overnight at 4ºC. Next day, coverslips were washed with PBS and incubated for 1 h with 1:1000

goat anti-mouse 532 secondary antibody (A-11002, Molecular Probes). Nuclei was labeled using Hoechst 33342 (1:2000) and coverslips were mounted with Vectashield (Vector Laboratories, H-1000-10). Photomicrographs were acquired with a LEICA SP5 confocal microscope using LAS software.

4.6 Cell transfection and fluorescence microscopy

To determine the subcellular localization of the Kv1.3 isoforms we co-transfected the previously generated plasmids containing the different forms of Kv1.3 fused to the fluorescence proteins mCherry or EGFP.

For transfection of 293HEK, cells were seeded into poly-l-lysine coated coverslips placed in 12 mm wells. Cells were transfected using 0,5 micrograms of plasmid and Turbofect Transfection Reagent (Fisher Scientific, R0531) at a ratio DNA: Turbofect of 1:2. Next day, cells were fixed with 4% paraformaldehyde, nuclei were labeled with Hoechst 33342 at 1:2000 and coverslips were mounted in Vectashield (Vector Laboratories, H-1000-10). Images were captured with the LEICA SP5 confocal microscope using LAS software.

Jurkat WT were transfected using the Neon Nucleofector. 2x 10^6 cells were resuspended in 100µL of Buffer R (Thermo Fisher) mixed with 5µg of plasmid DNA. Three pulses of 1600V/10 ms were applied to deliver the plasmid into the cells. Following electroporation, Jurkat cells were seeded into poly-l-lysine coated coverslips placed in 12 mm wells. Next day, cells were fixed with 4% paraformaldehyde, nuclei were labeled with Hoechst 33342 at 1:2000 and coverslips were mounted in Vectashield. Images were captured with the LEICA SP5 confocal microscope using LAS software.

4.7 Electrophysiological methods

Ionic currents were recorded using the patch clamp technique in cell-attached, whole-cell, or perforated-patch configurations at room temperature, as previously described in studies by Pilar Cidad et al. (2021) and Jiménez-Pérez et al. (2015). Transfected HEK or edited-Jurkat cells were plated on small poly-l-lysine-treated

glass coverslips in a recording chamber and perfused with bath solution by gravity. The patch pipettes had resistances ranging from 2 to 5 MΩ. For whole-cell studies, the bath solution composition was (mM): 141 NaCl, 4.7 KCl, 1.2 MgCl2, 1.8 CaCl2, 10 glucose, and 10 HEPES, pH 7.4 with NaOH, and the internal solution composition was (mM): 125 KCl, 4 MgCl2, 10 HEPES, 10 EGTA, 5 MgATP, pH 7.2 with KOH. For perforated-patch experiments, the pipette tip was briefly dipped in a solution containing (in mM): 40 KCl, 95 KGlutamate, 8 CaCl2, 10 HEPES, pH 7.2 with KOH and backfilled with the same solution containing amphotericin B (480 µg/ml).

Perforated-patch recordings were used for resting E_M (Resting membrane potential) measurements of Jurkat cells in the current-clamp configuration. Whole-cell current recordings were carried out in Jurkat cells. The biophysical and pharmacological characterization of the currents was performed using several different protocols, including current/voltage (I/V) curves, steady-state inactivation curves, voltage ramps, or repetitive depolarizing pulses, as previously described (119). Transfected HEK cell currents were studied using cell-attached experiments. In this case, after gigaseal obtention, cells were bathed in a solution intended to mimic intracellular media composition, containing (in mM): 150 KCl, 0.5 MgCl2.6H2O, 10 HEPES, and 1 EGTA, pH 7.2 with KOH, while the composition of the pipette solution (in mM): 120 NaCl, 30 KCl, 2 CaCl2, and 10 HEPES, pH 7.4 with NaOH was close to an extracellular medium. Current amplitude was measured with I/V curves or depolarizing pulses to +40 mV. The voltage dependence of Kv current inactivation was analyzed using a double pulse protocol consisting of a 2s prepulse from -100 to +40 mV in 20 mV increments, followed by a 100ms pulse to +40 mV. Use-dependent block was studied with trains of 25 pulses of 500ms duration at a frequency of 0.5 Hz from -100 to +40

mV.

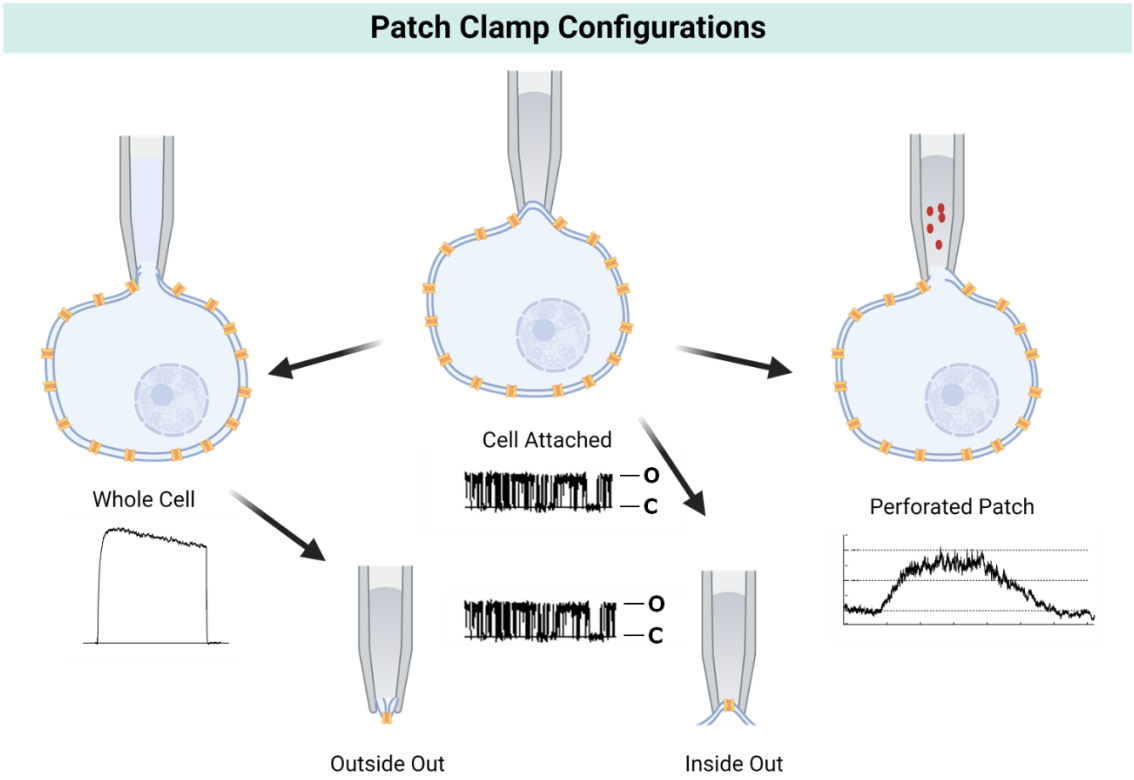

Figure M 16 Examples of Patch Clamp configurations to measure currents in isolated cells. 1. ***Whole-Cell Configuration****: involves forming a high-resistance seal between the recording pipette and the cell membrane, allowing direct access to the intracellular environment. This configuration enables precise voltage control and facilitates the measurement of total membrane currents, including both capacitive and ionic components.* ***2. Cell-Attached Configuration****, the patch pipette is attached to the cell membrane without breaking it. This configuration allows the measurement of currents at the localized membrane patch directly beneath the pipette tip. It is useful for studying single-channel properties, such as channel conductance, open-close kinetics, and pharmacological modulation, while preserving the cell's physiological environment.* ***3. Inside-Out Configuration****: The inside-out configuration involves excising a small patch of the cell membrane, resulting in the formation of an intracellular-facing membrane patch. This configuration enables the study of ion channels and receptors localized on the cytoplasmic side of the membrane. It provides precise control over the intracellular environment.* ***4 Outside-Out Configuration****, involves excising a membrane patch containing ion channels or receptors, resulting in an extracellular-facing membrane patch. This configuration allows the measurement of currents from ion channels exposed to the extracellular environment. It is valuable for studying ligand-gated channels, synaptic transmission, and drug-receptor interactions.* ***5. Perforated Patch Configuration****: combines aspects of both whole-cell and cell-attached configurations. It involves the addition of membrane-permeable pore-forming agents, such as gramicidin, to the recording pipette. These agents create small pores in the cell membrane, allowing selective ion permeation while preserving intracellular components. The perforated patch configuration offers stable voltage*

control, reduced dialysis of intracellular contents, and prolonged recording durations.

4.8 Functional Characterization

4.8.1 Cytokine Secretion

Determination of IL2 secretion in Jurkat T cells.

Jurkat T cells can produce large amounts of IL-2 after stimulation with phorbol esters or monoclonal antibodies against the T3 antigen. We decided to determine if there were differences in the secretion of IL2 in our clones. To this end, we quantified the concentration of IL2 secreted by our KO clones using an enzyme-linked immunosorbent assay (ELISA) (900-M12, Peprotech, USA) following manufacturer's instructions. Briefly, a standard curve was prepared from the solutions using PBS containing 0.1% BSA. 100 µL of the standard solutions and the samples were added into the wells of the ELISA plate in duplicate. Plate was incubated for 2 hours at room temperature. After incubation, plate was washed with wash buffer and, shaking gently 100 µL of biotinylated anti-IL2 antibody (provided in the kit) was added to each well. The plate was incubated for 1 hour at RT. Then, plate was washed and 100 µL of streptavidin-HRP (provided in the kit) was added to each well. Plate was incubated for 30 minutes at RT. Finally, after washing, 100 µL of substrate solution (provided in the kit) was added to each well. After 15 minutes, 50 µL of stop solution (provided in the kit) was added to each well to stop the reaction. The absorbance was read at 450nm. Analysis was performed by plotting the absorbance values for the standards against their corresponding IL2 concentrations on a graph, and determining the equation of the line of best fit using Microsoft Excel. The equation of the line was used to calculate the concentration of IL2 in the samples, using their absorbance values.

Jurkat T cells be stimulated with phorbol esters or monoclonal antibodies against the T3 antigen. We tested three different stimulations in our clones:

A. Monoclonal antibodies against the T3 antigen: αCD3 +αCD28

5µg/ml of mouse anti-human αCD3 (17281456, Invitrogen, USA) was fixed on a 96 well plate overnight. Next day, 3×10^5 Jurkat cells were plated and stimulated with 1 µg/ml of mouse anti human αCD28(12322193, Invitrogen, USA) and 1

µg/ml of IgG (H+L) F(ab′)2-Goat anti-Mouse (15470934, Invtrogen USA) for 16 hours. After stimulation, supernatants containing IL2 were recovered and stored at -80ºC until further use. In experiments analyzing the effect of PAP-1 or Margatoxin, cells were pre-treated 1 h before stimulation.

B. Phorbol esters:

Jurkat T-cells were seeded in 96 well plates (3×10^5 cells/well) in triplicates and stimulated for 16 hours with phorbol 12-myristate 13-acetate (PMA; 100 ng/ml) plus phytohemagglutinin (PHA; 1 µg/ml) in the absence or presence of Kv1.3 inhibitors PAP-1 and Margatoxin. After stimulation, supernatants containing IL2 were recovered and stored at -80ºC until further use.

C. Raji B cell-based conjugates.

In experiments using Raji B cell-based stimulation, Raji B cells were loaded with different concentrations of Staphylococcal enterotoxin E (ET404, Toxin Technology Inc., USA) for 30 min at 37°C and were washed in serum-free RPMI-1640 media to remove excess toxin. Next, 2×10^5 Jurkat cells were mixed with 10^5 SEE-loaded Raji B cells per well in a 96-well U-bottom plate. The plate was incubated at 37°C for 16 h. Following stimulation, supernatants containing IL2 were recovered and stored at -80ºC until further use. In experiments analyzing the effect of PAP-1 or Margatoxin, cells were pre-treated 1 h before stimulation. All experiments were performed in technical duplicate and biological triplicate.

D. Determination of IL2 and TNFα secretion in T cells.

IL2 and TNFα was also determined on CD4+ human T cells. CD4+ human T cells were stimulated with 1:1 CD3/CD28 coated Dynabeads (Thermo Fisher Scientific) for 16 hours at 37°C. Then, supernatants were recovered, and cytokines concentration was quantified by enzyme-linked immunosorbent assay (ELISA) (Peprotech, USA) according to manufacturer's instructions. In experiments analyzing the effect of the Kv1.3 inhibitors PAP-1 (100nM) and Margatoxin (10 nM), cells were pre-treated with the blockers 1 h before stimulation. All experiments were performed in technical duplicates and biological triplicates.

4.8.2 Apoptosis.

Jurkat KO clones presented a depolarized resting membrane in comparison with WT Jurkat. We decided to test if this difference could result in differences in apoptosis induction. To test that, Caspase-3/7 Detection Reagents (C10423, ThermoFisher) were used following manufacturer's instructions.

The mechanism of action of this protocol is based on the fact that the Caspase-3/7 Green Detection Reagent is initially non-fluorescent due to the presence of the DEVD peptide, which blocks the dye's ability to bind to DNA. Nevertheless, once caspase 3/7 activation occurs in apoptotic cells, the DEVD peptide is cleaved, allowing the dye to bind to DNA and generate a vivid, fluorogenic signal. The protocol was performed as follows, a 96 well plate was treated with poly-l-lysine for 10 minutes to facilitate the bound of the cells to the bottom of the plate. Jurkat cells were labeled with 2µM of Caspase-3/7 Green Detection Reagent and Hoescht 33342. After labeling, cells were cultured at 30.000 cells/well in PBS supplemented with 5%FBS. 1µM of staurosporin was used as apoptosis-inducing, 1% DMSO was added to the negative controls as a vehicle. The plate was incubated at 37ºC for 6 and 24h to allow caspase 3/7 to cleave the luminogenic substrate. After incubation, the samples were visualized with a plate reader cytation 5 (Agilent) that contains a fluorescence microscope equipped with a DS-Ri1 digital camera. From each well, at least 9 images were obtained using GFP and blue filters. The images were obtained using a 20X objective, and the same illumination conditions, diaphragm and condenser adjustments, exposure time, background correction, and color levels were applied to all images. The images were then analyzed using FIJI software, and

relative caspase activity was calculated by subtracting the background signal obtained from cells treated with vehicle from the signal obtained from cells treated with the apoptosis-inducing agent. The relative caspase activity was then normalized to the number of cells in each well by counting the total number of cells using Hoescht channel. The resulting data was presented as the percentage of apoptotic cells, which was calculated by dividing the number of caspase-positive cells by the total number of nuclei and multiplying the result by 100.

4.8.3 Intracellular calcium determination

For intracellular calcium measurements, Jurkat cells were seeded on poly-l-lysine treated glass coverslips. After 24 hours, cells were loaded with 2 µM of the fluorescent Ca^{2+} indicator Fluo-4-AM (Molecular Probes, Invitrogen, Oregon, USA) for 1 hour at room temperature. The cells were then transferred to an inverted microscope stage, treated with 200 nM Thapsigargin, and placed in a 0 mM Cl_2Ca tyrode's solution to remove intracellular Ca^{2+}. Following this, changes in intracellular Ca^{2+} levels in response to 2mM Cl2Ca tyrode's solutions were examined. At the end of the experiment, cells were exposed to 10 µM of the protonophore CCCP plus 5 µM of Ca^{2+} ionophore ionomycin to establish fmax. Intracellular calcium images were obtained using an inverted microscope, Eclipse TE (Nikon), with a Nikon CFI S Fluor (40X, NA=1.30) oil immersion objective and a Sensi Cam (PCO AG, Germany) camera. Imaging Workbench 4.0 software was used to acquire images, and background-subtracted fluorescence signals were expressed as f/(fmax-f).

4.8.4 Proliferation studies

The percentage of cells at the S phase was quantified using EdU (5-ethynyl-2´-deoxyuridine) incorporation. Briefly, HEK cells were transfected with WT-Kv1.3-EGFP plasmid, LongForm-EGFP plasmid, Short-Form-EGFP plasmid or EGFP-N1 plasmid acting as a negative control using Turbofect Transfection Reagent (R0531, Fisher Scientific) at a ratio DNA:Turbofect of 1:2. Next day, transfected cells were seeded into poly-l-lysine coated coverslips placed in 12 mm wells in technical triplicates. Next day, media was replaced with media containing 10 µM EdU for 30 minutes and proliferation was measured following Click-iT® EdU Imaging Cell Proliferation Assay instructions. Briefly, cells were washed with PBS and fixed with 4% paraformaldehyde. After washing with PBS, cells were permeabilized with 0.1% Triton X-100 in PBS. Then, Click-iT Plus reaction cocktail prepared according to manufacturer's instructions was added to each coverslip and incubated for 30 minutes at RT. After incubation, Hoescht 33342 was added to stain cell nuclei and then coverslips were washed to remove excess of dye. Finally, coverslips were mounted with Vectashield, and samples were

visualized with an Eclipse 90i fluorescence microscope (Nikon) equipped with a DS-Ri1 digital camera. The images were obtained using a 20X objective, and the same illumination conditions, diaphragm and condenser adjustments, exposure time, background correction, and color levels were applied to all images. The images were then analyzed using FIJI software, and the resulting data was presented as the percentage of proliferating cells, which was calculated by dividing the number of EdU-positive cells by the total number of nuclei and multiplying the result by 100.

4.8.5 Immunological synapses studies

Enterotoxin SEE (Staphylococcal Enterotoxin E) is a type of toxin produced by the bacterium Staphylococcus aureus. SEE is consider a superantigen, which means that it can activate large numbers of T cells in the immune system, leading to a massive inflammatory response, it causes non-specific activation of T cells, resulting in polyclonal T cell activation and massive release of cytokines. In an in vitro setting, SEE can be loaded onto Raji B cells, which act as antigen-presenting cells. The loaded Raji B cells can then be presented to Jurkat cells to create a Jurkat-Raji conjugate. This conjugate emulates the native activation of T cells through the T cell receptor (TCR) and major histocompatibility complex (MHC) creating an immunological synapse in the contact space between both cells (Figure M17).

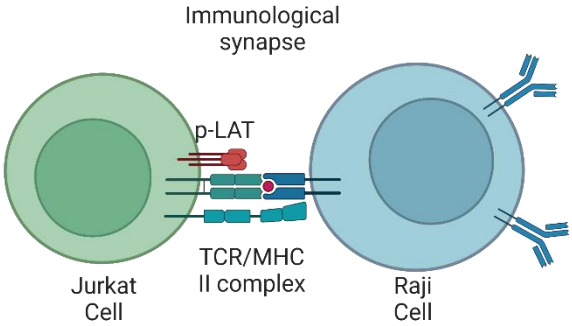

Figure M 17 The TCR from Jurkat T cell interacts with the SEE loaded MHC-II receptor from the Raji Cell to iniciate the immune response. The contact point between both will create a immunological synapses.

To create the conjugate Jurkat-Raji, Raji B cells were seeded at a concentration of 1x10^6 cells/mL and labeled with CellTracker Blue CMAC dye (10 µM, Thermo Fisher) in RPMI without FCS for 20 minutes at 37°C. The Raji cells were then treated with 100 ng/mL of SEE for 30 minutes at 37°C. The SEE-loaded Raji cells and Jurkat cells were cocultured on coverslips at a 1:1 ratio for 30 minutes at 37°C. The cells were subsequently washed with PBS and fixed with 4% paraformaldehyde, quenched with 10 mM glycine for 10 minutes, and permeabilized with staining buffer (PBS + 0.2% BSA + 0.05% saponin) for 30 minutes. The cells were then incubated with primary antibodies, human anti-GFP (Recombinant Antibody Platform, Institut Curie) and rabbit anti-pLAT (Cell Signaling) for 1 hour. After washing with staining buffer, the cells were incubated for 30 minutes with secondary antibodies, anti-Human Alexa-488, anti-rabbit Alexa-568 (Invitrogen, ThermoFisher), and phalloidin-647 (Invitrogen, Thermo Fisher) at a 1:500 dilution. The coverslips were mounted with Fluoromount G (SouthernBiotech, USA). Images were obtained using an inverted laser scanning confocal microscope (Leica DMi8, SP8 scanning head unit), equipped with HC PL APO CS2 63x/1.40 OIL objective. ImageJ software and compatible scripts were generated for automated or semi-automated analysis (Figure M18).

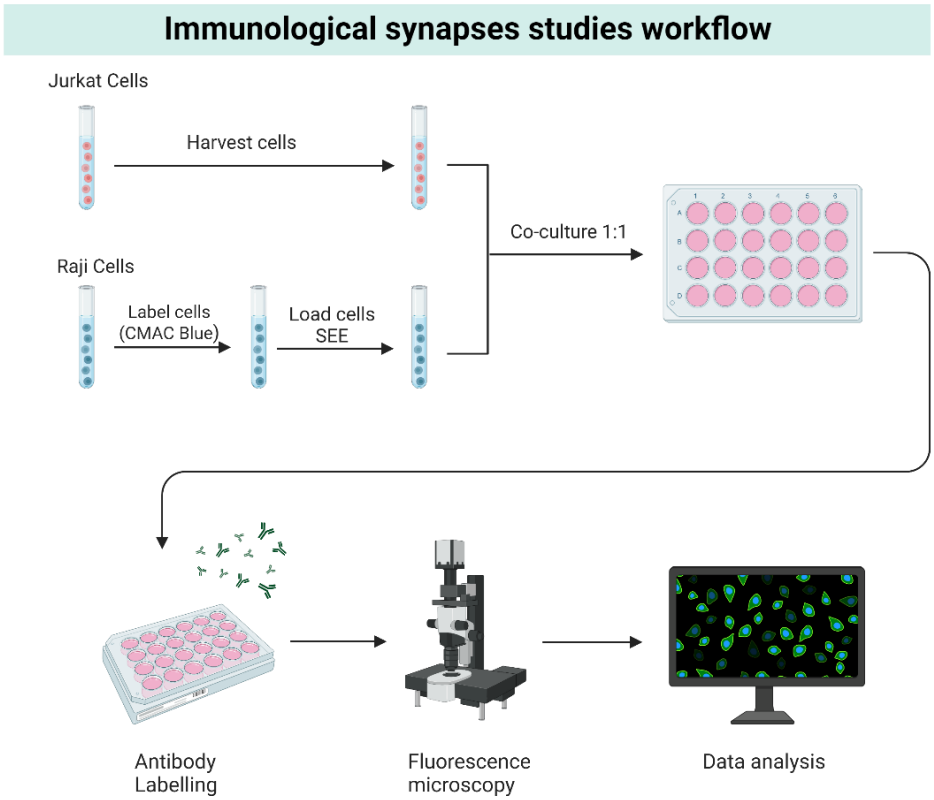

Figure M 18 Workflow used to measure the immunological synapse dynamics in our Jurkat clones.

Results

5. Results.

5.1 Generation of a genetically modified cell line for the study of the endogenous Kv1.3 channel.

The accurate detection of Kv1.3 protein under endogenous conditions has been hindered by the lack of reliable antibodies. To overcome this limitation, we decided to generate a Jurkat cell line in which the endogenous Kv1.3 channel was tagged with a signal peptide. This cell line allowed us to determine the expression, location, and changes of expression in the native Kv1.3 channels upon activation. We genetically modified two Jurkat cell lines to express the endogenous Kv1.3 channel fused with a tag protein. One of the cell lines was edited with a 3FLAG-2MYC (3F2M) peptide, while the other was modified with the fluorescent protein Neon Green (Figure R1).

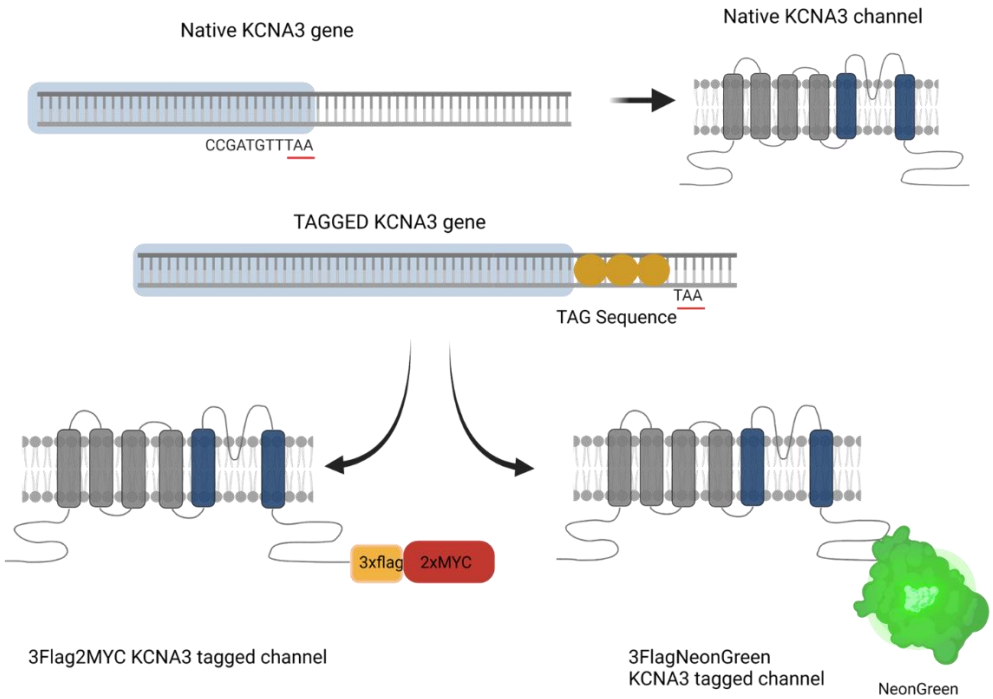

Figure R 1 Strategy performed to create a Jurkat cell line with the endogenous Kv1.3 protein tagged with a 3FLA-2MYC peptide or the NeonGreen protein.

To generate the modified cell lines, we performed a homologous recombination strategy at the *KCNA3* loci. Our strategy combined two key elements: firstly, the CRISPR-Cas9 system was used to target the *KCNA*3 gene and induce a Double

Strand Break (DBS), and secondly, AAV6 viral particles were used to deliver the DNA donor. The DNA donor contained two homology arms derived from the *KCNA*3 gene, flanking the exogenous TAG sequence (either 3FLAG-2MYC or 3FLAG-NeonGreen), as well as a blasticidin resistance gene. Subsequently, we isolated the edited cells through blasticidin selection (Figure R2).

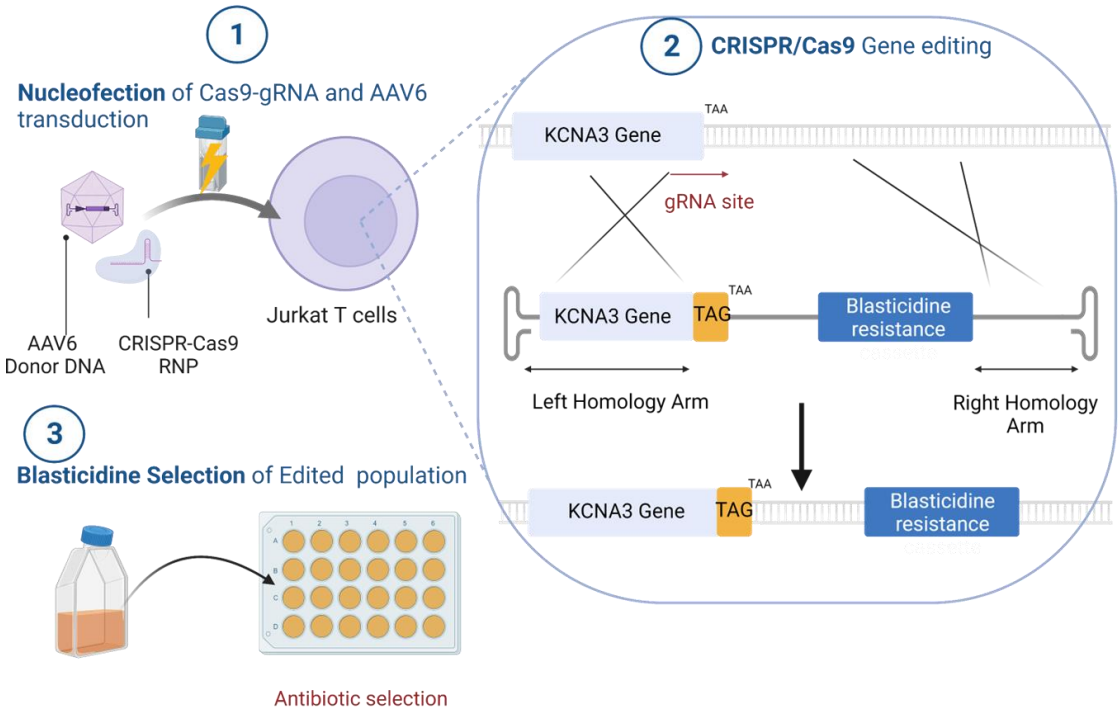

Figure R 2 Workflow of our strategy performed to create a Jurkat cell line with the endogenous Kv1.3 protein tagged with a 3FLA-2MYC peptide or the NeonGreen protein. Jurkat cells were nucleofected to deliver the RNP into the cells and transduced with AAV6s to introduce the DNA donor. After edition, edited cells were isolated by blasticidin selection.

To generate the AAV6 particles containing DNA donor, a homology recombination vector (pAAV-HomologyArms-TAG plasmid) was first constructed. The plasmid was obtained through the following steps (Figure R3):

1 - Left Homology Arm: a 1516 bp fragment containing the *KCNA3* gene was amplified from Jurkat genomic DNA using primers F1 and R1 and cloned into the AAV-MCS vector with the enzymes MluI and SalI.

2 - Blasticidin Resistance gene: a blasticidin cassette containing the promoter, the blasticidin resistance gene and a polyadenylation signal was amplified from a pBluescript II based plasmid previously generated in our lab with the primers F2 and R2 inserted after the Arm A using the enzymes SalI and EcoRI.

3 - Right Homology Arm: a 500bp fragment containing the downstream sequence of *KCNA3* was amplified from genomic Jurkat DNA with primers F3 and R3 and cloned into the vector using SalI/XhoI and RsrII.

4 - 3FLAG peptide insertion: A triple FLAG sequence was introduced right before the *KCNA3* stop codon by a directed mutation with primers F4 and R4.

5 - NheI site generation: a NheI restriction site was introduced before the triple FLAG sequence using a directed mutation with primers F5 and R5.

6 - Tag sequences insertion: The tag sequences of double Myc (F6/R6) and NeonGreen (F7/R7) protein were cloned using this NheI restriction site.

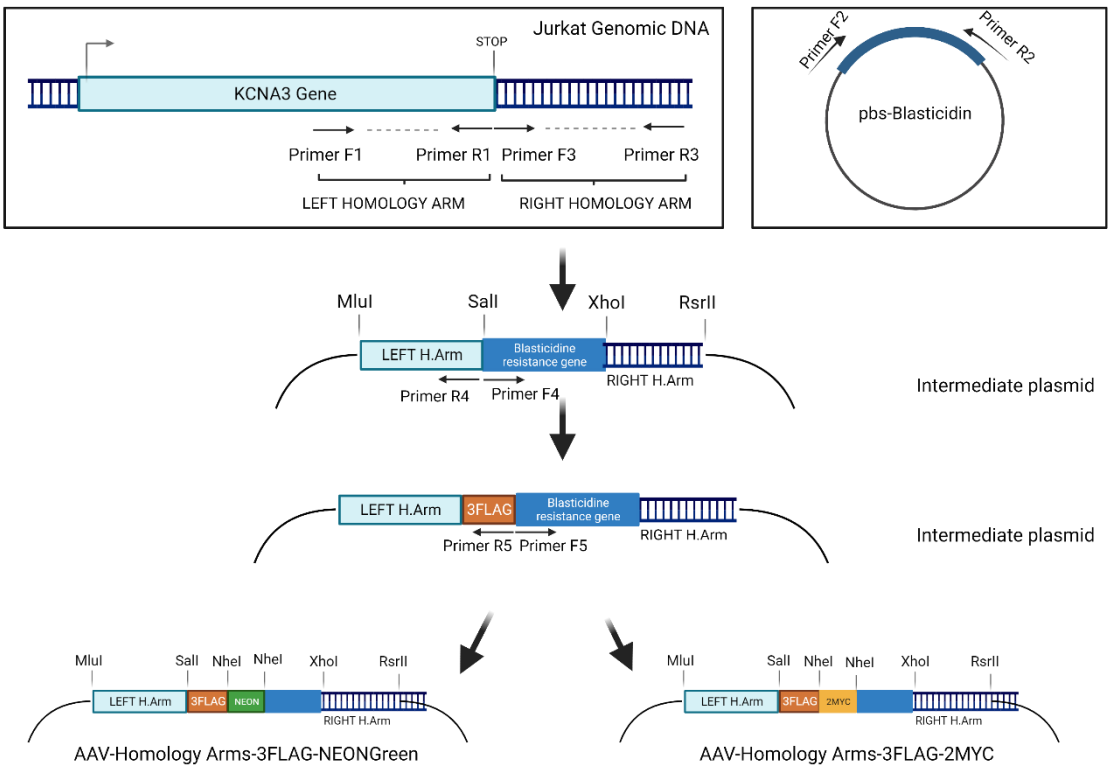

Figure R 3 Workflow of the generation of AAV-homology Arms-Tag plasmids. Primer sequences are indicated in Table 1.

The five DNA fragments were purified from agarose gel electrophoresis and digested with the appropriate enzyme. These fragments were then sequentially ligated into the pAAV-MCS vector. To confirm the correct generation of the plasmid, the complete vector was sequenced by Sanger Sequencing (Not

To produce AAV6-HomologyArms-TAG particles, 293FT cells were transfected using the pDGM6 plasmid and the pAAV-HomologyArms-TAG plasmid. After 72h of transfection cells were harvested and lysed with 5 freeze-thaw cycles.

Supernatant containing AAV6 particles was recovered, and a quantification of the viral titer was performed by qPCR. Viral titer determination is a key step for a successful gene editing experiment. Titration was performed by qPCR using primers targeting ITRs regions (Fx-Rx). A standard curve was generated diluting standards of the AAV-MCS vector (1:100, 1:1000, 1:10000, 1:100000) to estimate the titer of our AAV6 sample. AAV-MCS vector contains 4 ITRs, while the AAV6 only contains 2, because the plasmid is made up of a dsDNA and the AAV is made up of a ssDNA, so the corresponding correction must be made in the final calculation. The titers of the viruses were between 10^9 - 10^{10} viral particles/mL, which was considered within the optimal range.

To evaluate transduction efficiency of Jurkat T cells, AAV6 particles containing EGFP molecules were generated and transduced into Jurkat T cells. Different concentration of AAV6 particles were delivered into the cells alone or in combination with nucleofection. (Figure R4). Higher concentrations of AAV6-EGFP resulted in higher EGFP expression on the cells, reaching more than 90% expression of EGFP in 1/2 and 1/4 dilutions with and without nucleofection. The combination of nucleofection and transduction improved the transduction efficiency, but compromised the viability as we can observe less viable cells in the plots. A 1/8 dilution of the supernatant containing AAV6 (titer around 10^9 viral particles/mL) was sufficient to achieve almost 80% transduction efficiency.

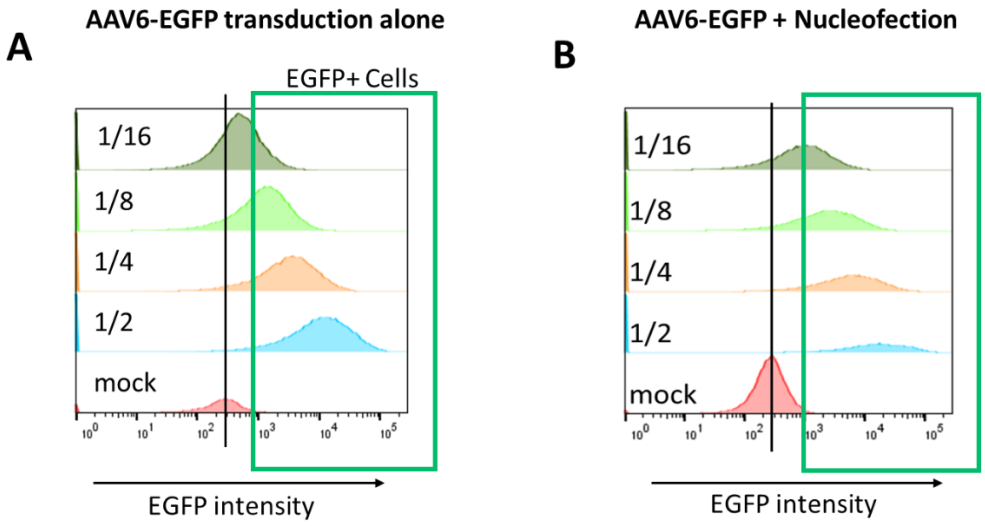

Figure R 4 Jurkat cells were transduced with different concentrations of AAV6-EGFP viral particles alone (Left panel) or in combination with Nucleofection (right panel). Representative flow cytometry plots measuring the EGFP intensity in the cells 24hous after transduction.

CRISPR-Cas9 tool was used to generate a Double Strand Break (DSB) at the 3' end of the *KCNA3* gene before the STOP codon. To this end, Cas9 and gRNA was delivered into Jurkat by nucleofection using Neon Electroporation System. Following electroporation, Jurkat cells were transduced with 10^6 AAV6-HomologyArms-TAG particles. Subsequently, edited cells were isolated by blasticidin selection (10ng/mL) for 3 days. Following selection with blasticidin, a limiting dilution was performed to establish individual clones (Figure R2). Isolated clones were analyzed by PCR to confirm the insertion of the signal tag in the *KCNA3* gene. The PCR analysis was carried out utilizing SEN primers that bind to the 5' end of the KCNA3 gene, along with ATS primers specifically designed for the 3FLAG sequence, which is exclusively present in the edited clones (Figure R5).

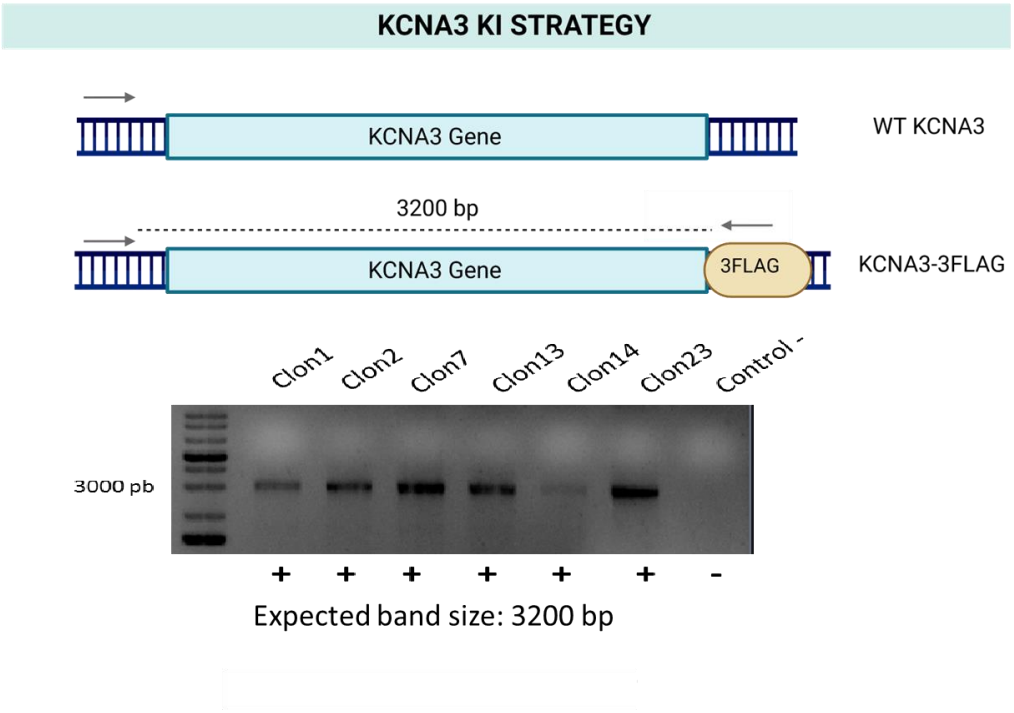

Figure R 5 Correct insertion of tag peptide at the KCNA3 gene was validated through PCR using specific primers for the KCNA3 gene.

When PCR confirmed insertion of the TAG peptide at the KCNA3 locus, the clones were Sanger Sequenced to confirm the in-frame TAG insertion at the specific position (Figure R6).

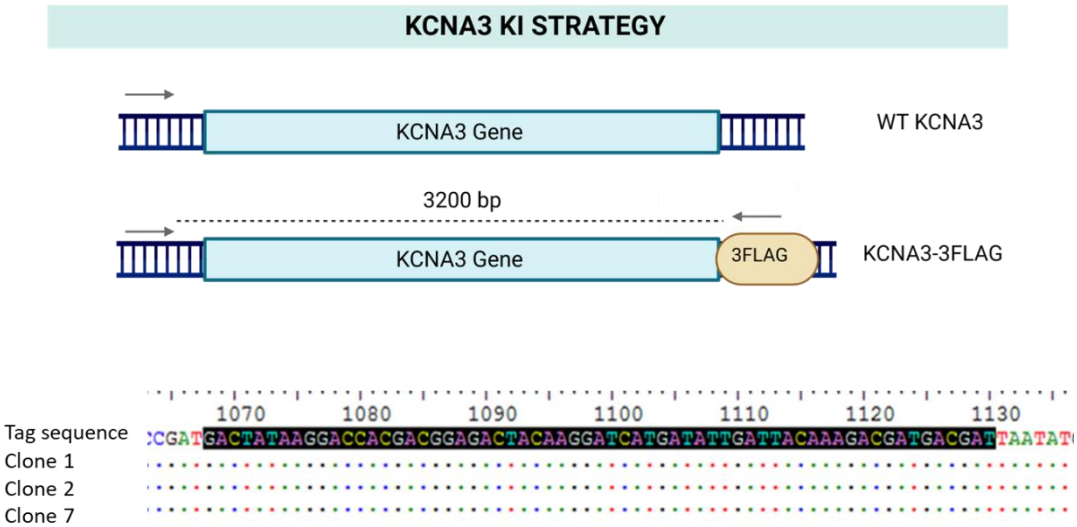

Figure R 6 Correct in- frame insertion of tag peptide at the KCNA3 gene was confirmed through Sanger Sequencing.

After sequencing, the clones were lysed to detect the presence of Kv1.3-tagged protein within the cells. Despite the Jurkat T cells having low levels of Kv1.3 expression, the cell lines produced enabled the detection of Kv1.3 protein through Western Blotting (in the Jurkat 3FLAG-2MYC cell line) using the antiFLAG antibody and flow cytometry (in the Jurkat 3FLAG-NeonGreen cell line) (Figure R7).

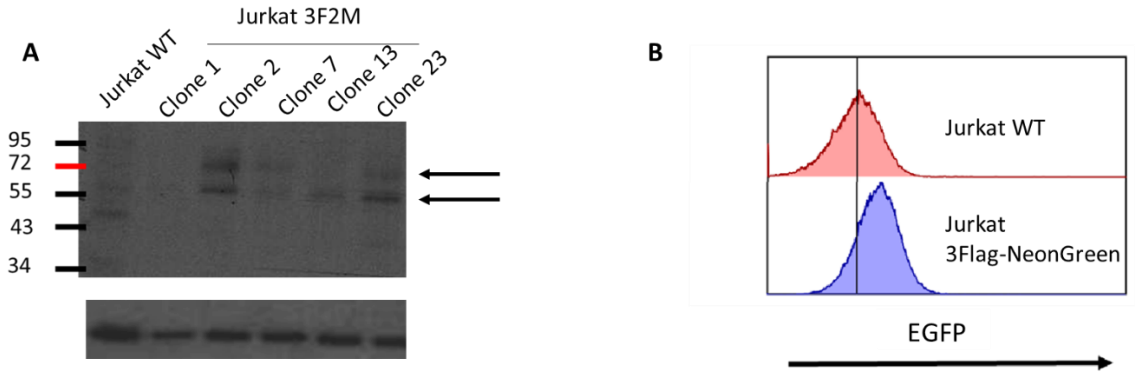

Figure R 7 ***(A)*** *Representative WesternBlotting membrane of total lisates from resting Jurkat WT (Left lane) and 3FLA2MYC edited clones. Membrane was incubated with antiFLAG M2 antibody.* ***(B)*** *Representative Flow cytometry plot of living Jurkat WT (Red) and Jurkat-3F-NeonGreen (Blue) cultures. The displacement of the blue curve with respect to the red one indicates a positive signal for NeonGreen protein expression.*

Although detection of the Kv1.3 channel in our cell lines was possible under native conditions, protein expression was very low. To increase the protein yield, we decided to perform an immunoprecipitation using total lysate from our Jurkat cells. This assay allowed us to detect more clearly the Kv1.3 protein in resting Jurkat cells. Surprisingly, we identified two protein bands other than the expected canonical channel whose protein size was calculated around 63-66KDa, a longer band with a molecular weight of around 70-80KDa and a shorter band of 43KDa.These three bands were observed when compared the WT Jurkat clone (No tag) with the Jurkat-3FLAG clone. N-Glycosidase enzyme was included in the samples as a control to determine if the new bands could correspond to a canonical band modified by strong glycosylation. Although all three bands were found to be slightly N-glycosylated, none of them disappeared after N-deglycosylation, indicating the presence of independent proteins (Figure R8).

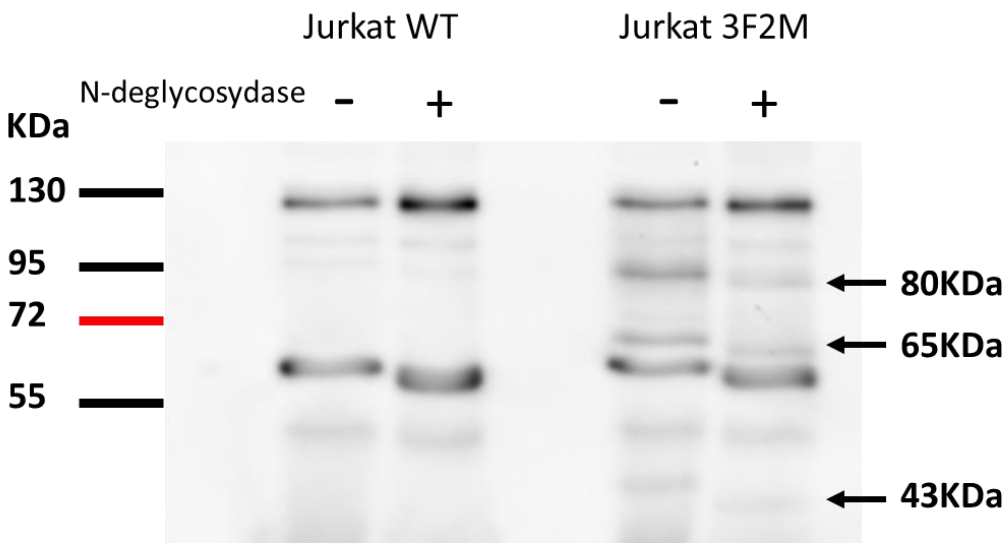

Figure R 8 Representative Western Blotting membrane of Immunoprecipitated Kv1.3-3FLAG2MYC from total lisates from resting Jurkat WT ***(Left Lane)*** *and 3FLA2MYC edited clones. Membrane was incubated with antiFLAG M2 antibody. Left lane of each sample was untreated while right lane was treated with N-Glycosidase enzyme to detect glycosylation in our samples. Stroger bands at 60KDa and 130KDa correspond to heavy and light chains of the antibodies used for immunoprecipitation that are recognized by the detection antibody.*

5.2 Endogenous Kv1.3 channels show different isoforms.

Western blot results from our Jurkat-3FLAG-2MYC cell line clearly showed that, in addition to the canonical 66KDa channel protein, two other undescribed proteins appeared on the gel. We wondered if these two bands corresponded to proteolytic cleaved products of the canonical band or if they could correspond to alternative isoforms translated from the Kv1.3 gene, which is composed of only one exon. Translation of different proteins from the same exon is common in prokaryotic organisms, but not in eukaryotic cells. Typically, eukaryotic mRNAs contain a single translation start site and encode a single functional protein product, but many studies have recently shown that eukaryotic ribosomes can also recognize multiple alternative translation start sites. The number of experimentally validated examples of alternative translation is rapidly increasing (120), and includes membrane ion channels such as the calcium channel Orail (121). We therefore hypothesized that our exon translates different isoforms of Kv1.3. To determine whether the observed bands corresponded to different Kv1.3 channel isoforms, we performed a bioinformatic search for translation initiation sites in the KCNA3 mRNA sequence. We identified four start codons that could be the origin of the proteins detected by Western blotting (Figure R9).

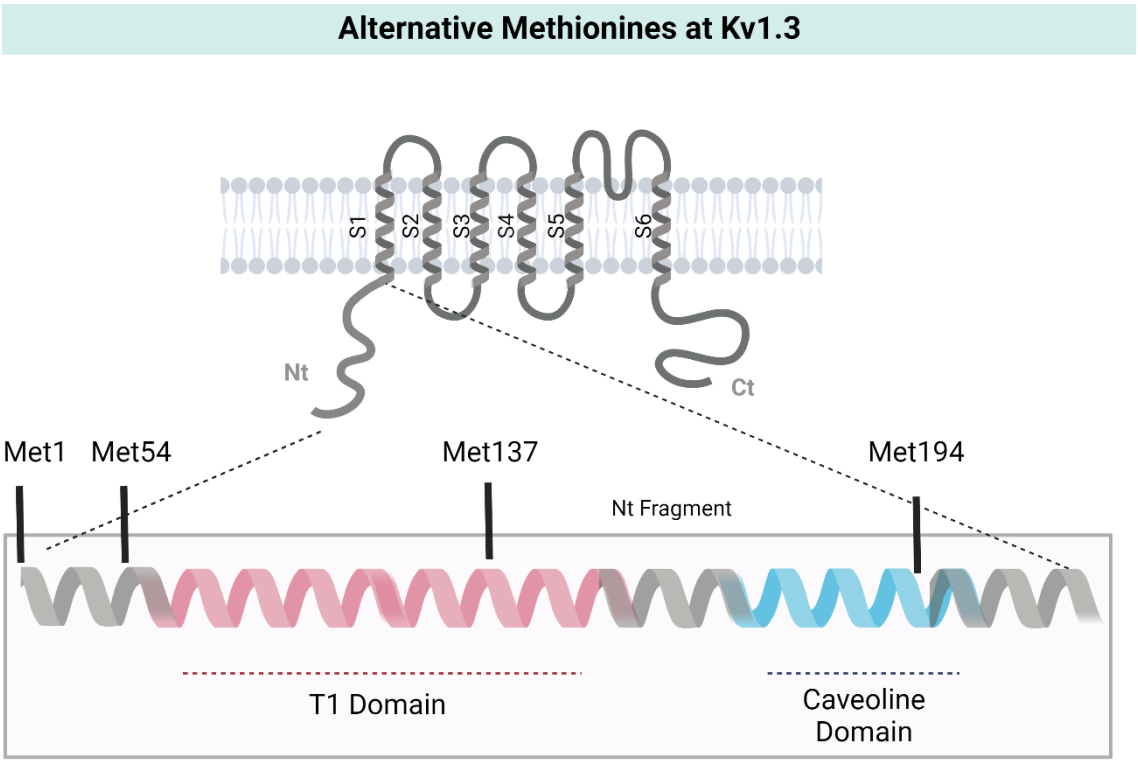

Figure R 9 Representation of the location of methionines found at the Nterminal fragment of Kv1.3.

The First Methionine identified was located at position 1 (Met1). This Methionine is present in a range of species, including humans, but is absent in rats and mice. The presence of this Methionine would lengthen the N-terminus of the Kv1.3 channel by 53 amino acids (Figure R10.A). The N-terminus fragment of Kv1.3 is responsible for the channel's tetramerization and transport to the plasma membrane. An expansion of this fragment may be involved in signaling changes (refer to Figure R9). In comparison to other members of the KCNA family (Kv1 family), the structure of Kv1.3 is highly conserved, but this Methionine is exclusively found in the Kv1.3 channel (Figure R10.B).

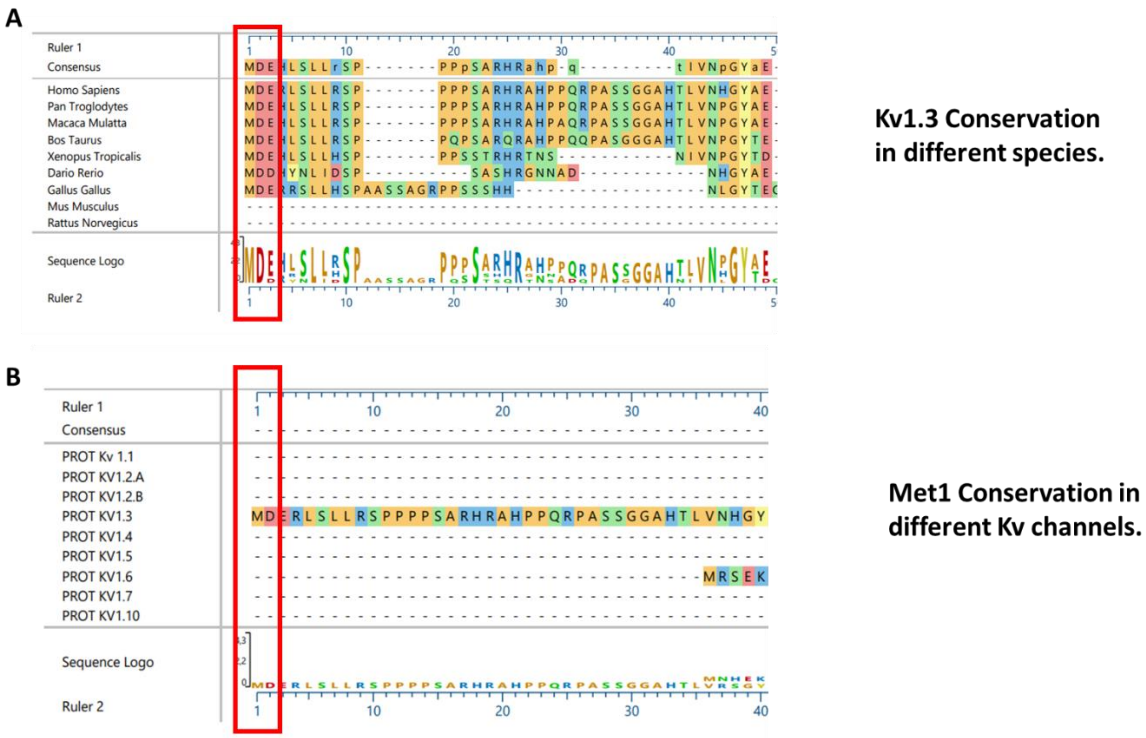

*Figure R 10 Alignment performed between the protein sequence of Kv1.3 in different model organisms **(A)** or members of human KCNA family **(B).** Red box shows the conservation of Met1. Alignment was performed using Cristal Omega model in Laser Gene software.*

The second Methionine (M1) was located at position 53 and it is the classically considered in literature as the “Canonical start of translation” in Kv1.3 due to its conservation in all model species (including mice and rat). The protein starting at this methionine has been extensively studied electrophysiologically and functionally over the last three decades due to their presence in mice and rat. We could also observe how this methionine was conserved in other KCNA channels (Figure R11).

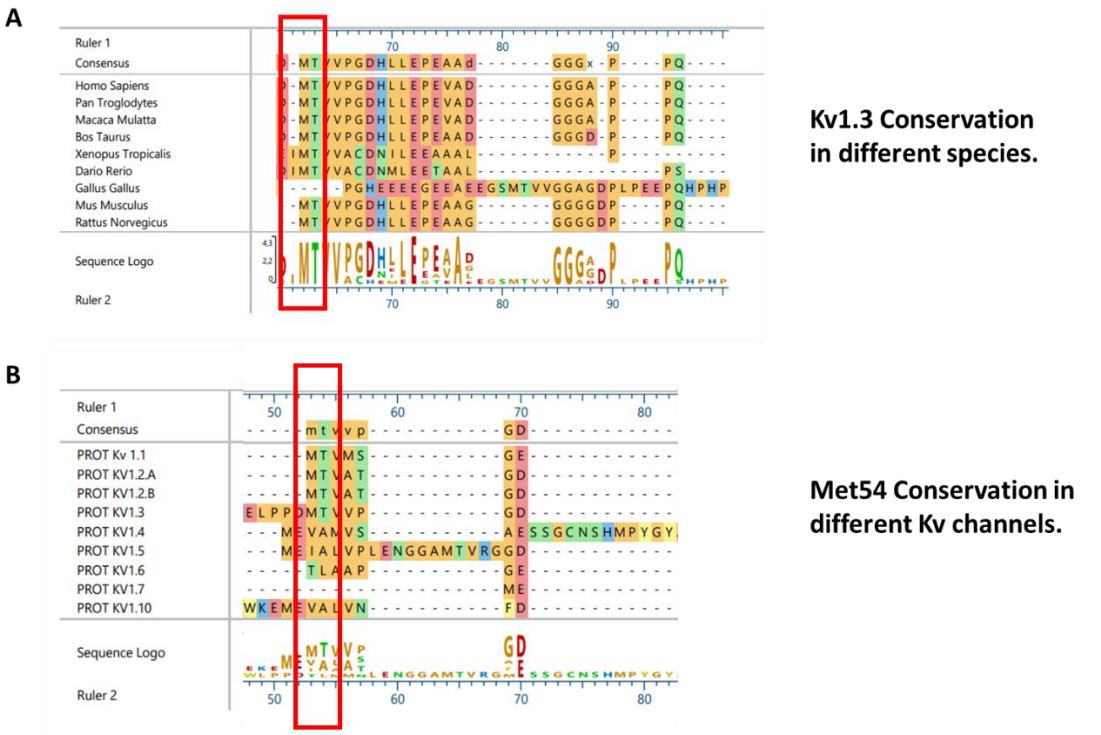

*Figure R 11 Alignment performed between the sequence of Kv1.3 in different model organisms **(A)** or members of human KCNA family **(B).** Red box shows the conservation of Met54. Alignment was performed using Cristal Omega model in Laser Gene software.*

Finally, we identified two additional Methionines at positions 137 and 194, which could translate proteins with molecular weights of approximately 49 and 43 KDa respectively. Both Methionines were situated in the N-terminal fragment of the protein, but they did not include the T1 tetramerization domain of Kv1.3. The protein produced from these Methionines would retain the six-helix fragment of the channel, but its location at the plasma membrane may be affected due to the missing fragment at the N-terminus. These Methionines were highly conserved not only in various species but also in other KCNA channels (Figure R12).

*Figure R 12 Alignment performed between the sequence of Kv1.3 in different model organisms **(A)** or members of human KCNA family **(B).** Red box shows the conservation of Met137 (Left) and Met 194 (right). Alignment was performed using Cristal Omega model in Laser Gene software.*

To confirm if the selected methionines could represent Translation Initiation Sites, we generated four plasmids containing the *KCNA3* gene tagged with the 3FLAG peptide with mutations to alanine of each putative starting methionine (Met 1, Met 53, Met 137 and Met 194) and we transfected HEK cells with those plasmids. If the bands observed by western Blotting were translated from the putative methionine, its mutation to an Alanine should abolish the translation of that isoform. We could clearly observe that mutation of the first methionine, (Met1, M0 in figure R12) abolished translation of the 75KDa band. Mutation of the second methionine (Met53, M1) eliminated the canonical 55-60KDa band. We couldn't observe any changes when mutating the third methionine (Met137), indicating that it was not a translation initiation site. Finally, mutation of the fourth methionine (Met194, M2) eliminated the 43KDa band (Figure R13). These results demonstrate that **there are at least 3 alternative translation initiation sites in the *KCNA3* coding region**.

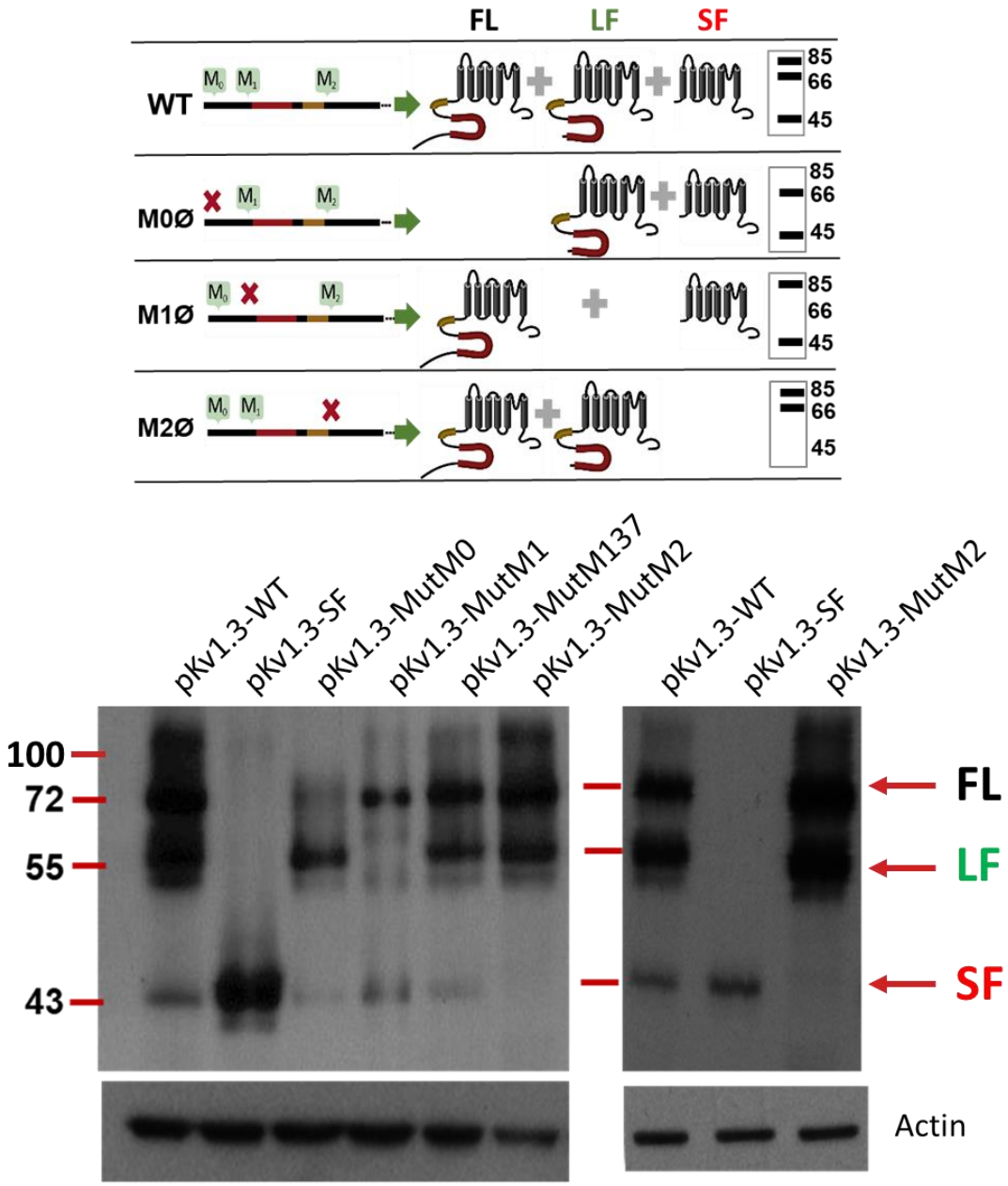

Figure R 13 ***(A)*** *Schematic representation of the position of the Kv1.3 Methionines M0, M1 and M2 and the expected outcome of their individual mutation to alanine (M0ø, M1ø, M2ø, see text for more details) in a Kv1.3-3Flag plasmid.* ***(B)*** *Representative immunoblots obtained with anti-Flag antibody on HEK cells lysates transfected with WT Kv1.3-3Flag plasmid (WT), SF-Kv1.3-3Flag plasmid encoding the 45KDa protein (SF) or the different point mutants M0-M3. M0-M2 mutants showed the band pattern depicted in the scheme of part A, while M3ø mutant (Met137) was not different from WT and is not shown in the scheme.*

After confirming the existence of three different isoforms in our Jurkat cells, we decided to study their localization and expression in order to identify their possible

function. We had previously confirmed that the basal expression of the three Kv1.3 isoforms in Jurkat was very low in resting conditions. Previous studies stated that Kv1.3 was involved in the activation and apoptosis pathways of T cells (87,122). We decided to study whether the expression of the channel could be upregulated by both pro-apoptotic and activating stimuli. To achieve this, we conducted a Western Blotting analysis after applying pro-apoptotic and activating stimuli. **The results showed that the three isoforms were upregulated when activating stimuli (PMA+ionomycin, PHA-P, and CD3+CD28) were applied, while the expression remained unchanged or slightly reduced after pro-apoptotic stimuli.** These findings suggest that the activation pathways of T cells stimulate the expression of Kv1.3 in all its forms (as shown in Figure R14). Surprisingly, Thapsigargin which is an inhibitor of the sarco/endoplasmic reticulum Ca^{2+} ATPase (SERCA), was the strongest up regulator of Kv1.3 isoforms. Thapsigarguin was described as a pro-apoptotic stimulus for Jurkat T cells (123).

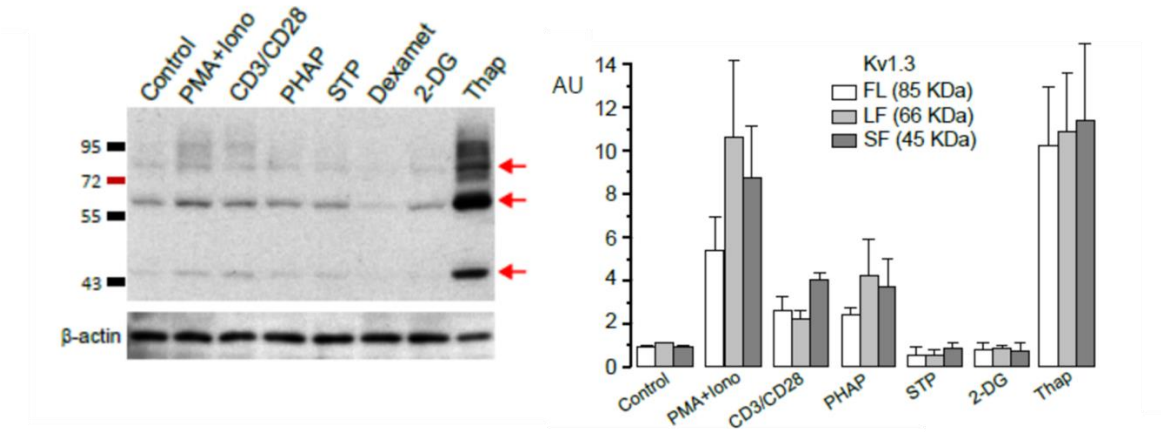

Figure R 14 Representative immunoblot obtained with the anti-Flag antibody from total Kv1.3-3Flag-2Myc Jurkat cell lysates at rest (left lane) or after incubation with the indicated activating or pro-apoptotic stimuli. The bar plot shows the protein quantification of the 85KDa (Kv1.3-FL), 66KDa (FL-Kv1.3) and 45KDa (SF-Kv1.3) after normalization with β-actin in arbitrary units. Each bar is the mean±SEM of 3-5 independent experiments.

We also confirmed the upregulation of Kv1.3 protein expression through Flow Cytometry using the Jurkat-NeonGreen Tagged cell line after treatment with PMA + Ionomycin and Thapsigargin stimuli. The results showed that Thapsigargin was

still the strongest stimulus for the upregulation of Kv1.3 expression (as depicted in Figure R15).

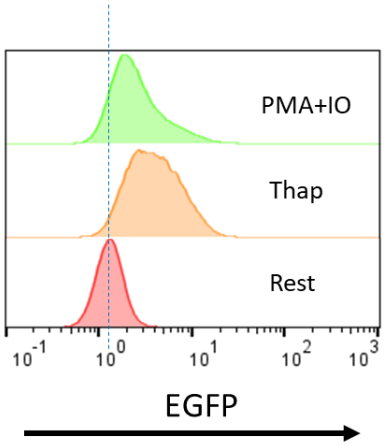

Figure R 15 Representative flow cytometry plot showing the expression of the Kv1.3-Neon protein in the Jurkat-NeonGreen cells. Kv1.3-NeonGreen is upregulated after the treatment with PMA+ionomycin and Thapsigarguin.

The upregulation of Kv1.3 channels after PMA +Ionomycin stimuli was previously reported in literature (124). Unexpectedly, our data showed that Thapsigargin represented the strongest upregulator of Kv1.3 isoforms. To gain a better understanding of this upregulation, we decided to quantify the expression of the protein over a period of 36 hours after the treatment. The results revealed that the upregulation of Kv1.3 expression began as early as three hours after the treatment and continued to increase for at least 36 hours (as shown in Figure R16). Furthermore, all three isoforms were upregulated with similar dynamics.

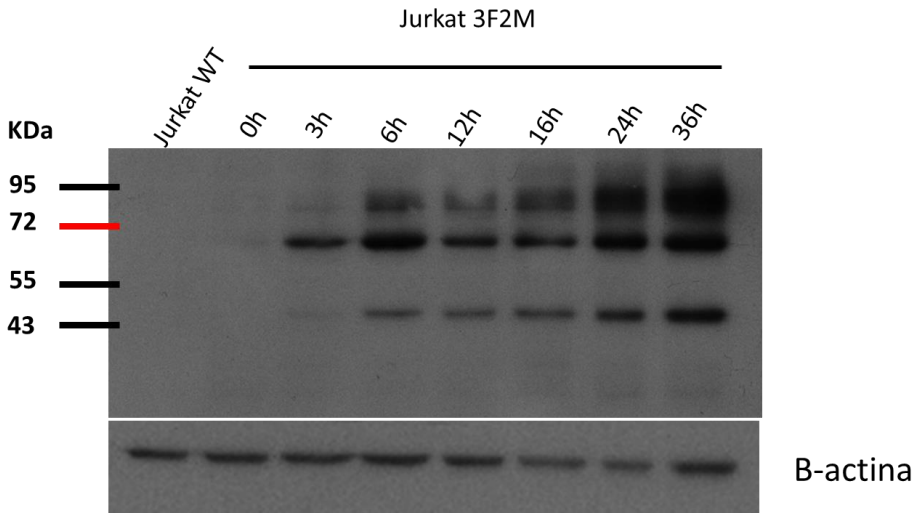

Figure R 16 Representative immunoblot obtained with the anti-Flag antibody from total Kv1.3-3Flag-2Myc Jurkat cell lysates at rest (left lane) or after incubation thapsigarguin at the indicated time.

Thapsigargin induces an elevation in intracellular calcium levels by depleting the reticulum. As no other apoptotic stimulus induced an increase in Kv1.3 expression, we questioned whether the upregulation of Kv1.3 was caused by the elevated intracellular calcium levels. To test this hypothesis, we stimulated our Jurkat-3F2M cell line with thapsigargin for 4 hours in complete medium with and without calcium (Figure R17). Our results clearly demonstrated that in the absence of extracellular calcium, Jurkat T cells were unable to upregulate Kv1.3.

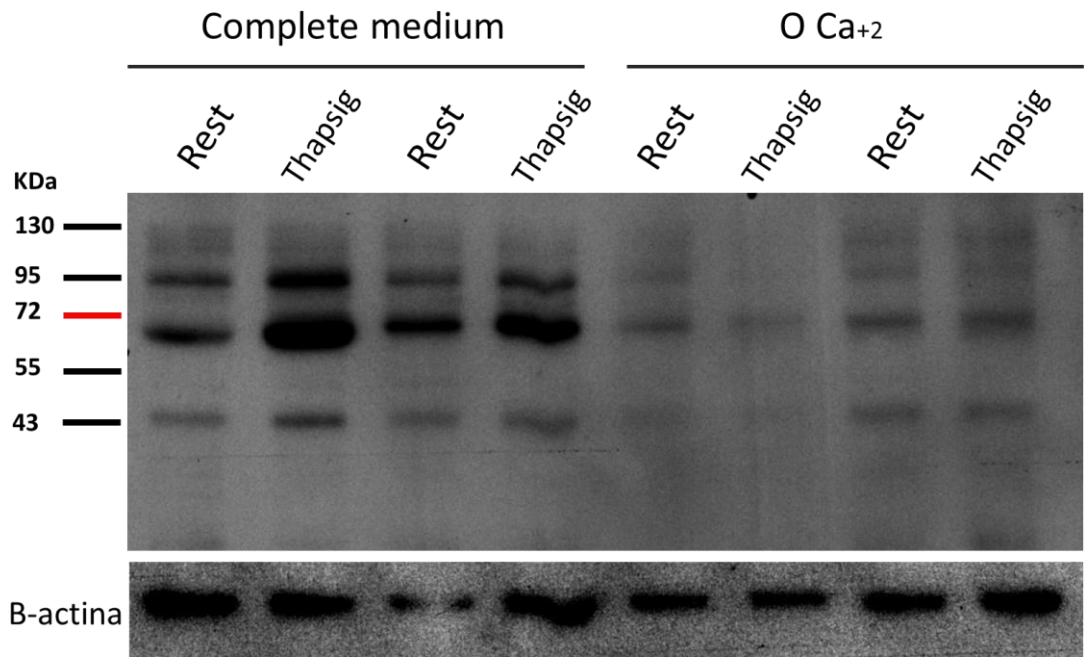

Figure R 17 Representative immunoblot obtained with the anti-Flag antibody from total Kv1.3-3Flag-2Myc Jurkat cell lysates at rest (left lane) or after incubation thapsigarguin for 4 hours in complete culture medium (left lanes) or in 0 Ca+2 medium.

As it appeared that calcium could be involved in the regulation of Kv1.3, we decided to investigate whether Kv1.3 was a gene regulated by the nuclear factor of activated T cells (NFAT). NFAT is a family of transcription factors that are regulated by calcium and play a key role in T cell activation and differentiation. T

cell receptor (TCR) activation leads to an increase in intracellular calcium, which activates calcineurin and results in NFAT dephosphorylation and nuclear translocation. At the nucleus, NFAT binds to the promoters of various genes involved in T cell activation, such as IL-2 (125)(See Figure R18.A). To test whether Kv1.3 was regulated by NFAT, we conducted a bioinformatics search of the KCNA3 promoter and identified the consensus NFAT binding sequence at nucleotide position -1229 (Figure R18.B). We then treated our cells with Cyclosporin A, an inhibitor of calcineurin and a positive regulator of NFAT, to determine whether Kv1.3 was regulated by NFAT. Our results showed that Kv1.3 upregulation after Thapsigarguin stimulation was not reduced by the addition of Cyclosporin A, suggesting that Kv1.3 was not regulated by NFAT under our experimental conditions.

A

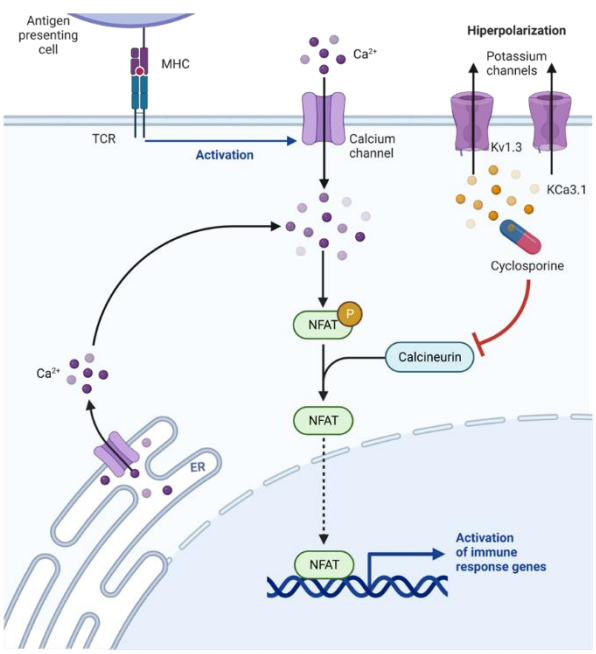

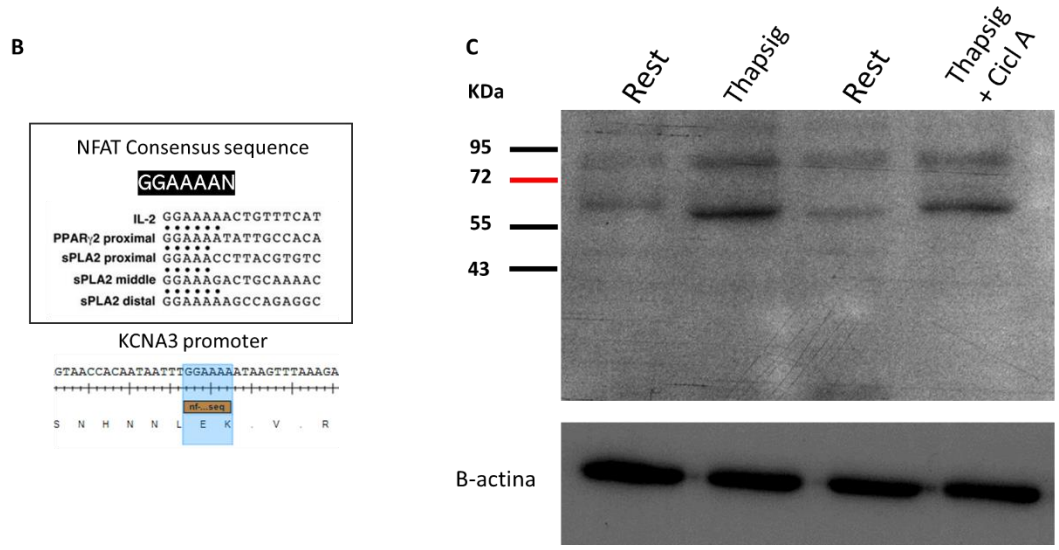

Figure R 18 ***(A)*** *NF-AT signaling pathway after TCR stimulation in T cells.* ***(B)*** *NFAT Consensus sequence is found in the KCNA3 promoter.* ***(C)*** *Representative immunoblotting showing how Kv1.3 is upregulated in Jurkat T cells after Thapsigarguin stimulation for 4 hours in presence or absence of Ciclosporin A.*

Further studies are necessary to fully comprehend the precise regulation of Kv1.3 by calcium. Based on our findings, we can conclude **that Thapsigargin is a potent upregulator of Kv1.3 channel isoforms**.

5.3 Functional characterization of Kv1.3 channel isoforms in HEK cells.

After identifying the new isoforms of Kv1.3, we aimed to investigate the functional implications of these unreported proteins. Specifically, we focused our interest on the canonical Kv1.3 protein (60 KDa) and the short 43KDa isoform (Short Form, SF) because they are present in our mice and rat models. The characterization of SF was particularly important because the mRNA encoding for this truncated protein may be present in commercially available Kv1.3 KO mice (126). The knockout mice were generated through the deletion of the 5p region of the kcna3 gene (as depicted in the top panel of Figure R19). However, the methionine 194,

which is responsible for translating the Short Form of Kv1.3, is still present in these mice. To verify if SF was being expressed in the KO mice, we conducted PCR analysis on samples obtained from macrophages of Kv1.3 KO mice and wild-type (WT) mice. We designed two sets of primers; the first set contained an SEN primer that hybridized at the deleted region, while the other had an SEN primer that bound to the region of the SF. The PCR was performed on cDNA samples obtained from RNA samples of KO and WT macrophages to examine the expression of the channel. We could clearly observe how the mRNA of **the SF of Kv1.3 was being expressed in the commercially available Kv1.3 KO mice** which makes us suspect that the mouse might not be a complete knockout for Kv1.3 (Figure R19). For this reason, we decided to generate a complete KO mouse that would eliminate the entire exon of Kv1.3, which will be explained in section 5.6 of this thesis.

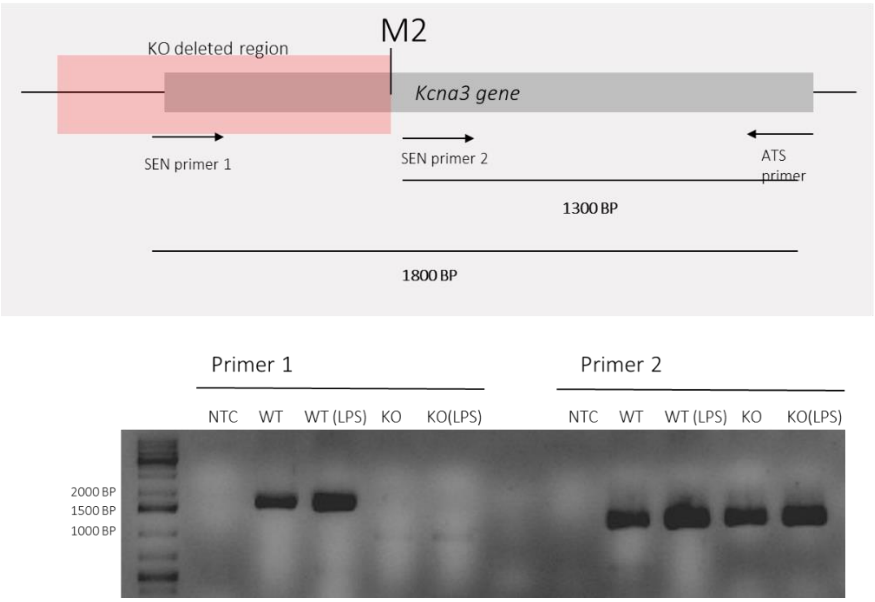

Figure R 19 Gel electrophoresis of polymerase chain reaction (PCR) products obtained with primers annealing in the 5' region of the kcna3 gene (absent in the Kv1.3 knockout [KO] mouse, or in the 3' region of the kcna3 gene (conserved in the Kv1.3 KO, S-2) and the same antisense primer (AS). PCR was performed of complementary DNA (cDNA) obtained from total RNA extracted from wild type (WT) and KO Kv1.3 mouse bone marrow derived macrophages at rest and after 6 h stimulation with 100 ng/mL of lipopolysaccharide (LPS) to induce Kv1.3 expression. NTC, no template control.

In order to characterize the function of the long and short isoforms independently, we decided to determine in which cell organelles they were localized. To this end, we used a heterologous expression system of HEK cells, and we created plasmids expressing either the canonical Kv1.3 protein alone (the long form, LF, carrying a mutation to alanine of the M2 methionine) or the short 43KDa isoform (short form, SF) as GFP or mCherry fusion proteins (Figure R20). Both plasmids were co-transfected in HEK cells. We could clearly observe how LF expression was mainly restricted to plasma membrane, while SF seemed almost exclusively intracellular. Surprisingly, no colocation between both isoforms was found suggesting complete independence between them and no heterotetramerization. These results are consistent with previous data in the literature showing that alternative translation generates protein isoforms that are, in most cases, targeted at different subcellular localizations (127). This differential targeting has also been reported for some other ion channels (128–130).

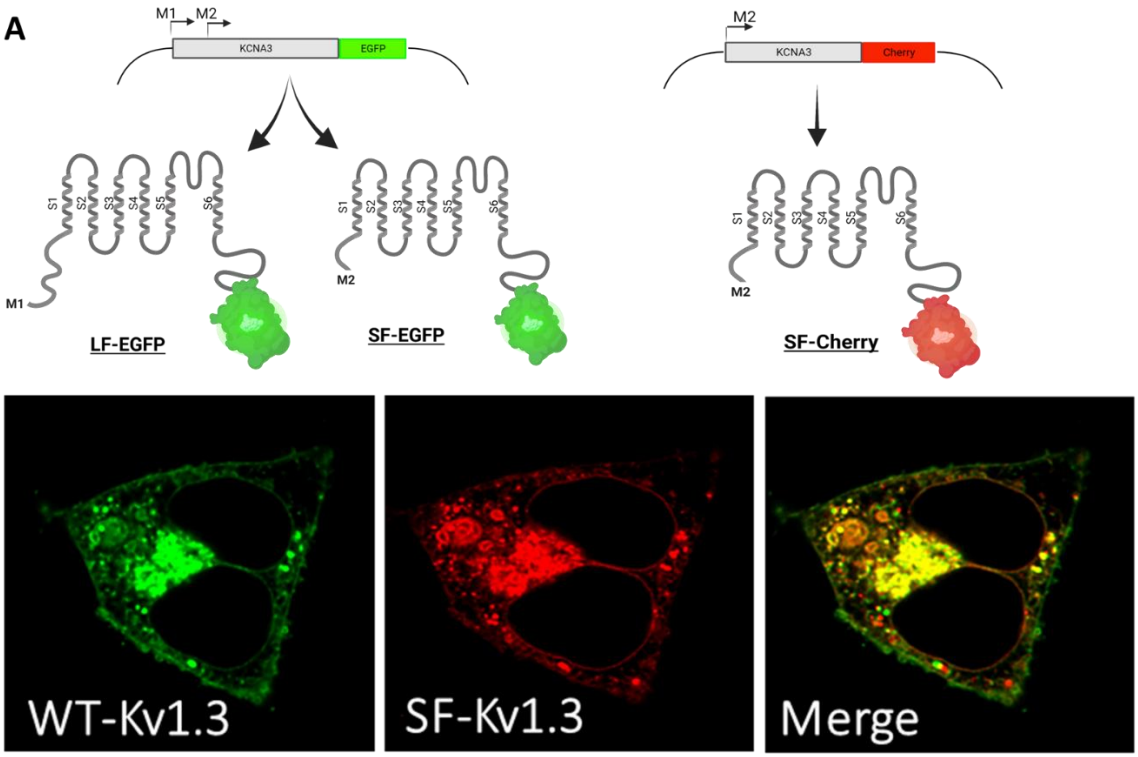

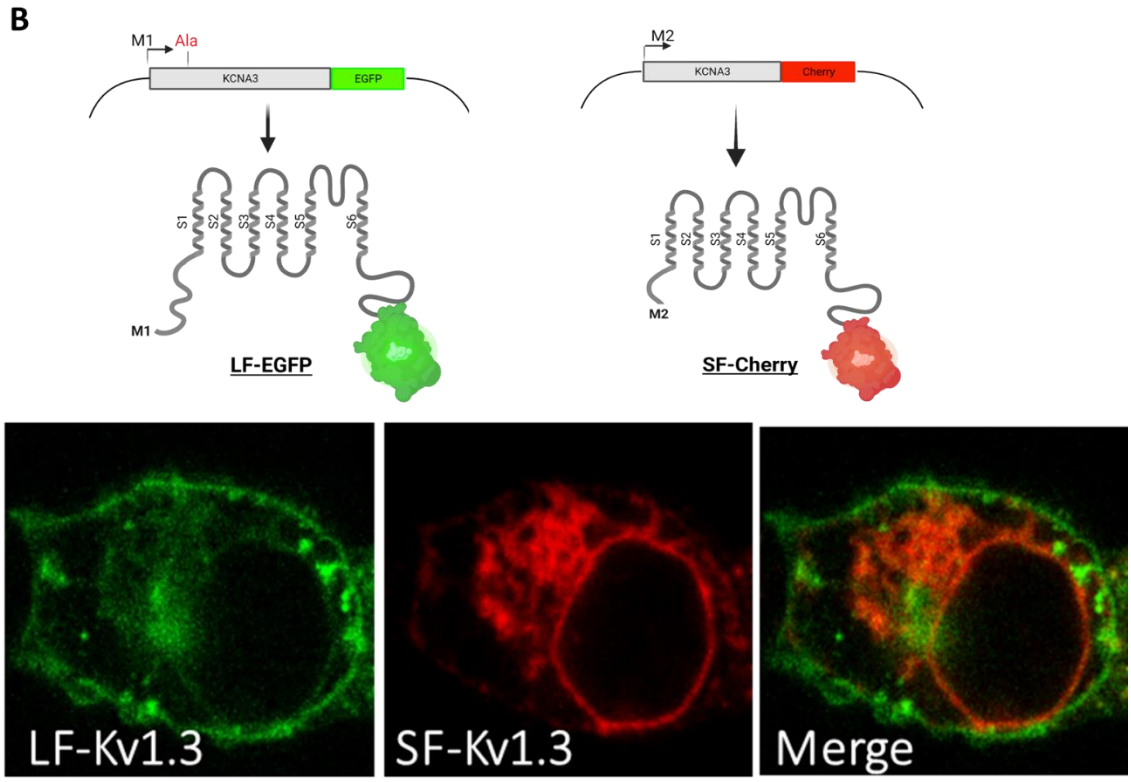

Figure R 20 Confocal microscopy image of transfected HEK cells highlighting the expression of Kv1.3 isoforms. A. WT channel (green) (LF+SF) and SF channel alone (red). B LF protein (green) alone and SF protein alone (red)

SF expression was located delimitating the nuclear envelope and was also observed showing partial location at the Endoplasmic Reticulum (Figure R21).

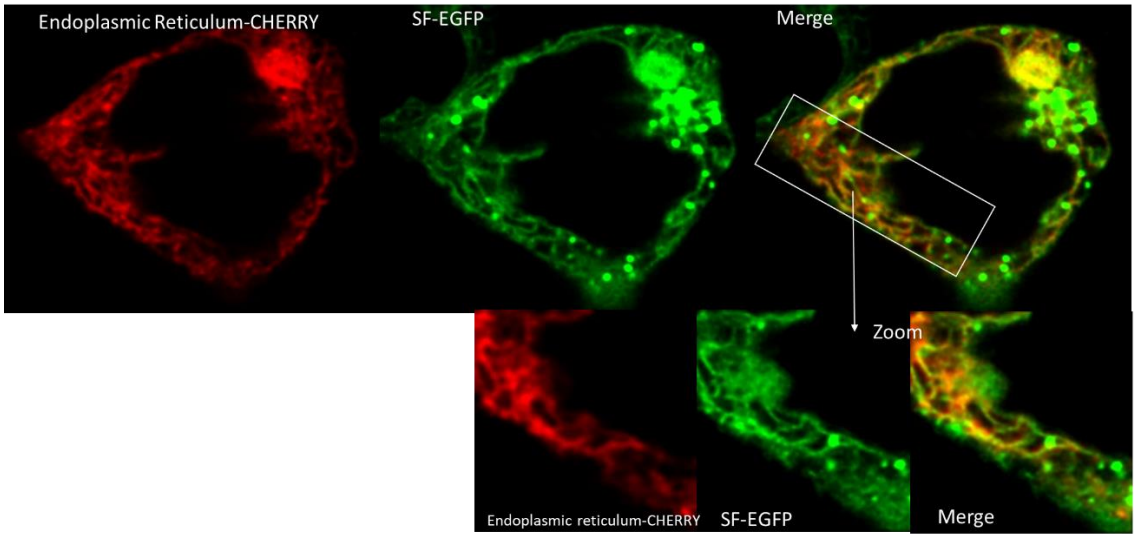

Figure R 21 Confocal microscopy image of transfected HEK cells highlighting the location of SF isoforms of Kv1.3. Endoplasmic Reticulum is shown in Red and the SF protein is shown in green. Partial colocalization is found.

The lack of membrane expression of the SF was also demonstrated by cotransfection of SF with Orai channel, whose expression is predominant at the plasma membrane (Figure R22). This combination confirmed that SF was not present at the plasma membrane.

With these results we could conclude that **LF was mainly expressed at the plasma membrane**, **SF is found intracellular** in the nuclear envelope and in the ER and **no interaction between both forms is found in HEK cells**.

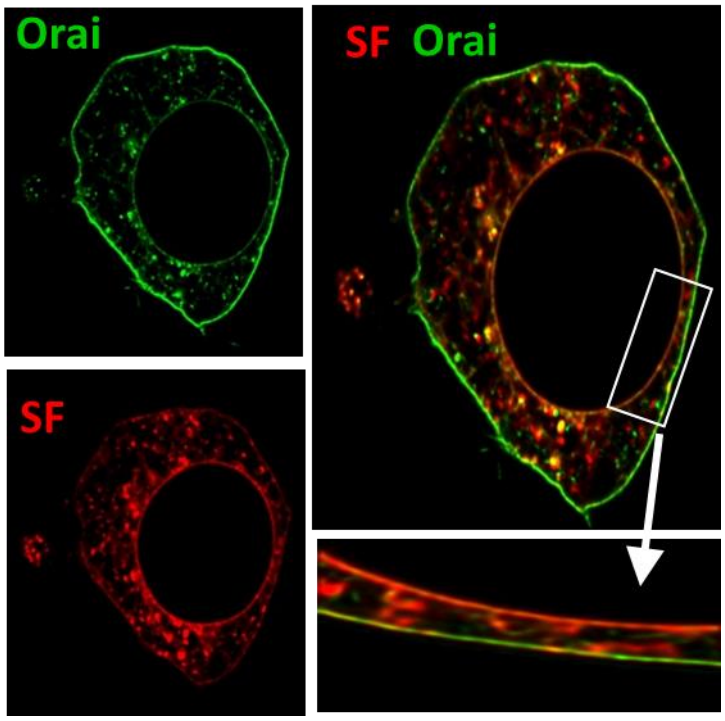

Figure R 22 Confocal microscopy image of transfected HEK cells highlighting the location of SF isoforms of Kv1.3. Plasma membrane is shown in Green and the SF protein is shown in Red.

Finally, we tried to confirm previously published data suggesting a mitochondrial location of Kv1.3 (131,132). To this end, we performed live cell confocal images of WT Kv1.3 channels (Both channels, LF and SF together) coexpressed with MitoTracker in HEK cells. However, contrary to the published results Kv1.3 proteins did not show colocalization with MitoTracker in our experimental conditions (Figure R23a). We confirmed this result in HEK fixed cells

cotransfected with SF or LF and the mitochondrial targeting signal (MTS) of the cytochrome c oxidase subunit 8A (COXa) fused to a mCherry protein as a mitochondria marker (mito-Cherry, Figure R23b). No colocalization between the COX protein and the Kv1.3 isoforms was found.

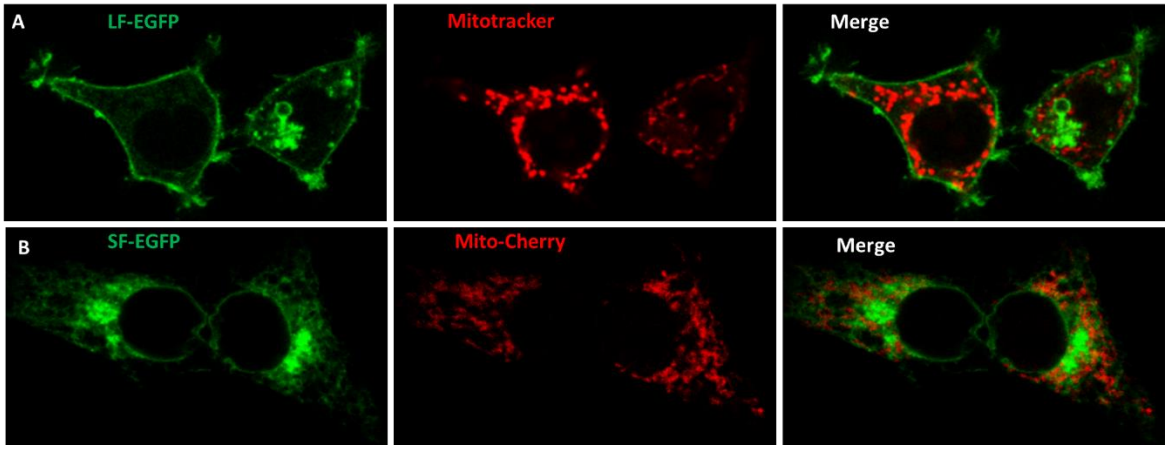

Figure R 23 Confocal microscopy image of transfected HEK cells highlighting the location of SF and LF isoforms of Kv1.3. Mitochondria is shown in Red and the LF protein (A) and the SF protein (B) are shown in green.

Although our results do not exclude the expression of some Kv1.3 channels at the mitochondria, they indicate that **mitochondria do not represent a preferential location for the descripted Kv1.3 channel isoforms**.

After confirming the different locations of both isoforms within the cells, we performed a functional characterization of these two isoforms, together with the WT Kv1.3 channels. To this end, we carried out Electrophysiological studies in transfected HEK cells with our generated plasmids (Figure R24). We studied the current density in depolarizing pulses to +40 mV, the steady-state inactivation (B), the use-dependent block upon high-frequency pulses (C) and the sensitivity to block with the selective blocker PAP-1 (D).

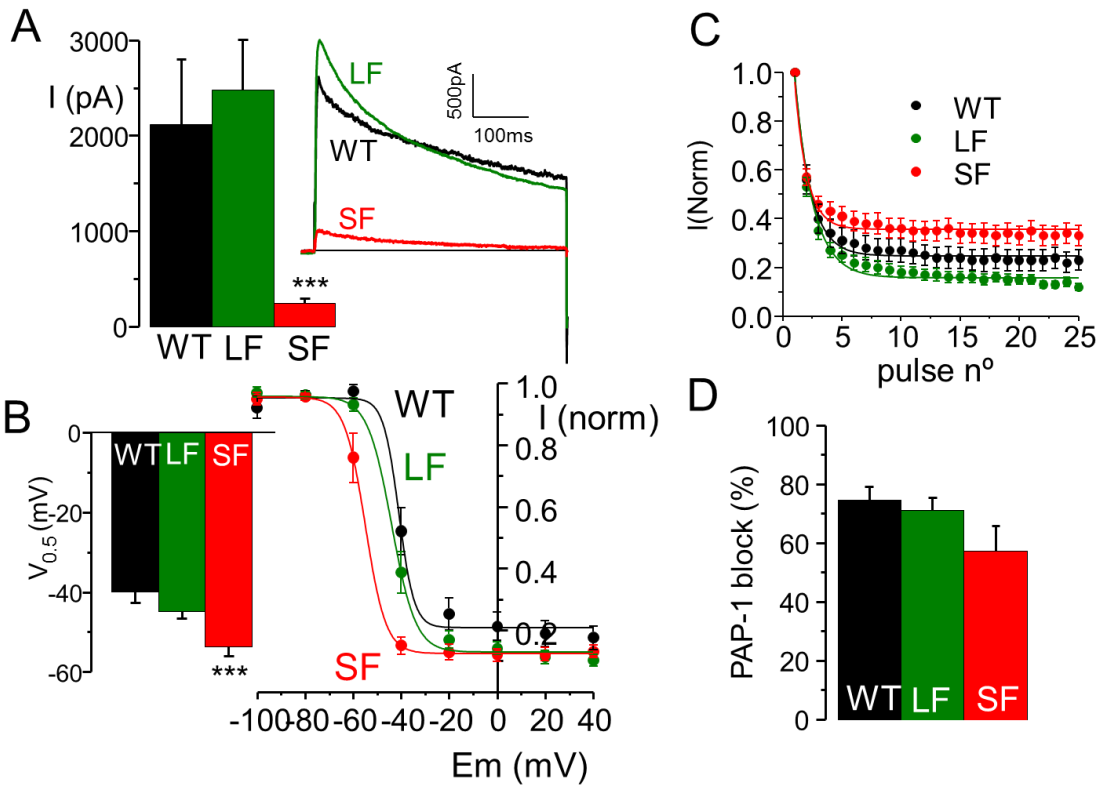

Figure R 24 Electrophysiological studies in transfected HEK cells with our generated plasmids. ***(A)*** *Current density in depolarizing pulses to +40 mV,* ***(B)*** *the steady-state inactivation,* ***(C)*** *the use-dependent block upon high-frequency pulses and* ***(D)*** *the sensitivity to block with the selective blocker PAP-1.*

LF overexpression elicited large Kv1.3 currents with kinetic and pharmacological properties indistinguishable from WT currents. In contrast, the Kv currents observed in SF-transfected cells showed a significantly smaller current amplitude and some kinetic differences with WT Kv1.3 currents, as a leftward shift of the inactivation curve. As membrane location of the SF constructs is scarce, a possible explanation for these results could be that SF channels do not form functional plasma membrane channels, but some of these SF subunits could be forming heteromultimeric Kv1 channels with endogenous Kv1.x channels in HEK cells. To test this hypothesis, first, we quantify by qPCR the expression of other members of Kv1 family in HEK cells (Figure R25A). We found that, apart from Kv1.3, Kv1.1 and Kv1.6 were the most expressed channels in those cells. Then, we designed siRNA against Kv1.1 and Kv1.6 to reduce the expression of those channels (Figure R25B). To test if SF could be forming channels with native Kv1.1 and Kv1.6, we cotransfected HEK cells with SF and mixture of siRNAs against

Kv1.1 and Kv1.6 channels and we could observe that there was a significant reduction of the total current density without changes in the kinetics of the currents (Figure R 25C).

<u>These results suggest that SF-mediated currents observed in HEK cells could be mediated by heteromultimers withing the SF-Kv1.3 isoform and other members of the Kv1 family.</u>

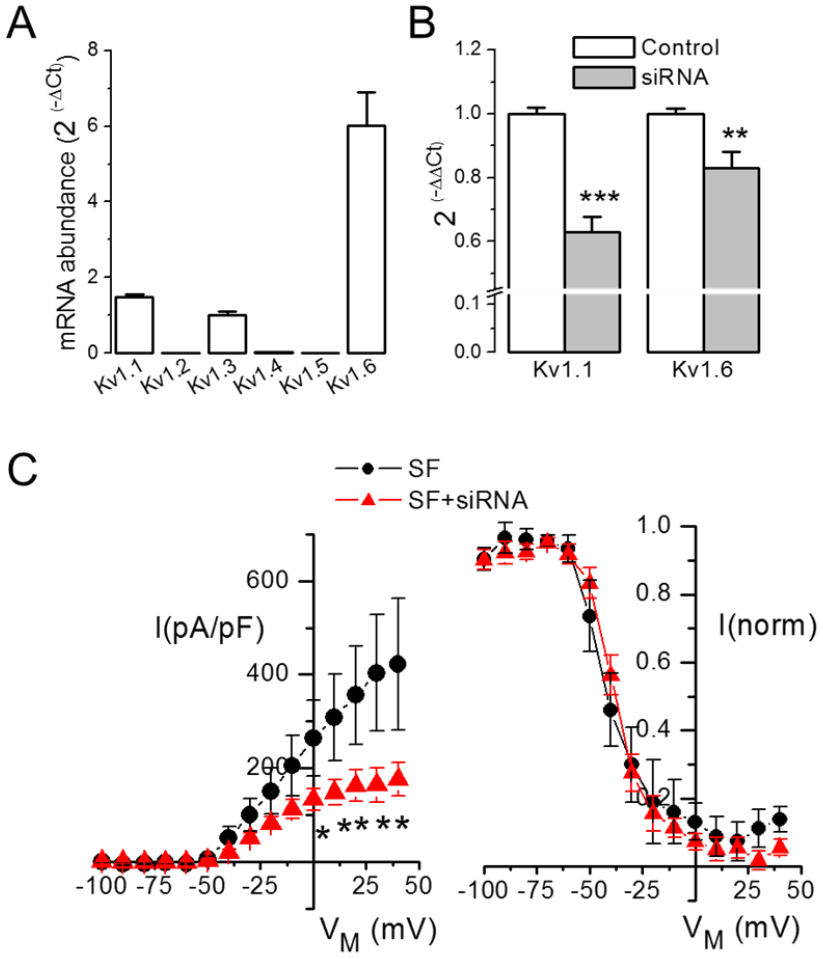

Figure R 25 ***(A)*** *mRNA abundance of other members of Kv1 family in HEK cells measured by qPCR.* ***(B)*** *Efectiveness of Kv1.1 and Kv1.6 siRNA in downregulating the expression of these genes in HEK cells measured by qPCR.* ***(C)*** *SF current was downregulated when siRNAs where coexpressed (red line.*

Finally, we studied the proliferation rate of transfected HEK cells with our plasmids which is a more integrated readout. To this, we transfected HEK cells with our plasmids expressing both Kv1.3 isoforms (WT) or the SF or LF isoforms alone. An empty EGFP plasmid was used as a negative control. EdU reactive

was used to measure the proliferation rate on HEK cells. As previously described (133), Kv1.3 WT overexpression increased HEK cell proliferation (Figure R26). This effect was reproduced with LF overexpression alone, while SF overexpression had no effect. This data suggests that LF is the responsible of inducing proliferation on HEK cells and that SF is not involved in the proliferative role of Kv1.3. As our data also show that SF is not located at the plasma membrane, this data also suggests **that Kv1.3 needs to be present at the plasma membrane to promote cell proliferation**.

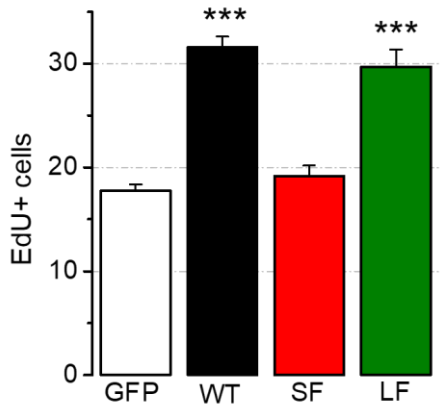

*Figure R 26 Role of Kv1.3 isoforms in proliferation. The proliferation rate of HEK cells transfected with the indicated plasmids was determined as a percentage of the proliferation observed in control conditions (green fluorescent protein [GFP]-transfected HEK cells) using 5-ethynyl-2-deoxyuridine (EdU) incorporation. Each bar is mean ± SEM, n = 6–15 data from 3 to 6 different experiments (***p < 0.001 vs. GFP).*

5.4 Contribution of Kv1.3 channels isoforms to Jurkat cell function

To further characterize this unreported SF isoform under endogenous conditions, we used the CRISPR-Cas9 system to generate Kv1.3-KO Jurkat clones (eliminating the full *KCNA3* gene) and SF Jurkat clones, expressing only the SF isoform which could represent the case of the Kv1.3 KO mice (Figure R27). Both SF and KO clones were created from the Kv1.3-3Flag2Myc Jurkat line using the CRISPR-Cas9 technology. To create the total KO, (Kv1.3-KO Jurkat clone), two gRNAs located at the beginning and at the end of the KCNA3 gene were selected using CRISPOR. The SF Jurkat clone was generated selecting two gRNAs located at the 5P region of the KCNA3 gene, to delete the region that it is not present at the SF. The screening of the resultant clones was made through Western Blotting to identify the lack of protein. (Figure R28)

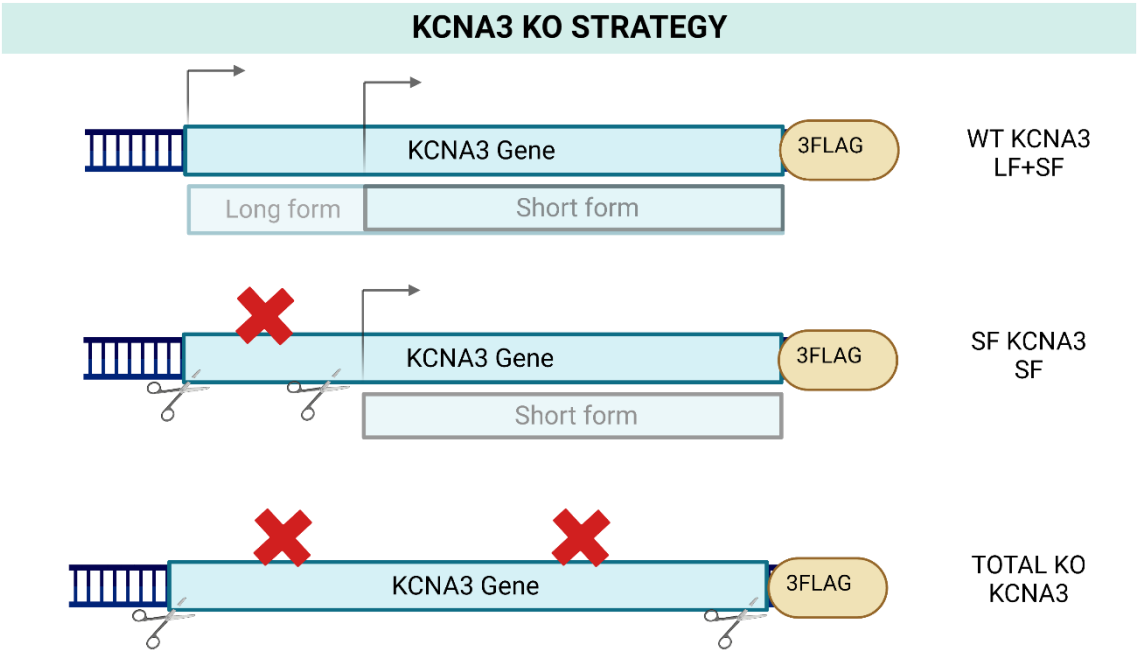

Figure R 27 Strategy to generate Jurkat Kv1.3 total KO and Jurkat SF (expressing only the SF) clones.

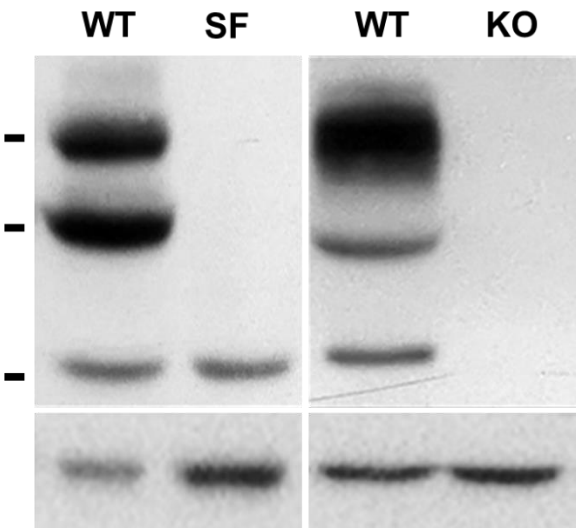

Figure R 28 Western Blot result showing the absence of all isoforms of Kv1.3 in the total KO Jurtak cell line (Right), and the presence of the SF alone in the Jurkat-SF cell line (left). Total lysates of Jurkat cells stimulated with Thapsigarguin were revealed using antiFlag M2 plasmid in each cell line of interest.

To identify the subcellular localization of native Kv1.3 in Jurkat cells, we stimulated Jurkat clones with PMA+ionomycin for 24 hours and performed immunocytochemistry using α-Myc antibody. Even in stimulated clones, Kv1.3 expression was quite low (Especially the SF clone) to perform robust cellular localization assays. Jurkat cells are small cells (11µm) in which the organelles are hard to identify correctly. We could observe how WT channels showed a distribution WT-Kv1.3-Flag Jurkat showed clear plasma membrane expression and SF proteins remained intracellular (similar to what we observed at HEK cells under heterologous conditions) (Figure R29).

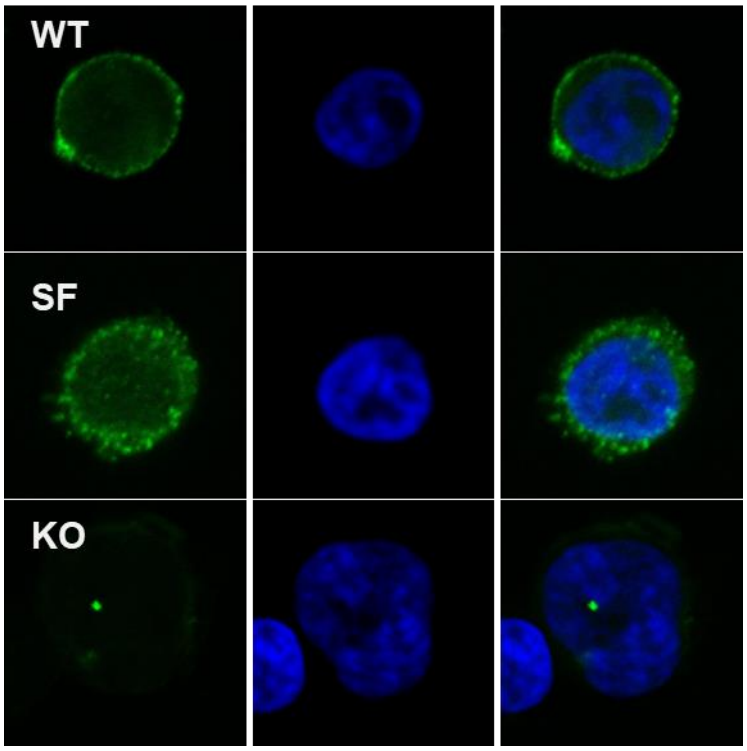

Figure R 29 Confocal microscopy image highlighting the expression of Kv1.3 channel (green) and nuclei (Blue) in the indicated Jurkat cell lines (WT-TAG, SF and KO). Kv1.3 protein was detected labelling the preparation with antiFLAG antibody + FITC secondary antibody to amplify the signal.

In agreement with the immunocytochemistry results, whole cell recordings did not show any Kv current in resting conditions or after 16h activation with PMA+Ionomycin in SF or KO clones. Meanwhile, WT edited clones exhibited Kv currents significantly upregulated upon activation (Figure R30). **This data confirms that SF protein does not form a functional K channel at the plasma membrane in an endogenous system.**

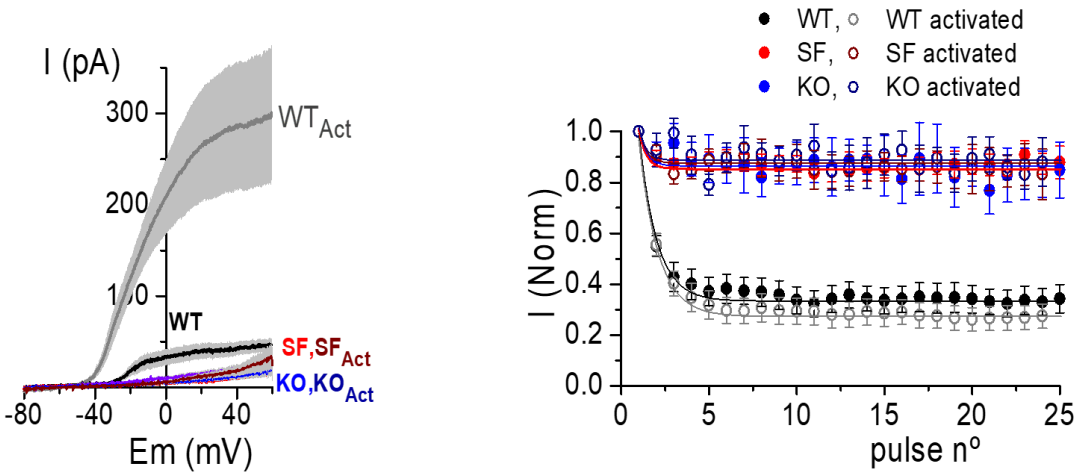

Figure R 30 Electrophysiological characterization of Jurkat KO and SF clones. (Left) Kv currents were elicited by 2 s voltage ramps from −80 to +60mV in WT, SF, and KO edited Jurkat cells at rest or activated (Act) by 16 h treatment with phorbol-12-myristate-13-acetate (PMA) + Ionomycin. (Right) The inset shows the use-dependent block analysis from a train of depolarizing pulses to +40mV. The peak amplitude (normalized to pulse #1) is plotted as a function of the pulse number in each experimental condition. Data are mean ± SEM of 18–26 cells in each condition. Cells were obtained from at least 4 different experiments and two independent Jurkat clones.

The absence of functional Kv currents in the plasma membrane of SF and KO clones was further confirmed with current-clamp experiments with the perforated-patch technique (Figure R31), which showed depolarizing resting E_M in both cases. **Resting E_M in the WT clones was significantly different** as it was the amplitude of the response to a depolarizing stimulus (an external solution with 60 mM K^+).

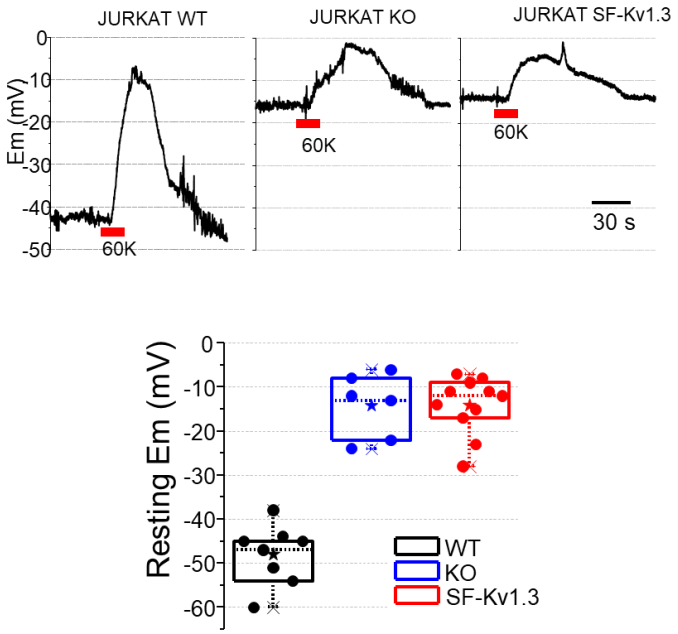

Figure R 31 Contribution of Kv1.3 channel isoforms to resting EM and Ca^{2+} influx. Representative traces of the resting EM recordings in wild type (WT), short form (SF), and knockout (KO) Jurkat cells with the current-clamp configuration, and the response to application of a 60mMK+ external solution. The box plot shows the average resting EM data in the three groups.

Hyperpolarized resting E_M of T cells due to Kv1.3 channels expression has been described to play an important role regulating Ca^{+2} entry (134), so we studied whether $[Ca^{+2}]_i$ or the kinetics of Ca^{+2} influx were affected in edited cells. Microfluorometric studies were carried out in Jurkat cells incubated with Fluo 4. After 10 min in a nominally-Ca^{+2} free external solution with 200nM thapsigargin, reintroduction of Ca^{+2} in the external solution led to an increase in the $[Ca^{+2}]_i$ that showed a larger magnitude and a faster kinetics in the WT Jurkat clones (Figure R32), as expected if the driving force for Ca^{+2} entry is dependent of resting E_M as described. However, we could no observed significant differences regarding the amplitude and kinetics of Ca^{2+} fluxes between SF and KO clones.

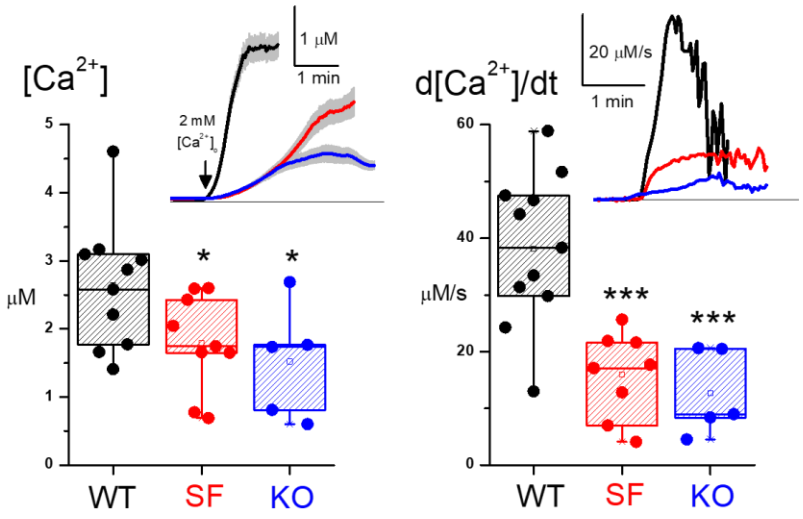

*Figure R 32 Box plots showing Fluo4-normalized fluorescence (as an indicator of [Ca^{2+}]) and the derivative of the fluorescence (dF/dt), as an indicator of the kinetics of Ca^{2+} influx) upon perfusion with a 2mM Ca^{2+} solution. Each dot is the average of 30–50 cells from an independent experiment and the insets show the mean ± SEM of all cells in one of these individual experiments in WT, SF, and KO as indicated. *p < 0.05; ***p < 0.001 versus WT.*

The difference in resting E_M and Ca^{2+} entry between WT and KO Jurkat cells prompted us to explore the role of Kv1.3 channel isoforms in T cell responses, by analyzing their contribution in the early steps after TCR stimulation. To this end, we studied the phosphorylation of proteins implicated in TCR induced signaling cascade such as phosphorylation of the CD3δ chain, of the ZAP-70 kinase (Zeta-chain-associated protein kinase 70) or of the linker for activation of T cells (LAT) as well as other signaling complexes further downstream in the signaling cascade such as PLCγ or ERK.

Phosphorylation of ERK in response to CD3/CD28 stimulation was reduced in KO Jurkat clones compared to WT or SF clones (Figure R33), suggesting a functional role for both the full length and the truncated protein in Jurkat cell activation.

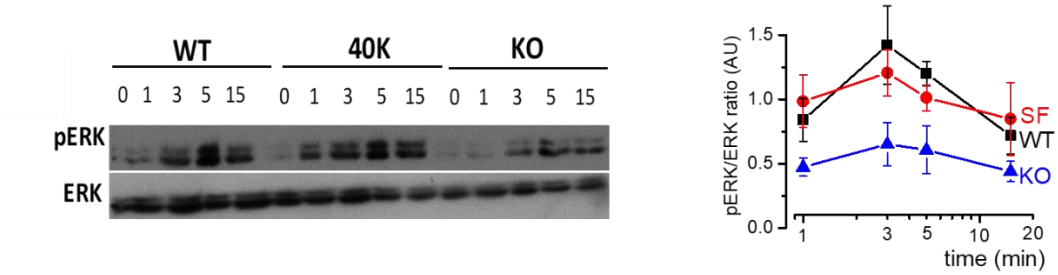

Figure R 33 Contribution of Kv1.3 channel isoforms to T-cell signaling pathways. Representatives immunoblot of total Erk and pErk protein obtained from wild type (WT), short form (SF), and knockout (KO) Jurkat cell lysates incubated in the presence of soluble CD3/CD28 + secondary crosslink antibody for the indicated time intervals. Erk phosphorylation was normalized to total Erk amount. The plot shows mean ± SEM, n = 3.

We also studied the characterization of phosphorylation of other proteins involved in the activation pathway. Our clones showed three different patterns (Figure R34):

CD3 and ZAP-70 were independent of Kv1.3 protein. Its phosphorylation patter was unaffected by the truncated isoform or the complete KO of the channel.

Some others required either the WT or the SF (as pERK), being significantly reduced only in KO clones. This was the case for PLC and LAT phosphorylation.

Full activation of one of them, SLP76, was only achieved in WT clones, being significantly reduced in both SF and KO cells.

These results suggest that **different Kv1.3 isoforms contributed differently to the early steps of T cell activation** after TCR stimulation.

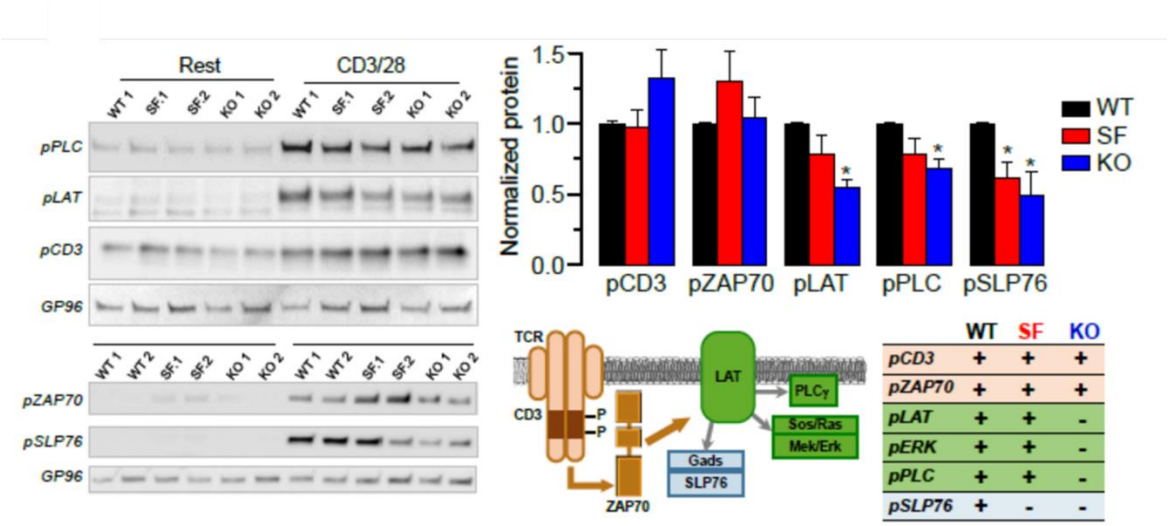

*Figure R 34 Contribution of Kv1.3 channel isoforms to T-cell signaling pathways. Representative immunoblots of the indicated proteins determined from Jurkat cell lysates (WT, SF, and KO) at rest and after incubation in the presence of plate fixed CD3/CD28 for 10 min. Quantification was performed using ImageJ and the amount of protein normalized for GP96 is represented in the bar graph. Mean ± SEM, n= 3-4 experiments. *p < 0.05 compared with WT. The scheme and the table depict the sequence of activation of the explored proteins, with a color code to indicate whether the activated proteins are independent of Kv1.3 expression (brown), dependent of Kv1.3 but not distinguishing between WT and SF (green), or with an absolute requirement for WT Kv1.3 (blue).*

Next, we explore whether these differences translate into functional T cell responses, and whether the SF-Kv1.3 protein may have a functional impact in T cell function despite not being able of forming a plasma membrane Kv channel. We studied cytokine IL2 secretion in our Jurkat cells. Under normal growth conditions little IL-2 is produce by Jurkat cells, only after stimulation substantial amounts of the cytokine are expressed. We test different stimuli to IL-2 secretion in our cultures. The levels of IL-2 in cell supernatants increased after treatment with PMA+PHA-P, polyclonal activation with anti-CD23/CD28 or exposure to Raji B-cells loaded with two different SEE concentrations (Figure R35). However, no differences in the response of the WT, SF or KO clones were observed. In fact, contrary to previous publications (135,136) , IL-2 secretion response was insensitive to selective Kv1.3 blockers such as PAP-1 or Margatoxin (MgTx).

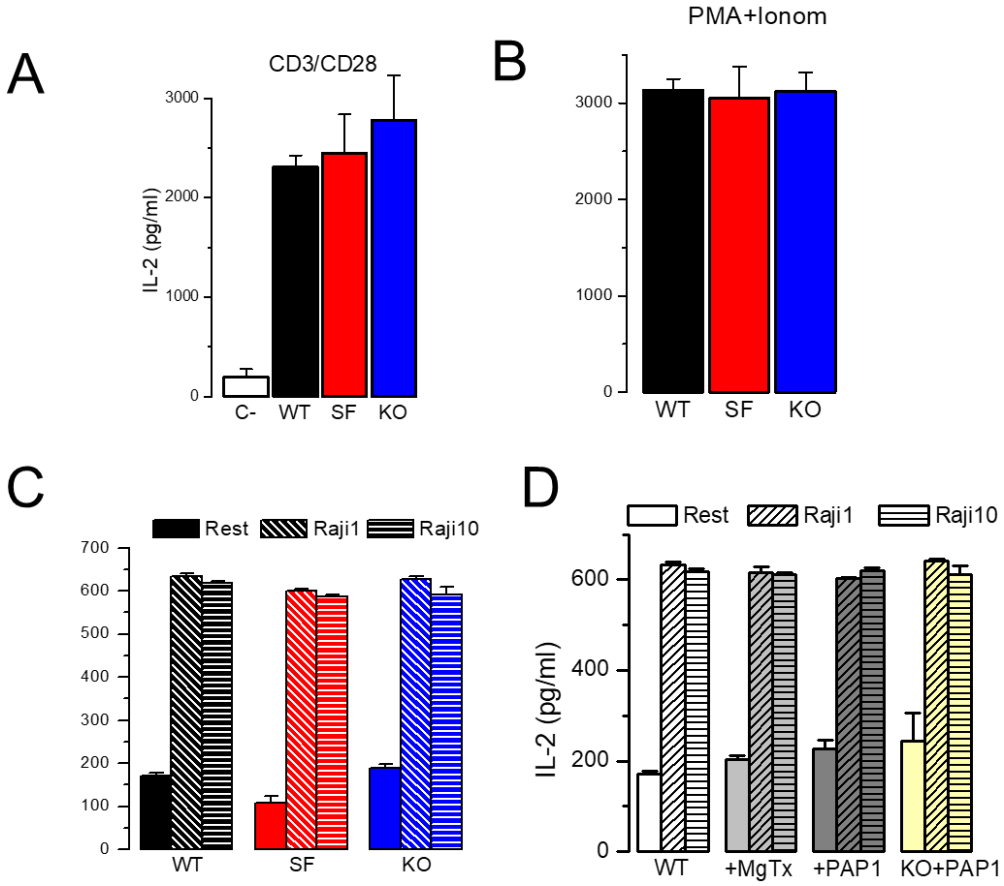

*Figure R 35 Role of Kv1.3 channel isoforms in cytokine secretion. The levels of interleukin 2 (IL-2) were quantified by enzyme-linked immunosorbent assay (ELISA) in supernatants from wild type (WT), short form (SF), and knockout (KO) Jurkat cell clones at rest or after 12–16 h of stimulation with **(A)** anti-CD23/CD28, **(B)** PMA+PHA-P, and **(C)** exposure to Raji B cells loaded with 1 ng/Ml 10 ng/mL of Staphylococcal enterotoxin E (SEE). **(D)** IL-2 secretion in response a Raji B-cell stimulation was measured in WT or KO Jurkat cells preincubated for 30 min with Kv1.3 inhibitors PAP-1 (100 nM) or Margatoxin (MgTx, 2 nM).*

We confirmed this result in native T-cells (Figure R36) in which IL-2 secretion was also unaffected after treatment with Margatoxin or PAP-1. In these later ones, the secretion of another cytokine, TNFα, was also unaffected by Kv1.3 blockers. Altogether, our data indicate that **Kv1.3 channels do not take part in stimulus-induced cytokine secretion** in these preparations. Our data does not exclude the possibility that the optimal stimulation conditions that we are using may be hiding differences in IL-2 secretion that may occur in vivo under physiological conditions.

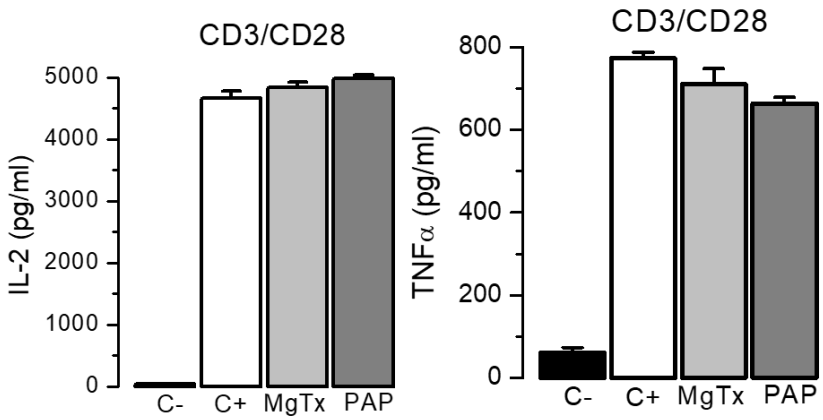

Figure R 36 IL2 and tumor necrosis factor-α (TNF-α) secretion were also quantified with ELISA in human-derived CD4+ T cells. Cells were preincubated with PAP-1 or MgTx before stimulation with CD3/CD28 for 16 h. Each bar (b–d) is mean ± SEM of at least three independent experiments.

We could not find any difference in our Knockout Jurkat clones regarding IL-2 cytokine; however some differences were found between the presence of SF or LF for SLP76 and LAT phosphorylation after TCR stimulation. Both cytosolic SLP76 and membrane-associated LAT are key adaptor proteins phosphorylated by TCR-associated ZAP70, forming microclusters at the Immunological Synapse (IS). Phosphorylation of LAT recruits SLP76 to the cell membrane, where they nucleate a multimolecular complex, which induces a host of downstream responses, including calcium influx, ERK phosphorylation, integrin activation and cytoskeletal reorganization. We speculated that decreased activation of these adaptors, by affecting their translocation and/or interaction with the proteins of the signaling complexes, will impact IS formation. The IS is a stable cell–cell junction between a T cell and an antigen-presenting cell (APC). The correct IS formation is crucial for T cell activation (137). For this reason, the exact manner in which IS is established and maintained is an area of great current interest. Kv1.3 had been described to be present at the IS, however its role has not been well understood. (52)

We explored the degree of Kv1.3 colocalization at the IS overexpressing GFP-labelled WT, LF or SF isoforms in Jurkat cells prior to Raji cells exposure. Confocal microscopy images (Figure R37) showed a restricted plasma membrane location for LF, with a distribution close to the cortical filamentous

actin, and at the IS area (labelled with pLAT). In contrast, GFP fluorescence of SF-transfected Jurkat cell was excluded from actin and pLAT labelled regions at the IS, being restricted to a perinuclear location. A combination of both patterns was observed, as expected, in the case of the WT Kv1.3 overexpression. We could conclude **that LF of Kv1.3 is recruited to the IS after Raji exposure while SF is not recruited**.

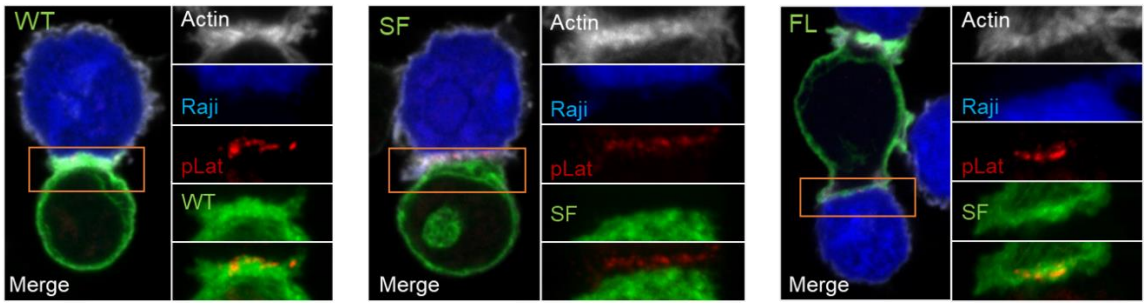

Figure R 37 Contribution of Kv1.3 channel isoforms to immunological synapse (IS) formation. Representative confocal microscopy images of Jurkat cells transfected with plasmids expressing Kv1.3 isoforms (wild type [WT], long form [LF], or short form [SF]) as enhanced green fluorescent protein (eGFP) fusion proteins (green). Transfected Jurkat cells were exposed to Staphylococcal enterotoxin E (SEE)-loaded Raji B cells and the IS was identified with pLAT staining (red). The actin cytoskeleton was labeled with phalloidin (white) and Raji cells were labeled with CellTracker Blue CMAC dye. Confocal representative images of each condition are shown and the square with the IS is expanded on the right side, to show the four individual channels and the combined green and red (Kv1.3 isoform and pLAT) to evidence the differences in their relative location in each isoform. The expanded images are z-projections of five to eight images around the z plane shown in the corresponding full image. Scale bar = 5 μm.

To explore whether this location is related to the efficiency of IS formation, we used the edited Jurkat clones stimulated with Raji cells to quantify the number of IS and the intensity of the pLAT signaling at the IS (Figure R38). Both parameters, quantity of IS and intensity of p-LAT, were significantly decreased in SF and KO clones. Altogether, these data indicate that full activation and **effective recruitment of LAT at the IS requires WT Kv1.3 channels**.

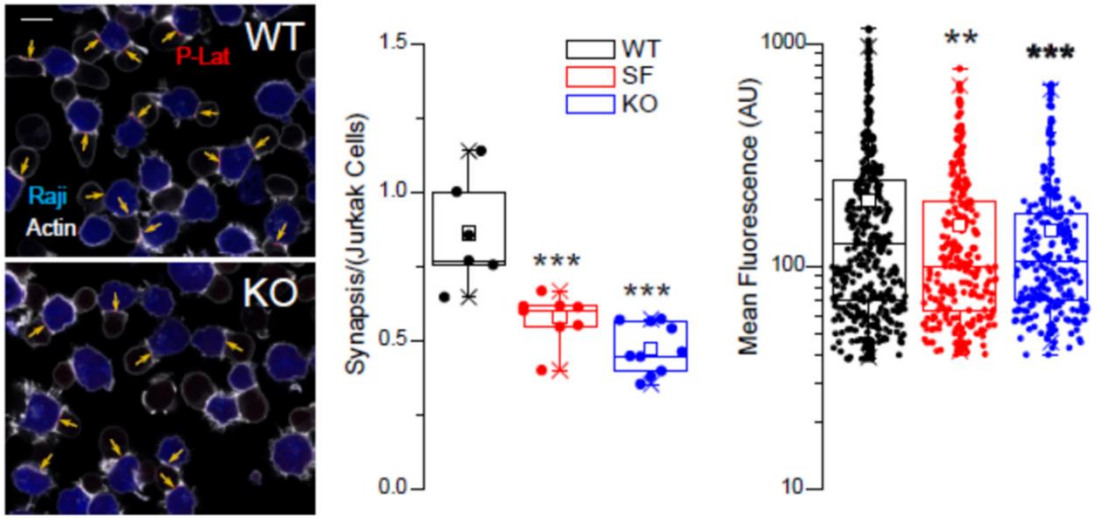

*Figure R 38 WT, SF, and knockout (KO) Jurkat cells were incubated in the presence of SEE-loaded Raji B cells for 10 min. pLAT, actin, and Raji cells are labeled as indicated and both the number of IS (arrows) normalized to Jurkat cell number and the product of the area and the intensity of the pLAT labeling were quantified in each condition. The plots show the average data from both parameters obtained from triplicates of at least three different experiments per condition. **p < 0.01; ***p < 0.001 versus WT. Scale bar = 10 µm.*

5.5 MitoKv1.3

The presence of Kv1.3 in the inner mitochondrial membrane is controversial. MitoKv1.3 has been described to play a role in the regulation of apoptosis in various tumor cell types (70,71). However, the N-terminus of Kv1.3 does not have a mitochondrial targeting signal, which is necessary to deliver the protein from the cytosol to the inner mitochondrial membrane.

The existence of at least three isoforms of Kv1.3 led us to hypothesize that mitochondrial Kv1.3 might exist as a different isoform from the other three previously described isoforms. To determine whether a new isoform could be targeted to the mitochondria, we performed a bioinformatic search for translation initiation sites in the KCNA3 mRNA sequence that could act as mitochondrial targeting sequences. Surprisingly, we identified a methionine at position Met358 with a predicted mitochondrial delivery of 93% (Figure R39).

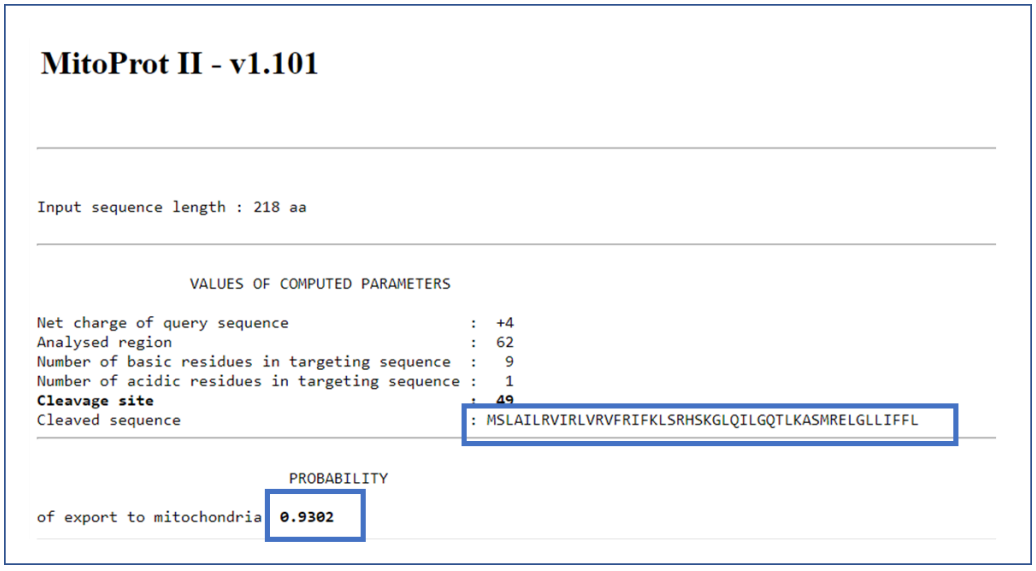

Figure R 39 MitoProt Software identified a possible mitochondrial targeting signal beginning at the Metionine 358 with a probability of mitochondrial import of 93%.

The most interesting feature of this possible new isoform was that the methionine was located at the beginning of the S4 helix, which corresponds to the voltage sensor domain of the channel and is the most conserved fragment of the channel between species and between other members of the Kv1 family (Figure R40).

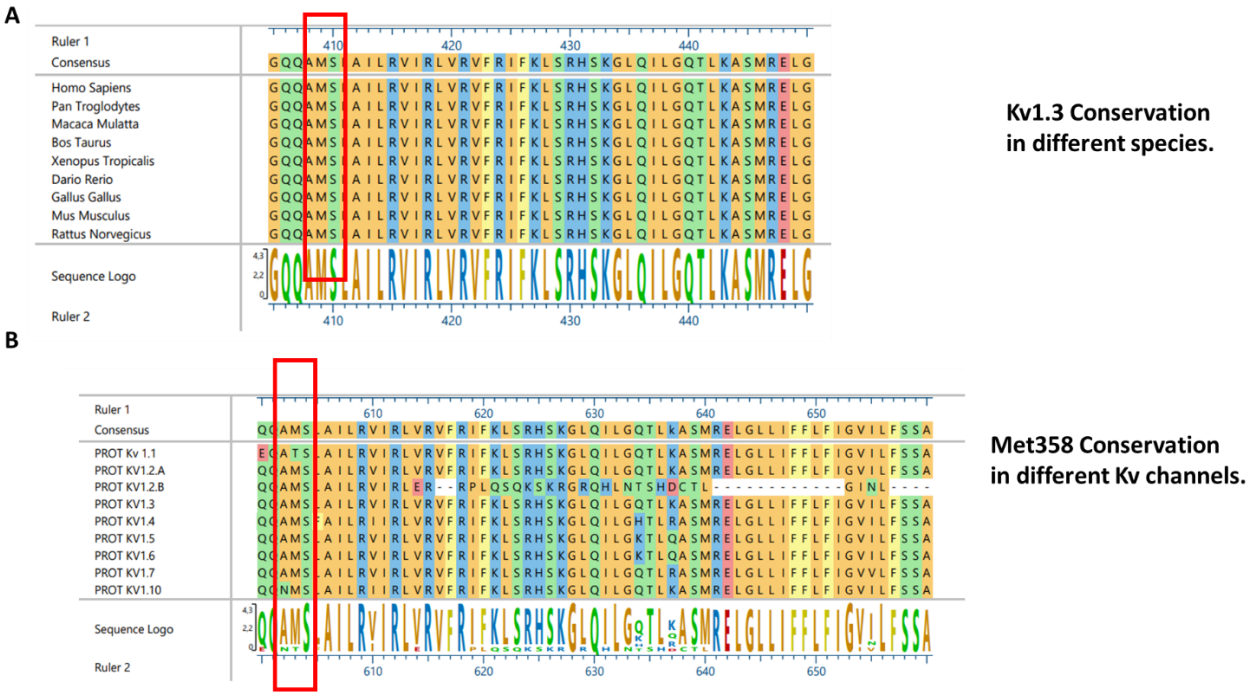

Figure R 40 Alignment performed between the sequence of Kv1.3 in different model organisms ***(A)*** *or members of human KCNA family* ***(B).*** *Red box shows the conservation of Met358.*

The S4 fragment would be cleaved after import at the mitochondria, leaving only the S5-P loop-S6 fragment at the mitochondrion (Figure R41). As mentioned in the introduction, the S5-P loop-S6 is the basic motif of all ion channels. It could tetramerize to form a channel, as occurs in the Kir family. This predicted new isoform was extremely interesting because it could resolve some of the discrepancies with the role of mitoKv1.3, it has a mitochondrial targeting signal to explain its import, it is not voltage dependent because the sensor domain is cleaved during mitochondrial import and its presence in the mitochondrion could be tightly regulated because the translation of the isoform could be regulated for the cell.

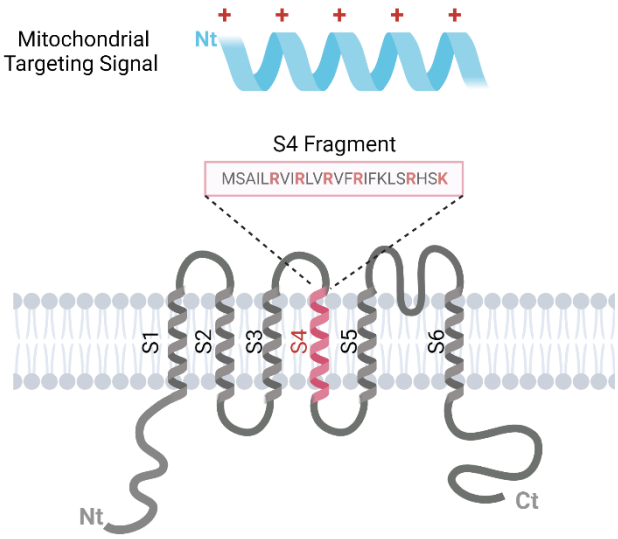

Figure R 41 The Mitochondrial targeting signal identified by Mitoprot corresponded with the S4 fragment of Kv1.3.

To determine whether this software-predicted isoform could exist in cells, we cloned its sequence flanked by flag into a pCDNA3 plasmid, transfected it into HEK cells and performed a Western blot (Figure R42). While we were able to detect the expected protein in the plasmid containing only the S4-S5-P loop-S6, this protein was not present in the WT sequence of the Kv1.3-3FLAG plasmid, suggesting that when the WT Kv1.3 mRNA was present, the mito isoform was not produced in transfected HEK cells.

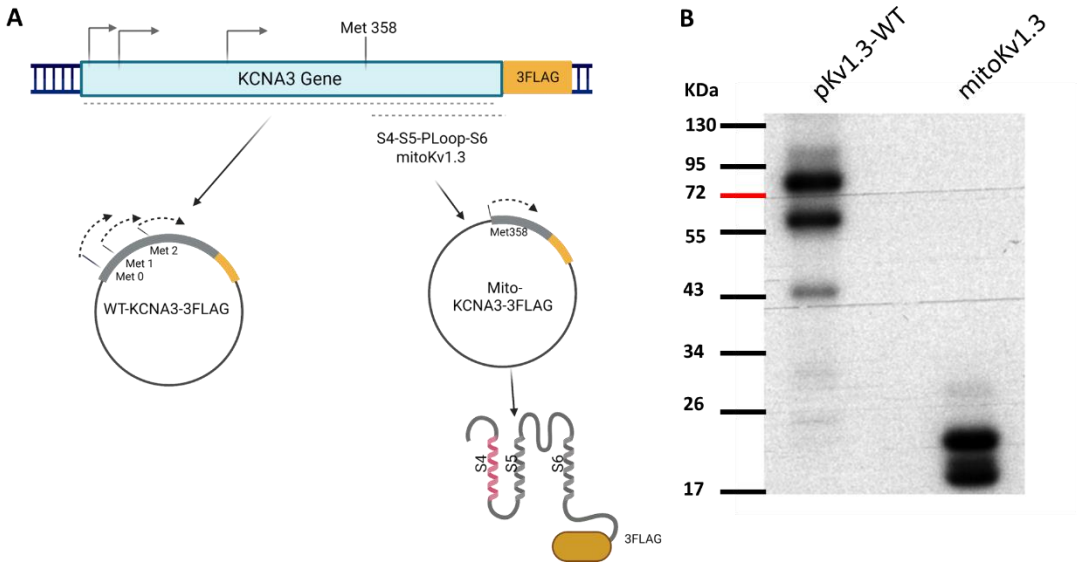

Figure R 42 ***(A)*** *A plasmid starting at Met358 OF Kv1.3 tagged with the FLAG peptide was generated to study the predicted isoform (mitoKv1.3).* ***(B)*** *Representative western blot of HEK lysates transfected with the WT Kv1.3-3FLAG plasmid or the predicted mitoKv1.3-3FLAG plasmid. No presence of the predicted mitoKv1.3 is observed in the WT Kv1.3 plasmid.*

Our hypothesis supported that mitoKv1.3 expression is tightly regulated by the cell, and it is translated to promote apoptosis in cells. Therefore, we tried to detect the expression of this isoform in our Jurkat cells after treatment with apoptotic inducers, but the isoform was not detectable under our experimental conditions (Figure R43).

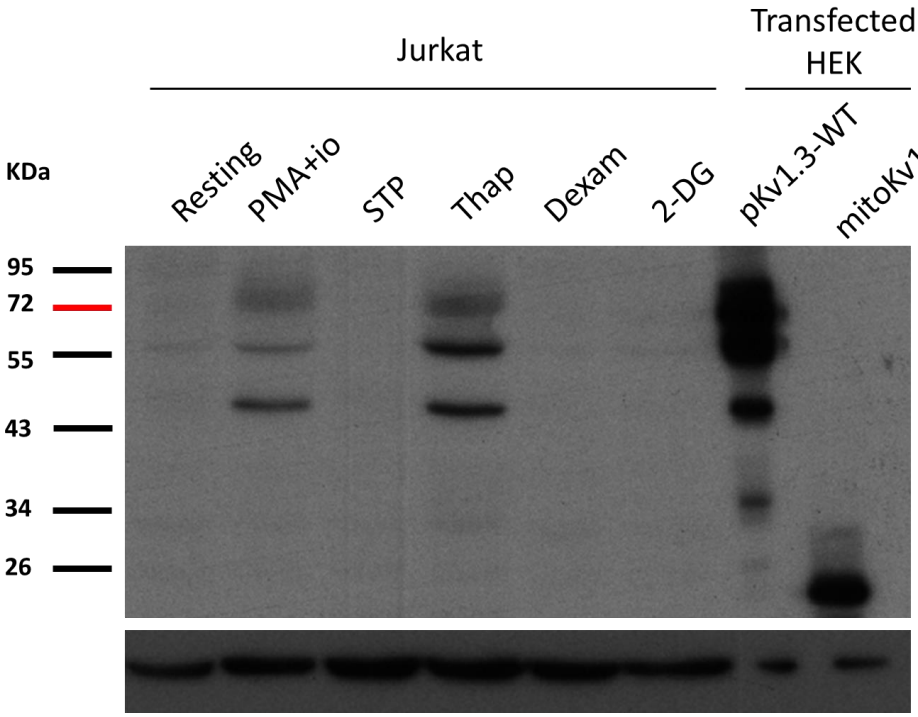

Figure R 43 Representative western blot of Jurkat-3FLAG2MYC cell line stimulated with proapoptotic stimuli (Staurosporin, Thapsigargin, Dexamethasone and 2-Deoxyglucose) and HEK cells transfected with the WT Kv1.3-3FLAG plasmid or the predicted mitoKv1.3-3FLAG plasmid. No presence of the predicted mitoKv1.3 is observed in the Jurkat-3F2M cell line after the proapoptotic stimuli.

Next, we measured the induction of apoptosis in our Jurkat clones after treatment with the pro-apoptotic stimuli staurosporine to test whether the deletion of the entire Kv1.3 gene in the KO clone might confer some resistance to apoptosis in this clone (Figure R44). However, no significant differences were observed between the clones suggesting no role of Kv1.3 in regulating staurosporin induced apoptosis in our model.

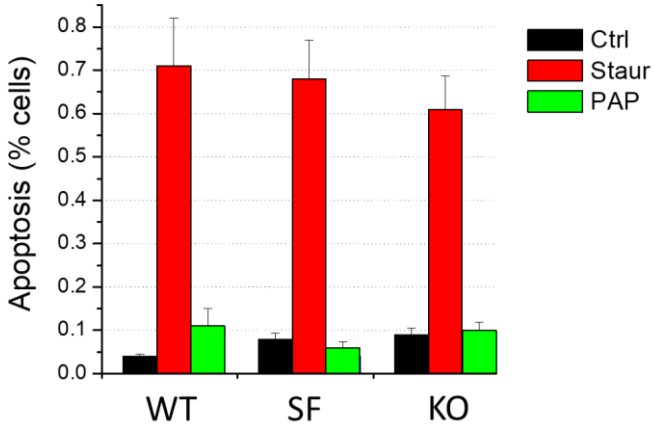

Figure R 44 Apoptosis induction in WT, SF, and KO was measured by detecting Caspase 3/9 cleavage 24 hours after stimulation. The results demonstrate increased apoptosis in all samples when treated with Staurosporine, but not with PAP-1 (Kv1.3 inhibitor). The differences in apoptosis induction among the three compounds under Staurosporine treatment were not statistically significant. The experiment was conducted with technical and biological triplicates.

The previous results suggested that the predicted mitoKv1.3 isoform was not being translated in our cells, or at least we were not able to detect it. We decided to clone the predicted mitoKv1.3 isoform (S4-S5-P loop - S6) and only the S4 fragment (predicted mitochondrial targeting sequence) into an EGFP plasmid and use confocal microscopy to localize the truncated proteins inside the cells. (Figure R45)

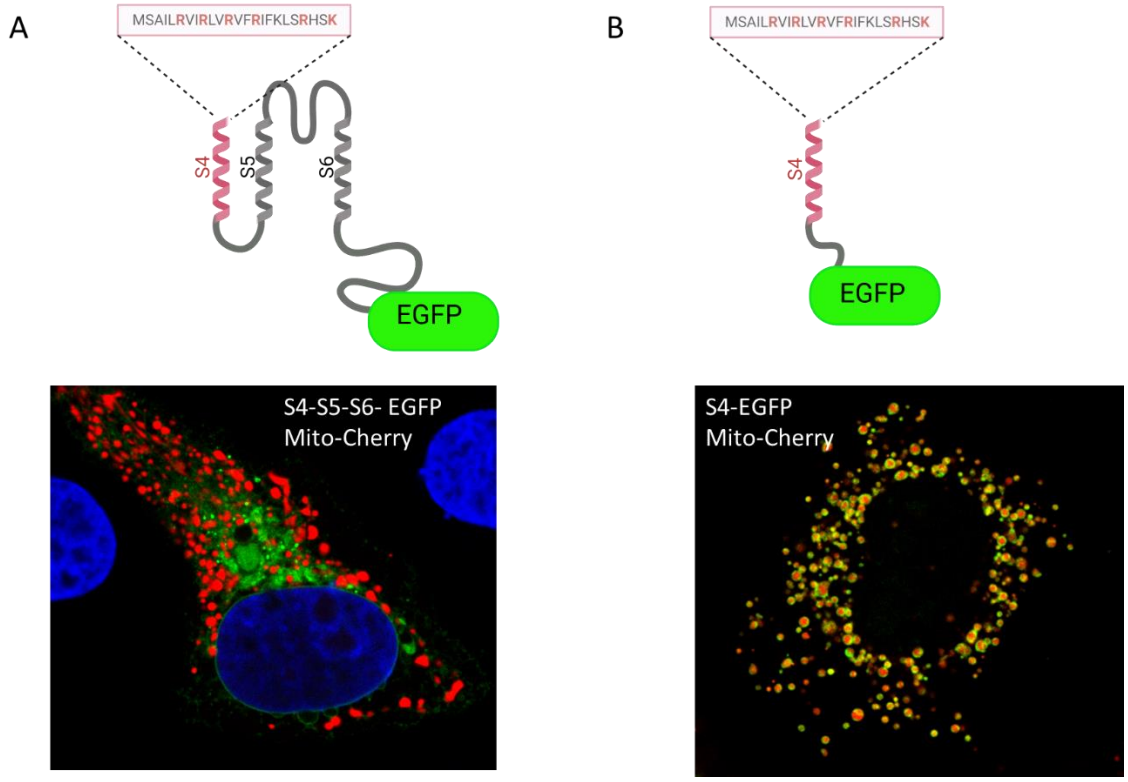

Figure R 45 Confocal microscopy image of transfected HEK cells highlighting the location of the predicted mitoKv1.3 ***(A)*** *and the S4 fragment of Kv1.3 alone fused to a EGFP* ***(B).*** *Mitochondria is shown in Red and the mitoKv1.3 protein* ***(A)*** *and the S4* ***(B)*** *are shown in green.*

Surprisingly, while the S4 cherry plasmid showed a clear mitochondrial localization, the mitoKv1.3 plasmid (S4-S5-P loop - S6 cherry) was not imported into the mitochondria. These results confirm that that the S4 fragment can be recognized by the cells as a mitochondrial targeting signal that can direct proteins (EGFP in this case) to the mitochondria. However, but when the rest of the channel is expressed (S4 to S6), the cell does not import this protein protein into the mitochondria. This unexpected result could be partially explained by the topology of both proteins, it has been previously reported in the literature that the S4 fragment alone can be integrated into a membrane with an efficiency of 92% (51), however transmembrane interactions, between S4-S5 and S6, could manifest as an altered protein conformation at the mitochondria, this hypothesis would be explained in more detail in the discussion section of this thesis.

5.6 Generation of complete KO Kv1.3 Mice.

As explained in section 5.3 of this thesis, the commercially available Kv1.3 KO mice still express SF (7). The knockout mice were generated by deleting the 5p region of the kcna3 gene, leaving the sequence encoding SF intact in the exon. We were able to observe how SF mRNA was expressed in the mice (Figure R21), but we were not sure about the implications of this isoform in the physiology of the mice, so we decided to generate a complete KO mouse by deleting the entire exon of Kv1.3.

To do this, we designed a strategy using CRISPOR to select two gRNAs, one at the beginning and one at the end of the KCNA3 gene. A single-stranded oligo was designed by fusing the 5P region (before the START codon) and the 3P region (after the STOP codon) of the gene to promote homologous recombination and enhance the complete deletion of the gene (Figure R46).

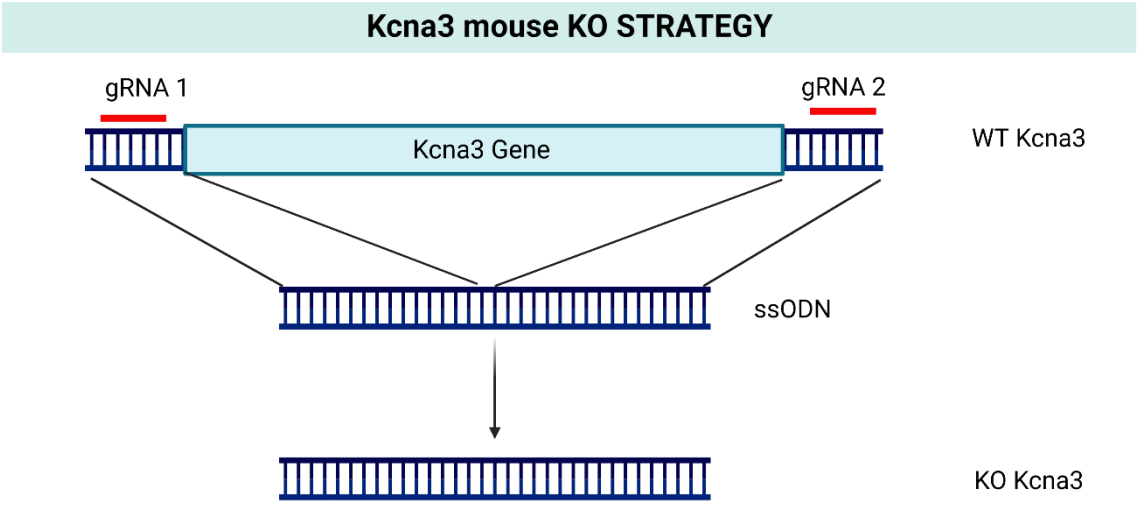

Figure R 46 Strategy performed to create a total Kv1.3 KO mice. 2 gRNA were selected at the beginning and at the end of the Kcna3 gene. A single stranded oligonucleotide was designed to promote homologous recombination between the ends of the gene facilitating the complete gene deletion.

The efficiency of selected gRNAs was tested using a T7 assay. The T7 endonuclease recognises and cleaves structural deformities in DNA heteroduplexes formed as a result of non-homologous end joining (NHEJ) repair

after a CRISPR-Cas9 experiment (Figure R47A). Murine Raw 264.7 cells were transfected with our designed gRNAs directed to the Kcna3 gene. DNA was purified and PCR was performed to amplify the Kcna3 gene. After, T7 assay was performed on the Kcna3 PCR product to determine the efficacy of each gRNA. The intensity of each band allowed us to calculate the gene editing percentage of our selected gRNAs, which was 51% for the 5P gRNA and 70% for the 3P gRNA (Figure R47B).

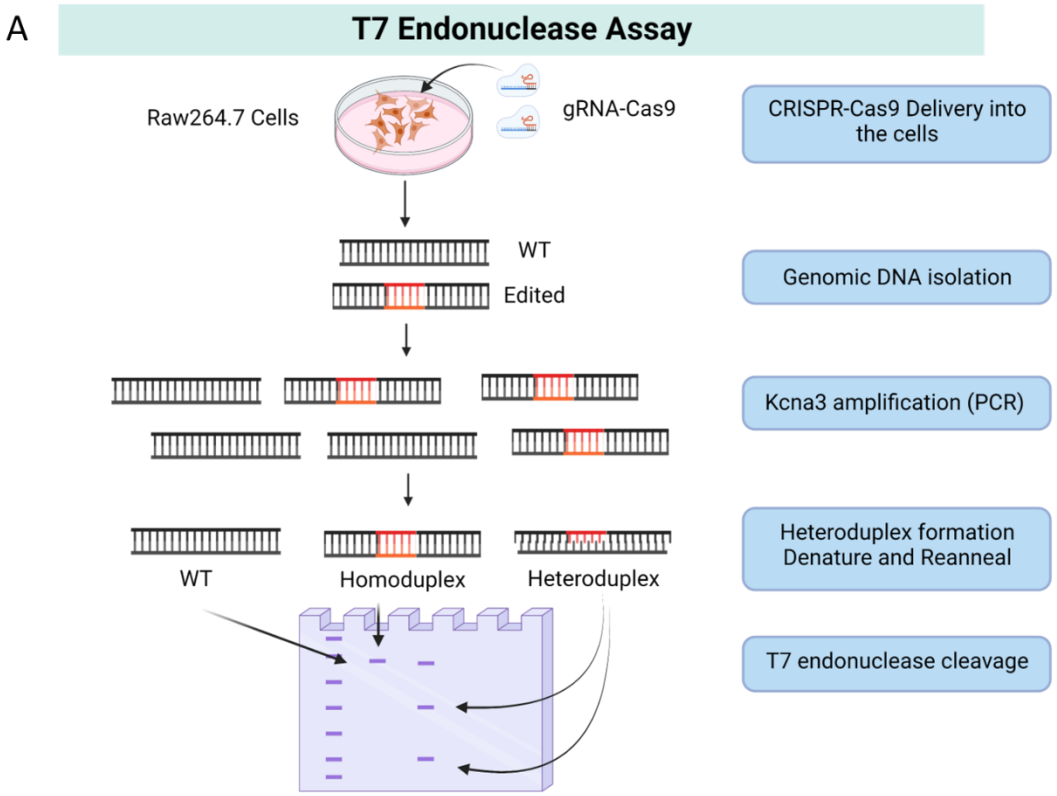

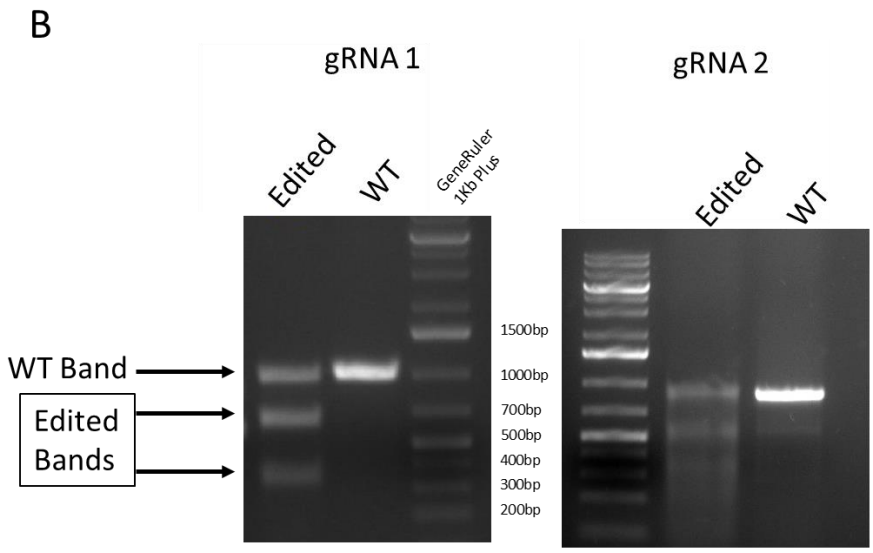

Figure R 47 ***(A)*** *Illustration showing the working principle of the T7 assay for CRISPR gRNA-mediated DNA cleavage.* ***(B)*** *Agarose gel electrophoresis image depicting a T7 assay to determine the cleavage efficacy of CRISPR gRNAs selected on the Kcna3 exont. The presence of cleaved DNA bands confirms the successful targeting and cutting by the gRNAs.*

After confirming the efficacy of our selected gRNA, the KO mice were generated by microinjecting the CRISPR components into mouse embryos at the University of Salamanca facility.

Three edited mice were obtained from 19 mice tested. Only one of them was edited with the correct sequence and showed a complete deletion of Kv1.3 in one of the exons (Figure R48).

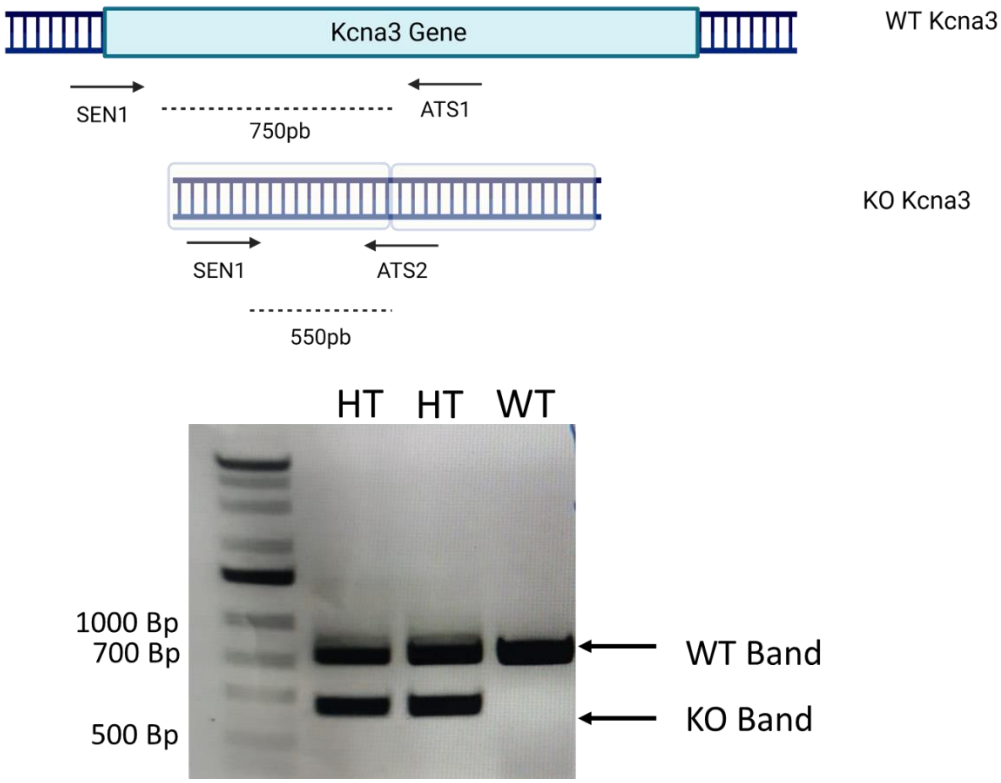

Figure R 48 Agarose gel of a PCR amplifying the Kcna3 gene in Kv1.3 edited mouse using specific primers for Kcna3 gene. HT means for Heterozygous mice that present one allele WT and one allele KO for Kv1.3.

This mouse was crossed with a C57B6 WT mouse to establish a pure background for 3 generations. Finally, a homozygous mouse was generated by crossing two heterozygous F3 mice. At the moment of writing this work we are in the process of obtaining enough homozygous mice in this controlled background to start characterizing them.

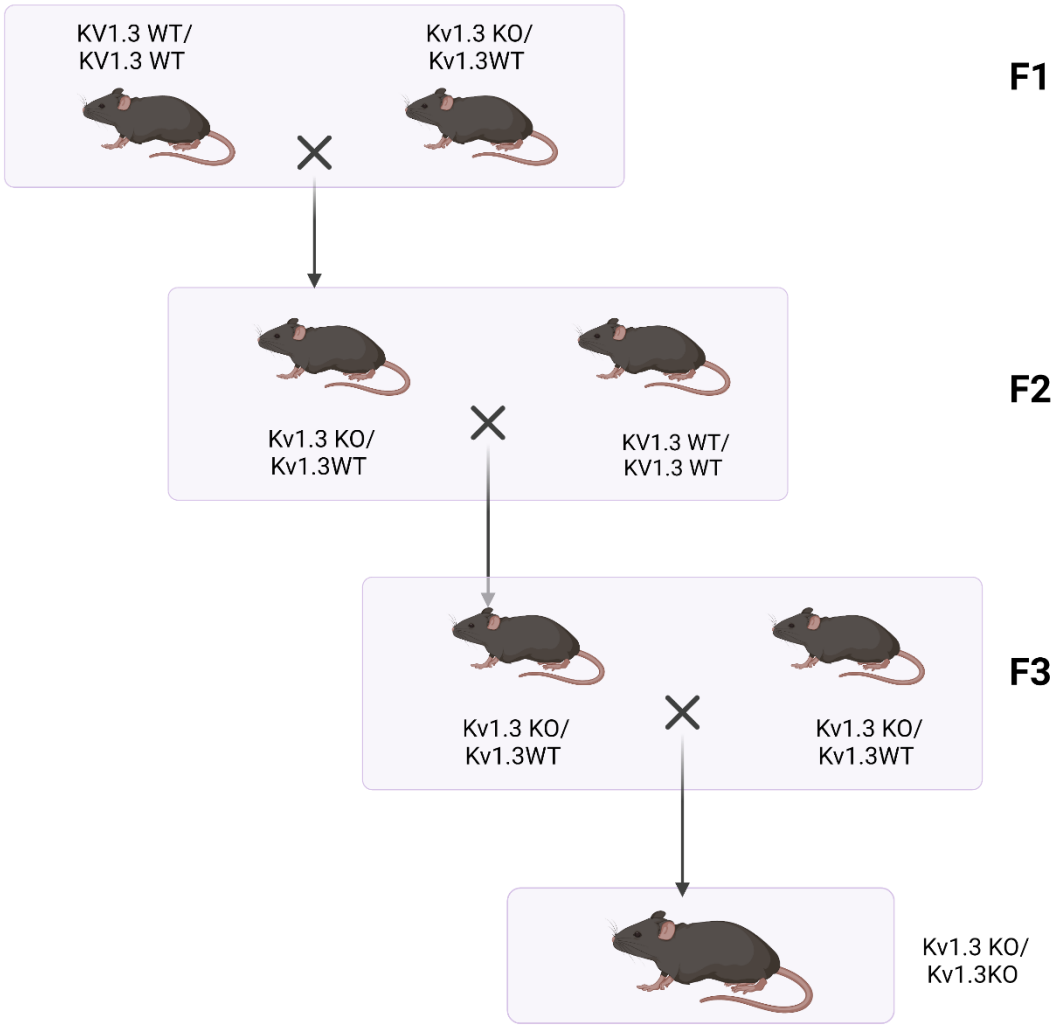

Figure R 49 Strategy of crossbreed performed for the obtention of a pure background Kv1.3 Knock-out mice from our heterozygous mice.

Discussion

6. Discussion

6.1 Tools for Kv1.3 channels study and their limitations

Lack of reliable antibodies against Kv1.3 have prevented its accurate detection under endogenous conditions. This has compelled the researchers to study Kv1.3 channel using heterologous models. In T cells that also express native channels, the overexpression of Kv1.3 WT or mutant channels has led to discrepancies that may affect the results. Moreover, because the majority of available antibodies lack specificity, using Kv1.3 antibodies as the only method to verify Kv1.3 functional expression led to confusing results. There are technical difficulties limiting the development of better Kv channels antibodies. The tiny surface loops on the channels have low immunogenicity, and their membrane architecture (multi-pass regions and multimeric structures) and high family-level amino acid conservation (which promotes immunological tolerance in host animals) make it challenging to develop a viable antibody against them (138,139).

In this thesis, we demonstrate that the use of gene-editing tools to obtain endogenously labelled Kv1.3 channels represents a powerful tool to elucidate channel function, providing unambiguous data on expression and location. Our laboratory have previously shown that in heterologous expression systems, the C-terminal fusion proteins had no effect on the expression, kinetics or regulation of the Kv1.3 channel protein (140). In our knock-in Jurkat clones, electrophysiological analysis revealed no differences in current amplitude, dynamics or response to stimulation compared to WT Jurkat.

Our strategy to generate the tagged Jurkat forced us to perform a limiting dilution step to isolate monoclonal cells edited with the correct tag sequence. The isolation of single clones is a potential limitation of this study, as single clones may behave differently from the multiclonal WT population. To minimize the impact of this limitation, we generated the KO and SF clones from the same monoclonal tagged WT (Jurkat-3Flag2Myc) and characterized at least 2-3 different clones from each construct so that any observed variances are likely attributed solely to the modified channel (or its absence in the KO).

The use of Jurkat cells as a study model represents another limitation of this work, as the expression of Kv1.3 in Jurkat cells is lower than in other T cells. Although Jurkat T cells are the most commonly used cell line to study T cells, the role of potassium channels may be attenuated in this cell line, obscuring potential results when compared to native T cells. In Jurkat, KCa currents were dominated by apamin-sensitive KCa2.2 channels, whereas only KCa3.1 currents are detected in healthy T cells and other leukaemic cell lines such as CEM and MOLT-3 cells (141). These data suggest that Jurkat cells may represent a special case and call for more extensive studies on primary leukaemic T cell lines. However, at the time we started this work, no efficient strategies had been developed to perform a knock-in tag in a primary T cell line sample. Furthermore, the CEM and MOLT-3 cell lines could have also served as suitable models for our study. However, there is limited literature available regarding the function of Kv1.3 in these cell lines, as most previous studies investigating Kv1.3 have been conducted using Jurkat cells. Considering the extensive body of knowledge and established protocols for Kv1.3 studies in Jurkat cells, we opted to utilize this cell line, while recognizing the limitations inherent to each model. The choice of Jurkat cells allowed us to build upon existing research and leverage the wealth of information available on Kv1.3 in this particular cell line. Nonetheless, future investigations exploring the function and regulation of Kv1.3 in other cell lines, such as CEM and MOLT-3, could provide valuable insights and enhance our understanding of the broader implications of Kv1.3 in different cellular contexts.

T cells are extremely difficult to transfect, so to overcome this limitation we decided to use a strategy that combines nucleofection to deliver the Cas9 components and AAV6 transduction, which has been described to have the greatest ability to transduce T cells (142), to deliver the donor DNA into the cells. Our strategy was shown to be efficient in modifying Jurkat T cells, and future studies in the laboratory will attempt to optimize the same strategy in primary T cells to obtain a population of human derived, healthy Kv1.3 tagged T cells that would allow the role of Kv1.3 to be studied under more native conditions. Similar strategy has been recently published but would need to be fine-tuned to have a high percentage of correctly edited cells for the detection of all potential isoforms.

This methodology was unfortunately outside the time frame available for this thesis (143).

6.2 Endogenous Kv1.3 channels express different isoforms.

We found endogenous expression of different Kv1.3 isoforms through alternative translation initiation sites that differ from the annotated AUG start codon.

Eukaryotic mRNAs were historically thought to rely exclusively on recognition and binding of their 5′ cap by initiation factors to effect protein translation. The canonical initiation of translation in eukaryotes begins with the recognition of the mRNA's 5' cap structure by the eukaryotic initiation factor 4F (eIF4F) complex. The eIF4F complex, facilitates the binding of the small ribosomal subunit (40S) to the mRNA. Once the 40S subunit is positioned on the mRNA, it scans the mRNA in a 5' to 3' direction until it encounters the start codon (AUG) within a favorable sequence context. The scanning process is facilitated by additional initiation factors. Upon recognition of the start codon, the eukaryotic initiation factors dissociate, and the large ribosomal subunit (60S) joins the complex, forming the 80S initiation complex. This marks the transition from initiation to the elongation phase of translation, where the ribosome synthesizes the polypeptide chain based on the mRNA's coding sequence (144) (Figure D1).

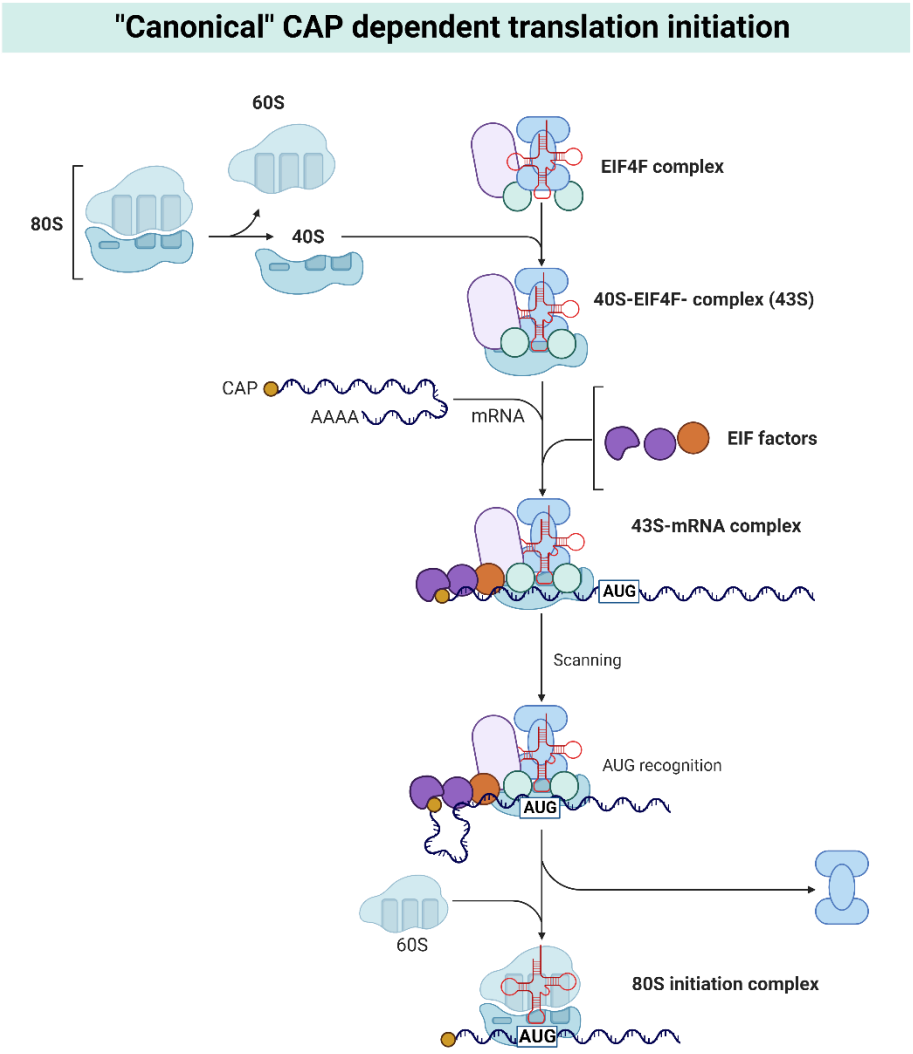

Figure D 1 The process of translation initiation in eukaryotic cells involves multiple steps and regulatory factors. This simplified illustration provides an overview of the main steps involved in translation initiation in eukaryotic cells. Detailed regulatory mechanisms and additional factors are not shown for simplicity.

While internal ribosome entry sites (IRESs) have been widely recognized as essential for cap-independent translation in many viral genomes, emerging evidence suggests that eukaryotic transcripts exhibit alternative translation initiation mechanisms. In recent years, it has become increasingly evident that non-canonical modes of translation initiation are not limited to viral genomes and that eukaryotic mRNAs can also undergo such processes. High-throughput

assays have identified thousands of mammalian transcripts with translation initiation occurring at non-canonical start codons, upstream of and within protein coding regions(145–147). In addition to IRES-mediated events, regulatory mechanisms of translation initiation have been described involving alternate 5′ cap recognition, mRNA sequence elements, and ribosome selection (148)

These mechanisms ensure translation of specific mRNAs under conditions where canonical cap-dependent translation is shut down and contribute to pathological states including viral infections, cardiac hypertrophy, and cancer (149,150).

The mechanisms governing the selection of start codons in mammalian cells are still not well understood. There are a small but growing number of mammalian mRNAs that start translation from a downstream in-frame AUG (or even a non-AUG codon), producing N-terminally truncated protein isoforms with various functional characteristics, this is the case of several growing factors like the fibroblast growth factor 2 (FGF2) and the vascular endothelial growth factor (VEGF) or numerous stress-induced proteins like the Stress-Activated Protein Kinase MK2 (130,151,152). The phosphatase and tensin homolog on chromosome ten (PTEN) is a tumor suppressor and an antagonist of the phosphoinositide-3 kinase (PI3K) pathway in which a translational variant, termed PTEN-Long, was identified from an alternative translation start site upstream of the ATG initiation sequence, adding 173 N-terminal amino acids to the normal PTEN open reading frame. PTEN-Long was described as a membrane-permeable lipid phosphatase secreted from cells and with the ability to enter other cells (153).

As a mechanism for protein function diversity, alternative translation generate protein isoforms which in most cases are targeted at different subcellular localizations, but maintained the same domain contents as the full-length isoforms (127). *Cai et al.* found that 85.7% of alternative translation events generated biological diversity, attributed to different subcellular localizations. **This is consistent with our data that showed non-overlapping locations for LF and SF isoforms** and it has also been reported for some other ion channels as the OraI channel (128–130).

In summary, the literature indicates that alternative translation start sites can be used to (i) compensate for inefficient translation from closely located start codons, resulting in the synthesis of slightly longer protein isoforms, (ii) direct the additional synthesis of N-truncated protein isoforms which exhibit distinct functional features such as altered subcellular localization. In the case of Kv1.3, we observed both types of isoforms: those initiating at M1 and M54, which share a similar structure but differ by 54 amino acids at the N-terminal region, and the isoform starting at Met197 (M2), which is a N-terminal truncated protein with a distinct subcellular localization.

It is possible that the presence of different isoforms is a common feature among all members of the Kv1 family, as they share high homology. To investigate this possibility, we performed a sequence alignment of all Kv1 channels and discovered that the Kv1.3 M2 methionine (which serves as the start codon for the SF isoform) is conserved in Kv1.1, Kv1.2, Kv1.5, and Kv1.10 channels (see figure xx). While the existence of a short isoform in these channels requires experimental confirmation, it is noteworthy that KCNA genes are ancient genes found in bacteria and archaea, and the expression of multiple isoforms from a single mRNA could represent an evolutionary remnant in mammalian cells. Moreover, it has been reported that other families of voltage-dependent potassium channels, such as the Voltage-activated human ether-á-go-go–related gene (hERG) family, which exhibit greater genomic structural complexity, can generate isoforms that bear structural similarities to our SF isoform. These isoforms are regulated by alternative splicing (154).

The M2 methionine is located at amino acid position 194, resulting in a protein missing 194 amino acids from the N-terminus when compared to the M0 and M1 proteins. M2 protein lacks two important channel regions, the tetramerization domain (T1) and the caveolin binding domain. T1 has been described as essential for tetramerization between the four subunits, but our heterologous experiments indicate that under heterologous conditions the SF can tetramerize and form channels at the plasma membrane, but at a less efficient rate than the FL channel. These results suggest that in heterologous systems the T1 is not essential for the channel to tetramerize. In these experiments, HEK cells were used to transfect SF Kv1.3 plasmids. HEK cells endogenously express other Kv1

channels different from Kv1.3, we showed how potassium currents were reduced when siRNAs against other Kv1 channels were co-transfected suggesting than SF of Kv1.3 could form heterotetramers with other family members of Kv1. The recorded currents in HEK cells transfected with SFSF was partially located at the plasma membrane, however, as showed in the fluoresce microscopy studies, the plasma membrane was not the preferential location of the SF. The SF was mainly located intracellular and in the nuclear membrane. The caveolin binding domain at the N-terminal of Kv1.3 was described to be important to regulate the targeting of the channel to the plasma membrane (11,12), the lack of this domain in the SF could partially explain why the SF is not preferentially delivered to the plasma membrane.

In Jurkat cells, no Kv1.3 current was found either in the KO clones or in the SF. These data suggest that under endogenous conditions SF does not form ion channels or that these ion channels are not located at the plasma membrane but in some intracellular organelles or in the nuclear membrane. The presence of Kv1.3 at the nucleus of cells was previously described (157). To determine whether SF formed channels in the nuclear membrane, we attempted to isolate nuclei from Jurkat cells and perform patch clamp experiments in these nuclei. However, while we were able to isolate well-preserved nuclei and perform patch clamp experiments on them, the outer membrane of the nuclei was consistently lost during the extraction process, making it impossible to record a current that we could unequivocally attribute to Kv1.3 (Figure D2).

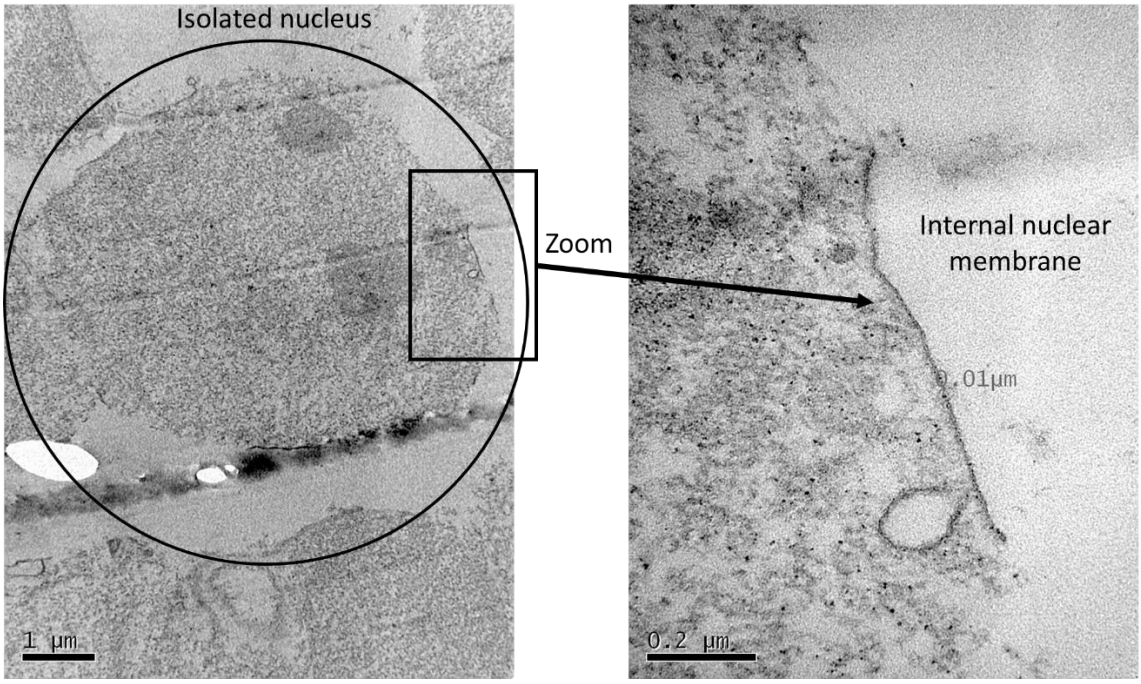

Figure D 2 Transmission electron microscopy showing a preparation of Jurkat isolated nucleus. Only the internal membrane is present in the preparation.

Further studies are needed to determine whether the SF forms a channel in the nuclear membrane of cells. As one of the main roles of Kv1.3 in the plasma membrane is the regulation of cell volume, the hypothesis that the SF could also regulate nuclear volume is interesting, especially considering the importance of nuclear volume in immune cells. One of the unique characteristics of immune cells is their ability to migrate throughout the body. To this end, the nucleus plays a critical role, and its movement, positioning and deformation strongly impact cell migration (158). During cell migration, the movement of the nucleus must be coordinated with the cytoskeletal dynamics at the leading edge and trailing end (159). Nuclear morphology and biomechanics have already been described to be particularly important in the context of neutrophil migration during immune responses. Neutrophils have an especially deformable nucleus, and the nucleus is a key determinant of neutrophil migration (160).

The previous understanding of the nuclear envelope (NE) was extremely limited, reducing it to a mostly inactive physical barrier that served only to divide the cytoplasm from the nucleoplasm. However recent data in the literature is suggesting that NE has enormous importance in cellular physiology. It has been

suggested that the NE is a key integrator of both mechanical and chemical inputs and has been described as a sensor/transducer of these mechanical signals, enabling cells to precisely control gene transcription and cellular signaling (161).

Some nuclear ion channels have been described to have a role in regulating cellular signaling pathways. The calcium dependent potassium channel BKca was described to play a key role in regulating nuclear Ca^{2+} and NF-κB-p65 nuclear translocation in myometrial smooth muscle cells (162). Our data suggests that plasma membrane Kv1.3 isoforms contribute to regulation Ca^{2+} influx at the cytosol, it would be interesting to test if SF is implicated in the regulation of Ca^{2+} influx in the nucleus.

In T cells, it was described how upon antigen presentation, NE composition changes with lamin A and C being upregulated. This upregulation was described to accelerate the immunological synapse formation between T lymphocytes and antigen presenting cells (163). Despite the fact that ion channels at the NE have not received much attention specifically due to technical challenges, certain potassium channels have been reported (164). Nuclear KCa1.1 channels were described to regulate cAMP response element binding protein (CREB) phosphorylation in RAW264.7 macrophages (165).

Our data suggest that SF could be present at the nuclear membrane and have a role in immune synapsis formation, however further studies are required to fully characterize the SF present in the NE of lymphocytes and its functional role(s) at this location.

6.3 Regulation of Kv1.3 isoforms in Jurkat cells.

The expression of the three isoforms of Kv1.3 was extremely low in the resting state of Jurkat T cells and was **upregulated after treatment with T cell activation** stimuli (PMA+ionomycin, PHA-P and CD3+CD28) (Figure D3). This upregulation of Kv1.3 channel after antigen recognition was previously described in literature (87,122).

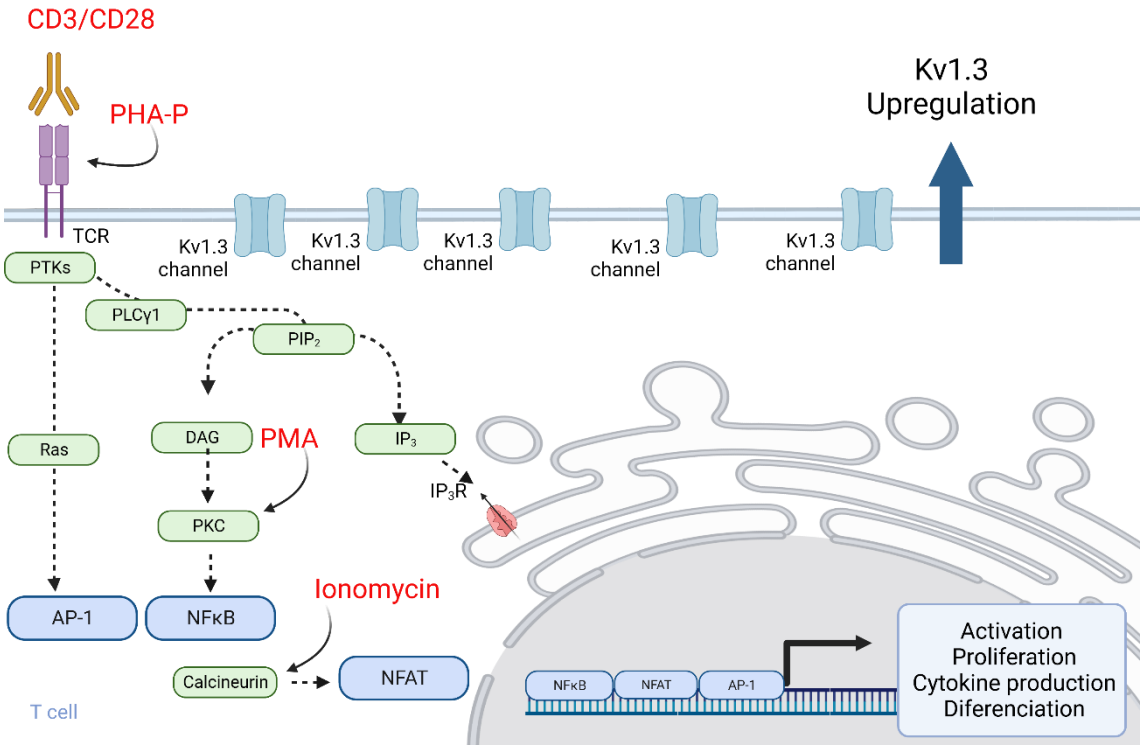

Figure D 3 Several T cell stimuli upregulated the expression of the three isoforms of Kv1.3. Stimuli tested are indicated in red.

Surprisingly, Thapsigargin (SERCA inhibitor) which was described as a pro-apoptotic stimuli for Jurkat T cells (123), was the strongest Kv1.3 up regulator of Kv1.3 isoforms, whereas other pro-apoptotic treatments had no effect on Kv1.3 expression. Thapsigargin is a potent inhibitor of the sarco/endoplasmic reticulum Ca^{2+}-ATPase (SERCA) pump, which leads to an increase in cytosolic calcium levels and the induction of endoplasmic reticulum (ER) stress (166).

ER stress is a cellular stress response that is activated when the ER is overwhelmed by unfolded or misfolded proteins, and it can lead to the activation of the unfolded protein response (UPR). ER stress promotes general inhibition of translation initiation to decrease the ER's protein folding load. Global translation suppression is accompanied by the targeted activation of translation for important UPR regulators and the transcription of downstream stress-response genes(167). Interestingly, **most of the genes upregulated during ER stress present non-canonical translation initiation** (Cap-independent translation), like the transcription factor ATF4 (167,168). Most of the genes

upregulated by thapsigargin are transcription factors or genes involved in apoptosis like ARF, p73, Apaf1, SEC24A(169,170).

As no other proapoptotic stimuli upregulated Kv1.3 expression we hypothesized that may the increase of intracellular calcium promoted by thapsigargin could be the signal to Kv1.3 upregulation. Calcium signaling is essential for T cell activation, several cytokines like IL-2 and proliferation factors are regulated by calcium related pathways in T cells. We found that in the absence of extracellular calcium Jurkat T cells were unable to upregulate Kv1.3, suggesting that calcium may be involved in the regulation of Kv1.3 in T cells. The regulation of Kv1.3 by calcium has not been previously described, but calcium regulates several genes associated with T-cell activation via the NFAT transcription factors (125). While Kv1.3 promoter poses the consensus NFAT binding sequence, the addition of Cyclosporin (NFAT pathway inhibitor) did not prevent Kv1.3 upregulation after thapsigargin treatment suggesting that Kv1.3 was not regulated by NFAT under our experimental conditions (Figure R.18). Further studies are necessary to fully comprehend the precise regulation of Kv1.3 by calcium. Based on our findings, we can conclude **that Thapsigargin is a potent up regulator of Kv1.3 channel isoforms**. However, it is still unclear whether this upregulation is a result of the increased intracellular calcium caused by Thapsigargin, by an unknown role of Kv1.3 in the UPR or by an unspecified effect of Thapsigargin in Jurkat Cells. Therefore, additional research is required to elucidate the underlying mechanism of Thapsigargin-induced upregulation of Kv1.3 channels. The utilization of alternative SERCA inhibitors, such as cyclopiazonic acid (CPA), could be advantageous. Unlike thapsigargin, CPA is a reversible inhibitor of SERCA that induces an intracellular Ca^{2+} increase but does not reportedly trigger the unfolded protein response (UPR). Exploring the use of CPA or other SERCA inhibitors may provide valuable insights into the regulation of Kv1.3 by calcium concentration without activating UPR pathways (171).

6.4 Contribution of Kv1.3 isoforms to T cell function.

The exact role of Kv1.3 in T cell function is still not well understood. Our data suggest that the **LF of Kv1.3 is responsible for controlling resting E_M in Jurkat T cells**. Knockout KO an SF clones exhibited a depolarized resting E_M Previous literature described that both Kv1.3 and KCa3.1 were essential to control the membrane potential after TCR activation. However, kinetic models have demonstrated that Kv1.3 primarily governs the membrane potential of T cells, thereby regulating Ca^{2+} influx through CRAC channels (172).

Kv1.3-mediated protein-protein interactions also control the activation of numerous signaling pathways in addition to regulating EM. In lipid rafts of Jurkat cells, Kv1.3 has been shown to co-localize with the TCR/CD3 complex and redistribute to the IS. (124,173,174). According to our results, only the **LF of Kv1.3 colocalizes with the TCR/CD3 complex**. Ion channels at the IS could contribute to regulate the local ion composition in the restricted volume of the synaptic space, modulating the function of voltage-gated channels and other molecules. In addition, Kv1.3 interaction with membrane associated proteins (such as integrin β or actin cytoskeleton), or kinases at the IS has also been reported to participate in activating signaling in T cells (175–178). The functional role of the mechanisms involving Kv1.3 in T cell activation is under debate. While certain studies associate the immunomodulatory effects of Kv1.3 channels in T cells with their capacity to regulate K^+ concentrations, as evidenced by the lack of effect observed with poreless mutant channels (179), alternative research indicates that non-conducting Kv1.3 channels can still fulfill a similar role to wild-type channels in immune synapse (IS) formation (173).

Unexpectedly, our Jurkat clones expressing only SF or even the KO cells maintained their capacity to perform effector functions including cytokine secretion. At the level of single cells, Kv1.3 channel blockers completely eliminate channel function. However, when functional readouts such as proliferation or cytokine production are used, only partial inhibition of T cell responses is observed, with highly variable results ranging from insignificant to more than 80%

block (135,180–182). The cytokine results obtained in our clones may be attributed to compensatory currents that were not investigated, as has been observed in other models. Recently, a study conducted on Kcna3-/- rats showed that Kv1.3 knockout T cells retained their effector function without any compromise. This was attributed to a compensatory upregulation of KCa3.1, which facilitated T cell proliferation and effector responses (183). However, this KCa3.1 seemed not to be upregulated in our Jurkat cells (data not shown). Moreover, other channel types apart from K^+ channels, (CRAC channels, or certain TRP channels such as TRPV1 or TRPM4) also have a role in T cell activation (184–186). Nonetheless, the lack of Kv1.3-induced significant alterations in cytokine secretion prompted us to investigate the involvement of Kv1.3 in intermediate signaling pathways.

After antigen presentation by the APC, TCR signal transduction is initiated by the phosphorylation of TCR and CD3 chains followed by recruitment and phosphorylation of the ZAP70 kinase. These early events are followed by the phosphorylation of adaptor molecules, regarded as signalling hubs for TCR signal diversification. LAT and SLP76, the best characterized adaptor molecules in T cells, exert their functions by mechanisms relying not only on the signalosomes formation but also on their specific location at the cell membrane (187,188). Phosphorylation of membrane-bound LAT activates PLCγ, Ras-MAPK pathway, and SLP76. pSLP76 is recruited to the IS, where it binds integrin VLA-4 (α4β1), stabilizes PLCγ and Ras-MAPK pathways and regulates other pathways dependent of VLA-4 ligation, including NFAT and NF-kB activation, cytokine production and proliferation (189). These effectors regulated cytoskeletal morphology, which is influenced by integrin ligation, hence, SLP76 represents an integrator for both TCR and integrins signals. (Figure D3)

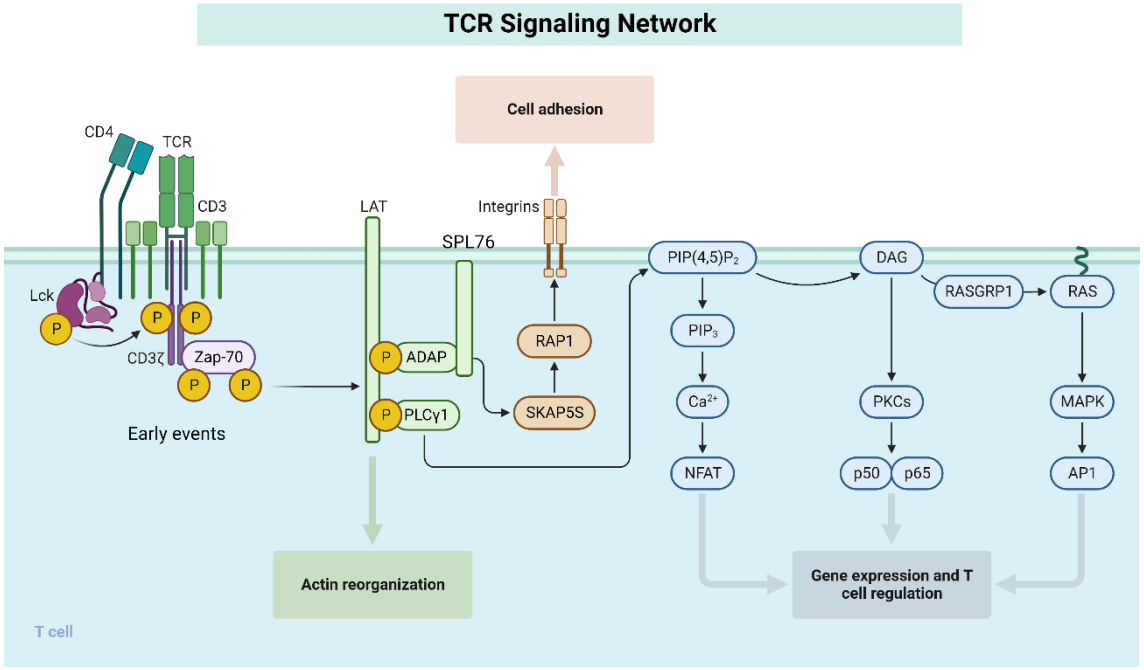

Figure D 4 This figure summarizes the key steps and molecules involved in the signaling cascade triggered by T lymphocyte activation. The intricate interplay of these signaling events orchestrates the immune response and subsequent T cell functions.

Like SLP76 and LAT, both the ion pore function and the subcellular localization of Kv1.3 channels appear to play a significant role in T cell activation at the immune synapse (IS). Our findings demonstrate that Kv1.3 channels play a distinct role in the investigated steps of signal transduction, with an intriguing differential contribution between the wild-type (WT) and (SF) isoforms. While Kv1.3 channels are not necessary for the proximal events of T cell receptor (TCR) signaling, such as CD3 or ZAP70 phosphorylation, they do participate in more distal events, including linker activation and the activation of various signaling pathways (such as PLCγ and ERK). Notably, while the intracellular SF isoform retains the functionality of WT-Kv1.3 in activating LAT, ERK, and PLCγ, it cannot fully substitute for Kv1.3's role in SLP76 recruitment. These results may indicate either the requirement of an ion-conducting channel at the cell membrane for SLP76 activation or the significance of protein localization. Further studies on the effect of a pore dead channel on SLP76 activation are needed to distinguish between these two possibilities. However, Kv1.3 channels have been previously described to associate with integrins contributing to actin polymerization (175–177), which is consistent with the importance of integrin binding for SLP76 translocation and activation.

While the absence of WT channels was found to alter the TCR-induced phosphorylation of certain signaling molecules, no significant changes in cytokine production by activated Jurkat or primary CD4+ T lymphocytes were detected in our samples. This could be due to the optimal conditions used for cytokine production, which may have masked partial inhibition. Dose-response experiments with different concentrations of stimuli could be an interesting approach or the isolation of the different subpopulations of CD4+T cells to distinguish if there is some inhibition in some of the subpopulations.

Nevertheless, we were able to confirm that these deficiencies in the TCR signaling pathways shown in the absence of WT-Kv1.3 led to altered IS formation. Although there were differences in protein phosphorylation observed between **SF and KO clones, both exhibited a significant decrease in the number and size of IS formed.** These changes may be attributed to alterations in molecular interactions and membrane potential.

6.5 Kv1.3 in mitochondria.

In addition to its expression at the plasma membrane, several studies have investigated the presence and function of the Kv1.3 channel in the inner mitochondrial membrane of both cancer cells and T cells. A PAP-1 and Margatoxin-sensitive K^+ current has been described in the mitochondria of these cells (131,132,190). This MitoKv1.3 has also been described to play a role in the regulation of apoptosis in various tumor cell types (70,71). In all cases, a protein of the same molecular weight as the canonical Kv1.3 channel was identified. However, in our research we were unable to detect WT Kv1.3 channels (or the LF or SF isoforms) in the mitochondria. Furthermore, no differences in apoptosis induction were found in our clones when comparing WT with SF or KO after treatment with staurosporin, suggesting that Kv1.3 does not play a role in apoptosis in these cells. While this result is consistent with previously published studies in adipocytes (191), some authors claim that inhibition of Kv1.3 in cancer cells promotes apoptosis (70,72).

The existence of at least three isoforms of Kv1.3 led us to hypothesize that mitochondrial Kv1.3 might exist as a different isoform from the other three previously described isoforms as different isoforms often results in different locations within the cell.

We found that the S4 transmembrane helix has the signature of the canonical MTS (an alternating pattern of hydrophobic and positively charged residues forming an amphipathic helix) and identified an in-frame AUG codon upstream of this region that could be used by the cell to generate a truncated isoform (mito-Kv1.3). This truncated isoform of Kv1.3 would contain only two alpha helices (S5-S6) and the p-loop, similar to the original 2TM potassium channel found in many bacteria and archaea and the Kir family. This truncated isoform would not be voltage dependent because the S4 fragment (sensor domain) would be cleaved after import into the mitochondria, and it would form a pore in the mitochondria. However, our Western blot analysis did not provide evidence for the existence of this predicted isoform in endogenous or heterologous processing of the Kv1.3 channel.

Moreover, from the colocalization studies overexpressing mito-Kv1.3 we conclude that if this truncated isoform were expressed, it will not be directed to the mitochondria. However, when we expressed the S4 alone, it was imported to the mitochondria. These results suggests that cells can recognize the S4 fragment as a mitochondrial targeting signal, but when the rest of the channel is expressed, the cell does not import the protein into the mitochondria. This unexpected result could be partially explained by the topology of both proteins, it has been previously reported in the literature that the S4 fragment alone can be integrated into a membrane with an efficiency of 92% (51), however transmembrane interactions, between S4-S5 and S6, could manifest as an altered protein conformation at the mitochondria.

Our results do not exclude the presence of some isoforms of Kv1.3 in the mitochondria, but we can conclude that none of the isoforms studied in this work has a preferential location for the mitochondria. Further studies, benefiting from the tools developed here, will be necessary to resolve this controversy.

6.6 Importance of the study of Kv1.3 in T cells and future perspectives.

Kv1.3 channels have been shown to play a significant role in T cell-mediated immune responses, making them a potential target for therapeutic intervention in autoimmune disorders. To date, autoimmune disorders affect a significant proportion of the population and can cause significant morbidity and mortality. Rheumatoid arthritis, multiple sclerosis, and type 1 diabetes are all autoimmune disorders that can significantly impact quality of life and reduce life expectancy. Although Kv1.3 inhibitors did not block IS formation (135), they have been shown to decrease Ca^{2+}-induced pathways in TEM cells of animal models and patients with multiple sclerosis, rheumatoid arthritis and type I diabetes (135,192,193) offering an opportunity to ameliorate autoimmune responses. There are several mechanisms that connect the functional expression of Kv1.3 channels to T cell responses, but their specific roles in pathophysiological conditions remain unclear. A better understanding of these mechanisms would be useful in designing more precise and effective therapeutic tools. By gaining a deeper understanding of these processes, researchers can develop therapies that target specific mechanisms and improve outcomes for patients with autoimmune diseases.

Moreover, Kv1.3 has also been implicated in various aspects of cancer biology. It has been recognized as a potential therapeutic target due to its involvement in cancer progression and metastasis. Kv1.3 channels has been described to be upregulated in cancer cells, and their activity has been linked to cell proliferation and survival. An increased expression of Kv1.3 channels was observed in the case of breast, colon, smooth muscle, skeletal muscle and lymph node cancer and in mature neoplastic B cells in chronic lymphocytic leukemia (194). Inhibition of Kv1.3 channels has been shown to reduce cancer cell growth and induce apoptosis in vitro and in vivo mice models (70–72,195). Understanding the role of Kv1.3 in cancer provides insights into its potential as a therapeutic target for cancer treatment. Targeting Kv1.3 channels may offer opportunities to develop

novel anti-cancer strategies aimed at inhibiting cancer cell proliferation, migration, and invasion, as well as overcoming drug resistance.

In this thesis we have described for the first time the endogenous expression of several Kv1.3 channel isoforms in Jurkat cells, showing different location and functional contribution to cell signaling. In particular, the effects on TCR signal transduction of the SF evidence that some of the functions of Kv1.3 channels do not require their presence at the plasma membrane. Altogether, we have developed a powerful tool for exploring regulation of endogenous channels translation and trafficking. On a more general aspect, we demonstrated that, despite being encoding by a single exon, KCNA3 gene gives rise to several isoforms with different location and function, uncovering a previously overlooked mechanism to increase protein diversity. Given the high homology among Kv1 subfamily members, this could represent a conserved mechanism for other Kv channels.

This work also opens future lines of investigation for our laboratory. The role of Kv1.3 channel isoforms needs to be studied in more physiological models, for which the generation of knock-in (KI) in primary T cells will be attempted, and a total Kv1.3 knockout (KO) mouse has been generated with a pure C57B6 background. In this mouse model, the complete exon of Kv1.3 has been deleted, thereby eliminating all potential isoforms. This model will allow validation of the data obtained here in an animal model and enable us to study the influence of Kv1.3 isoforms on different populations of T lymphocytes and in other cell types of interest.

Conclusions

7. Conclusions

1. **Generation of Jurkat KI cell lines for Kv1.3, Kv1.3-3Flag2Myc, enabled us to accurately locate the endogenous protein.**

2. **The KCNA3 coding region contains at least three alternative translation initiation sites and produced at least three different isoforms.**

   2.1 The longest isoform (starting at Met1) would result in a longer N-terminus channel, located at the plasma membrane which is present in human and in various species except for rats and mice.

   2.2 The isoform starting at methionine 53 (M1 or LF) was considered the canonical Kv1.3 in literature, is conserved across species including mouse and rat. It is located at the plasma membrane, and it form functional Kv1.3 channels. It is essential to control cell proliferation in HEK cells.

   2.3 Isoform starting in methionine 194 (M2 or SF) is a N-terminal truncated isoform that conserve intact the six transmembrane helix and the C terminal of the protein. This isoform is located intracellular, and it does not form functional channels at the plasma membrane. It is highly conserved in various species and other KCNA channels. The commercially available KO mice from Jacksonville could express this protein.

3. **The three isoforms of Kv1.3 were upregulated upon T cell activation stimuli AND** thapsigargin treatment, while pro-apoptotic stimuli had minimal effects on their expression.

4. **LF (long form) was predominantly expressed at the plasma membrane, while SF was found intracellularly in the nuclear membrane and ER, with no observed interaction between the two forms in HEK cells.**

5. **None of the Kv1.3 isoforms preferentially localized to mitochondria.**

6. SF of Kv1.3 may form heteromultimers with other members of the Kv1 family.

7. **Resting membrane potential (E_M) and Ca^{2+} influx in T cells is regulated by the membrane isoforms of Kv1.3.**

8. **Different Kv1.3 isoforms contribute differently to the early steps of T cell activation after TCR stimulation.** However, Kv1.3 channels do not participate in stimulus-induced cytokine secretion in our system.

9. LF of Kv1.3 is recruited to the immune synapse (IS) upon Raji exposure, while SF is not recruited. **Full activation and effective recruitment of LAT at the IS require WT Kv1.3 channels.**

10. A total knockout (KO) mouse model for Kv1.3 was successfully generated.

8. References

1. Jiménez-Pérez L, Cidad P, Álvarez-Miguel I, Santos-Hipólito A, Torres-Merino R, Alonso E, et al. Molecular Determinants of Kv1.3 Potassium Channels-induced Proliferation. J Biol Chem. 2016 Feb 12;291(7):3569–80.

2. Moran Y, Barzilai MG, Liebeskind BJ, Zakon HH. Evolution of voltage-gated ion channels at the emergence of Metazoa. Anderson PAV, editor. J Exp Biol. 2015 Feb 15;218(4):515–25.

3. Durell SR, Hao Y, Nakamura T, Bakker EP, Guy HR. Evolutionary Relationship between K+ Channels and Symporters. Biophys J. 1999 Aug 1;77(2):775–88.

4. Anderson PAV, Greenberg RM. Phylogeny of ion channels: clues to structure and function. Comp Biochem Physiol B Biochem Mol Biol. 2001 May 1;129(1):17–28.

5. Schrempf H, Schmidt O, Kümmerlen R, Hinnah S, Müller D, Betzler M, et al. A prokaryotic potassium ion channel with two predicted transmembrane segments from Streptomyces lividans. EMBO J. 1995 Nov 1;14(21):5170–8.

6. Doyle DA, Cabral JM, Pfuetzner RA, Kuo A, Gulbis JM, Cohen SL, et al. The Structure of the Potassium Channel: Molecular Basis of K+ Conduction and Selectivity. Science. 1998 Apr 3;280(5360):69–77.

7. Murata Y, Iwasaki H, Sasaki M, Inaba K, Okamura Y. Phosphoinositide phosphatase activity coupled to an intrinsic voltage sensor. Nature. 2005 Jun;435(7046):1239–43.

8. Ramsey IS, Moran MM, Chong JA, Clapham DE. A voltage-gated proton-selective channel lacking the pore domain. Nature. 2006 Apr;440(7088):1213–6.

9. Pongs O. Molecular biology of voltage-dependent potassium channels. Physiol Rev [Internet]. 1992 Oct 1 [cited 2023 Feb 23]; Available from: https://journals.physiology.org/doi/10.1152/physrev.1992.72.suppl_4.S69

10. Salkoff L, Baker K, Butler A, Covarrubias M, Pak MD, Wei A. An essential 'set' of K+ channels conserved in flies, mice and humans. Trends Neurosci. 1992 May 1;15(5):161–6.

11. Butler A, Wei A, Baker K, Salkoff L. A Family of Putative Potassium Channel Genes in Drosophila. Science. 1989 Feb 17;243(4893):943–7.

12. Catterall WA, Lenaeus MJ, Gamal El-Din TM. Structure and Pharmacology of Voltage-Gated Sodium and Calcium Channels. Annu Rev Pharmacol Toxicol. 2020;60(1):133–54.

13. Strong M, Chandy KG, Gutman GA. Molecular evolution of voltage-sensitive ion channel genes: on the origins of electrical excitability. Mol Biol Evol. 1993 Jan 1;10(1):221–42.

14. Nowycky MC, Fox AP, Tsien RW. Three types of neuronal calcium channel with different calcium agonist sensitivity. Nature. 1985 Aug;316(6027):440–3.

15. Catterall WA. Voltage-Gated Calcium Channels. Cold Spring Harb Perspect Biol. 2011 Jan 8;3(8):a003947.

16. Santiago AR, Carvalho CM, Carvalho AP, Ambrósio AF. Differential contribution of L-, N-, and P/Q-type calcium channels to [Ca2+]i changes evoked by kainate in hippocampal neurons. Neurochem Res. 2008 Aug;33(8):1501–8.

17. Catterall WA. Forty Years of Sodium Channels: Structure, Function, Pharmacology, and Epilepsy. Neurochem Res. 2017 Sep 1;42(9):2495–504.

18. Hibino H, Inanobe A, Furutani K, Murakami S, Findlay I, Kurachi Y. Inwardly rectifying potassium channels: their structure, function, and physiological roles. Physiol Rev. 2010 Jan;90(1):291–366.

19. Inanobe A, Matsuura T, Nakagawa A, Kurachi Y. Structural diversity in the cytoplasmic region of G protein-gated inward rectifier K+ channels. Channels Austin Tex. 2007;1(1):39–45.

20. Glaaser IW, Slesinger PA. Structural Insights into GIRK Channel Function. Int Rev Neurobiol. 2015;123:117–60.

21. Martin GM, Patton BL, Shyng SL. KATP channels in focus: Progress toward a structural understanding of ligand regulation. Curr Opin Struct Biol. 2023 Apr;79:102541.

22. Isomoto S, Kondo C, Kurachi Y. Inwardly rectifying potassium channels: their molecular heterogeneity and function. Jpn J Physiol. 1997 Feb;47(1):11–39.

23. Renigunta V, Schlichthörl G, Daut J. Much more than a leak: structure and function of K_2p-channels. Pflugers Arch. 2015 May;467(5):867–94.

24. Miller AN, Long SB. Crystal structure of the human two-pore domain potassium channel K2P1. Science. 2012 Jan 27;335(6067):432–6.

25. Braun AP. Two-pore domain potassium channels. Channels. 2012 May 1;6(3):139–40.

26. Bocksteins E. Kv5, Kv6, Kv8, and Kv9 subunits: No simple silent bystanders. J Gen Physiol. 2016 Feb;147(2):105–25.

27. Kv8.1, a new neuronal potassium channel subunit with specific inhibitory properties towards Shab and Shaw channels. | DrugBank Online [Internet]. [cited 2023 Mar 6]. Available from: https://go.drugbank.com/articles/A143623

28. Sano Y, Mochizuki S, Miyake A, Kitada C, Inamura K, Yokoi H, et al. Molecular cloning and characterization of Kv6.3, a novel modulatory subunit for voltage-gated K(+) channel Kv2.1. FEBS Lett. 2002 Feb 13;512(1–3):230–4.

29. Vergara C, Latorre R, Marrion NV, Adelman JP. Calcium-activated potassium channels. Curr Opin Neurobiol. 1998 Jun;8(3):321–9.

30. Sancho M, Kyle BD. The Large-Conductance, Calcium-Activated Potassium Channel: A Big Key Regulator of Cell Physiology. Front Physiol [Internet]. 2021 [cited 2023 Mar 6];12. Available from: https://www.frontiersin.org/articles/10.3389/fphys.2021.750615

31. Wallner M, Meera P, Toro L. Determinant for beta-subunit regulation in high-conductance voltage-activated and Ca(2+)-sensitive K+ channels: an additional transmembrane region at the N terminus. Proc Natl Acad Sci U S A. 1996 Dec 10;93(25):14922–7.

32. Latorre R, Castillo K, Carrasquel-Ursulaez W, Sepulveda RV, Gonzalez-Nilo F, Gonzalez C, et al. Molecular Determinants of BK Channel Functional Diversity and Functioning. Physiol Rev. 2017 Jan;97(1):39–87.

33. Zahra A, Liu R, Han W, Meng H, Wan Q, Wang Y, et al. KCa-Related Neurological Disorders: Phenotypic Spectrum and Therapeutic Indications. Curr Neuropharmacol. 2022 Dec 8;

34. Köhler R, Kaistha BP, Wulff H. Vascular KCa-channels as therapeutic targets in hypertension and restenosis disease. Expert Opin Ther Targets. 2010 Feb;14(2):143–55.

35. Bhattacharjee A, Joiner WJ, Wu M, Yang Y, Sigworth FJ, Kaczmarek LK. Slick (Slo2.1), a rapidly-gating sodium-activated potassium channel inhibited by ATP. J Neurosci Off J Soc Neurosci. 2003 Dec 17;23(37):11681–91.

36. Dryer SE. Na(+)-activated K+ channels: a new family of large-conductance ion channels. Trends Neurosci. 1994 Apr;17(4):155–60.

37. Bhattacharjee A, Kaczmarek LK. For K+ channels, Na+ is the new Ca2+. Trends Neurosci. 2005 Aug;28(8):422–8.

38. Kaczmarek LK. Slack, Slick, and Sodium-Activated Potassium Channels. ISRN Neurosci. 2013 May 13;2013:354262.

39. Barcia G, Fleming MR, Deligniere A, Gazula VR, Brown MR, Langouet M, et al. De novo gain-of-function KCNT1 channel mutations cause malignant migrating partial seizures of infancy. Nat Genet. 2012 Nov;44(11):1255–9.

40. Heron SE, Smith KR, Bahlo M, Nobili L, Kahana E, Licchetta L, et al. Missense mutations in the sodium-gated potassium channel gene KCNT1 cause severe autosomal dominant nocturnal frontal lobe epilepsy. Nat Genet. 2012 Nov;44(11):1188–90.

41. Hodgkin AL, Huxley AF. A quantitative description of membrane current and its application to conduction and excitation in nerve. J Physiol. 1952 Aug 28;117(4):500–44.

42. Arévalo-Martínez M, Cidad P, García-Mateo N, Moreno-Estar S, Serna J, Fernández M, et al. Myocardin-Dependent Kv1.5 Channel Expression Prevents Phenotypic Modulation of Human Vessels in Organ Culture. Arterioscler Thromb Vasc Biol. 2019 Dec;39(12):e273–86.

43. Post MA, Kirsch GE, Brown AM. Kv2.1 and electrically silent Kv6.1 potassium channel subunits combine and express a novel current. FEBS Lett. 1996 Dec 9;399(1–2):177–82.

44. González T, David M, Moreno C, Macías A, Valenzuela C. Kv1.5-Kv beta interactions: molecular determinants and pharmacological consequences. Mini Rev Med Chem. 2010 Jun;10(7):635–42.

45. Martens JR, Kwak YG, Tamkun MM. Modulation of Kv channel alpha/beta subunit interactions. Trends Cardiovasc Med. 1999 Nov;9(8):253–8.

46. Gu Y, Barry J, McDougel R, Terman D, Gu C. Alternative splicing regulates kv3.1 polarized targeting to adjust maximal spiking frequency. J Biol Chem. 2012 Jan 13;287(3):1755–69.

47. Zandany N, Marciano S, Magidovich E, Frimerman T, Yehezkel R, Shem-Ad T, et al. Alternative splicing modulates Kv channel clustering through a molecular ball and chain mechanism. Nat Commun. 2015 Mar 27;6:6488.

48. Hall MK, Weidner DA, Edwards MAJ, Schwalbe RA. Complex N-Glycans Influence the Spatial Arrangement of Voltage Gated Potassium Channels in Membranes of Neuronal-Derived Cells. PloS One. 2015;10(9):e0137138.

49. Cerda O, Trimmer JS. Analysis and functional implications of phosphorylation of neuronal voltage-gated potassium channels. Neurosci Lett. 2010 Dec 10;486(2):60–7.

50. Jindal HK, Folco EJ, Liu GX, Koren G. Posttranslational modification of voltage-dependent potassium channel Kv1.5: COOH-terminal palmitoylation modulates its biological properties. Am J Physiol Heart Circ Physiol. 2008 May;294(5):H2012-2021.

51. Tu L, Wang J, Helm A, Skach WR, Deutsch C. Transmembrane biogenesis of Kv1.3. Biochemistry. 2000 Feb 1;39(4):824–36.

52. Sebestyén V, Nagy É, Mocsár G, Volkó J, Szilágyi O, Kenesei Á, et al. Role of C-Terminal Domain and Membrane Potential in the Mobility of Kv1.3 Channels in Immune Synapse Forming T Cells. Int J Mol Sci. 2022 Mar 18;23(6):3313.

53. Shen NV, Chen X, Boyer MM, Pfaffinger PJ. Deletion analysis of K+ channel assembly. Neuron. 1993 Jul;11(1):67–76.

54. Long SB, Campbell EB, MacKinnon R. Crystal Structure of a Mammalian Voltage-Dependent Shaker Family K+ Channel. Science. 2005 Aug 5;309(5736):897–903.

55. Pérez-García MT, Cidad P, López-López JR. The secret life of ion channels: Kv1.3 potassium channels and proliferation. Am J Physiol-Cell Physiol. 2018 Jan;314(1):C27–42.

56. Tajti G, Wai DCC, Panyi G, Norton RS. The voltage-gated potassium channel KV1.3 as a therapeutic target for venom-derived peptides. Biochem Pharmacol. 2020 Nov;181:114146.

57. Gubič Š, Hendrickx LA, Toplak Ž, Sterle M, Peigneur S, Tomašič T, et al. Discovery of KV1.3 ion channel inhibitors: Medicinal chemistry approaches and challenges. Med Res Rev. 2021;41(4):2423–73.

58. Schmitz A, Sankaranarayanan A, Azam P, Schmidt-Lassen K, Homerick D, Hänsel W, et al. Design of PAP-1, a selective small molecule Kv1.3 blocker, for the suppression of effector memory T cells in autoimmune diseases. Mol Pharmacol. 2005 Nov;68(5):1254–70.

59. Vennekamp J, Wulff H, Beeton C, Calabresi PA, Grissmer S, Hänsel W, et al. Kv1.3-blocking 5-phenylalkoxypsoralens: a new class of immunomodulators. Mol Pharmacol. 2004 Jun;65(6):1364–74.

60. Fadool DA, Tucker K, Pedarzani P. Mitral cells of the olfactory bulb perform metabolic sensing and are disrupted by obesity at the level of the Kv1.3 ion channel. PloS One. 2011;6(9):e24921.

61. Sarkar S, Nguyen HM, Malovic E, Luo J, Langley M, Palanisamy BN, et al. Kv1.3 modulates neuroinflammation and neurodegeneration in Parkinson's disease. J Clin Invest. 2020 Aug 3;130(8):4195–212.

62. Koshy S, Huq R, Tanner MR, Atik MA, Porter PC, Khan FS, et al. Blocking KV1.3 Channels Inhibits Th2 Lymphocyte Function and Treats a Rat Model of Asthma *. J Biol Chem. 2014 May 2;289(18):12623–32.

63. Vicente R, Escalada A, Villalonga N, Texidó L, Roura-Ferrer M, Martín-Satué M, et al. Association of Kv1.5 and Kv1.3 contributes to the major voltage-dependent K+ channel in macrophages. J Biol Chem. 2006 Dec 8;281(49):37675–85.

64. Deutsch C. The Birth of a Channel. Neuron. 2003 Oct 9;40(2):265–76.

65. Martínez-Mármol R, Pérez-Verdaguer M, Roig SR, Vallejo-Gracia A, Gotsi P, Serrano-Albarrás A, et al. A non-canonical di-acidic signal at the C-terminus of Kv1.3 determines anterograde trafficking and surface expression. J Cell Sci. 2013 Dec 15;126(Pt 24):5681–91.

66. Szabò I, Bock J, Jekle A, Soddemann M, Adams C, Lang F, et al. A novel potassium channel in lymphocyte mitochondria. J Biol Chem. 2005 Apr 1;280(13):12790–8.

67. Jang SH, Byun JK, Jeon WI, Choi SY, Park J, Lee BH, et al. Nuclear Localization and Functional Characteristics of Voltage-gated Potassium Channel Kv1.3 *. J Biol Chem. 2015 May 15;290(20):12547–57.

68. Zhu J, Yan J, Thornhill WB. The Kv1.3 potassium channel is localized to the cis-Golgi and Kv1.6 is localized to the endoplasmic reticulum in rat astrocytes. FEBS J. 2014 Aug;281(15):3433–45.

69. Capera J, Navarro-Pérez M, Moen AS, Szabó I, Felipe A. The Mitochondrial Routing of the Kv1.3 Channel. Front Oncol. 2022 Mar 24;12:865686.

70. Szabó I, Bock J, Grassmé H, Soddemann M, Wilker B, Lang F, et al. Mitochondrial potassium channel Kv1.3 mediates Bax-induced apoptosis in lymphocytes. Proc Natl Acad Sci U S A. 2008 Sep 30;105(39):14861–6.

71. Peruzzo R, Mattarei A, Romio M, Paradisi C, Zoratti M, Szabò I, et al. Regulation of Proliferation by a Mitochondrial Potassium Channel in Pancreatic Ductal Adenocarcinoma Cells. Front Oncol. 2017;7:239.

72. Leanza L, Henry B, Sassi N, Zoratti M, Chandy KG, Gulbins E, et al. Inhibitors of mitochondrial Kv1.3 channels induce Bax/Bak-independent death of cancer cells. EMBO Mol Med. 2012 Jul;4(7):577–93.

73. Severin F, Urbani A, Varanita T, Bachmann M, Azzolini M, Martini V, et al. Pharmacological modulation of Kv1.3 potassium channel selectively triggers pathological B lymphocyte apoptosis in vivo in a genetic CLL model. J Exp Clin Cancer Res CR. 2022 Feb 16;41(1):64.

74. Zoghi S, Masoumi F, Rezaei N. Chapter 1 - The immune system. In: Rezaei N, editor. Clinical Immunology [Internet]. Academic Press; 2023 [cited 2023 Mar 22]. p. 1–46. Available from: https://www.sciencedirect.com/science/article/pii/B9780128180068000050

75. Gocke AR, Lebson LA, Grishkan IV, Hu L, Nguyen HM, Whartenby KA, et al. Kv1.3 Deletion Biases T Cells toward an Immunoregulatory Phenotype and Renders Mice Resistant to Autoimmune Encephalomyelitis. J Immunol. 2012 Jun 15;188(12):5877–86.

76. Alam R, Gorska M. 3. Lymphocytes. J Allergy Clin Immunol. 2003 Feb;111(2 Suppl):S476-485.

77. von Andrian UH, Mackay CR. T-cell function and migration. Two sides of the same coin. N Engl J Med. 2000 Oct 5;343(14):1020–34.

78. Testi R, Phillips JH, Lanier LL. T cell activation via Leu-23 (CD69). J Immunol Baltim Md 1950. 1989 Aug 15;143(4):1123–8.

79. Yarkoni S, Kaminitz A, Sagiv Y, Yaniv I, Askenasy N. Involvement of IL-2 in homeostasis of regulatory T cells: the IL-2 cycle. BioEssays News Rev Mol Cell Dev Biol. 2008 Sep;30(9):875–88.

80. Cahalan MD, Chandy KG. The functional network of ion channels in T lymphocytes. Immunol Rev. 2009 Sep;231(1):59–87.

81. Nohara LL, Stanwood SR, Omilusik KD, Jefferies WA. Tweeters, Woofers and Horns: The Complex Orchestration of Calcium Currents in T Lymphocytes. Front Immunol [Internet]. 2015 [cited 2023 Mar 13];6. Available from: https://www.frontiersin.org/articles/10.3389/fimmu.2015.00234

82. Lioudyno MI, Kozak JA, Penna A, Safrina O, Zhang SL, Sen D, et al. Orai1 and STIM1 move to the immunological synapse and are up-regulated during T cell activation. Proc Natl Acad Sci U S A. 2008 Feb 12;105(6):2011–6.

83. Bertin S, Raz E. Transient Receptor Potential (TRP) channels in T cells. Semin Immunopathol. 2016 May;38(3):309–19.

84. TRP expression pattern and the functional importance of TRPC3 in primary human T-cells - PubMed [Internet]. [cited 2023 Mar 14]. Available from: https://pubmed.ncbi.nlm.nih.gov/21215279/

85. Acharya TK, Tiwari A, Majhi RK, Goswami C. TRPM8 channel augments T-cell activation and proliferation. Cell Biol Int. 2021;45(1):198–210.

86. Schenk U, Frascoli M, Proietti M, Geffers R, Traggiai E, Buer J, et al. ATP inhibits the generation and function of regulatory T cells through the activation of purinergic P2X receptors. Sci Signal. 2011 Mar 1;4(162):ra12.

87. Chiang EY, Li T, Jeet S, Peng I, Zhang J, Lee WP, et al. Potassium channels Kv1.3 and KCa3.1 cooperatively and compensatorily regulate antigen-specific memory T cell functions. Nat Commun. 2017 Mar 1;8:14644.

88. NFAT proteins: key regulators of T-cell development and function | Nature Reviews Immunology [Internet]. [cited 2023 Mar 5]. Available from: https://www.nature.com/articles/nri1632

89. Nicolaou SA, Neumeier L, Steckly A, Kucher V, Takimoto K, Conforti L. Localization of Kv1.3 Channels in the Immunological Synapse Modulates the Calcium Response to Antigen Stimulation in T Lymphocytes1. J Immunol. 2009 Nov 15;183(10):6296–302.

90. Nicolaou SA, Neumeier L, Takimoto K, Lee SM, Duncan HJ, Kant SK, et al. Differential calcium signaling and Kv1.3 trafficking to the immunological synapse in systemic lupus erythematosus. Cell Calcium. 2010 Jan 1;47(1):19–28.

91. Dustin ML. Chapter 11 - The Immunological Synapse. In: Bradshaw RA, Dennis EA, editors. Handbook of Cell Signaling (Second Edition) [Internet]. San Diego: Academic Press; 2010 [cited 2023 Mar 22]. p. 71–5. Available from: https://www.sciencedirect.com/science/article/pii/B9780123741455000115

92. Chimote AA, Hajdu P, Kottyan LC, Harley JB, Yun Y, Conforti L. Nanovesicle-targeted Kv1.3 knockdown in memory T cells suppresses CD40L expression and memory phenotype. J Autoimmun. 2016 May;69:86–93.

93. Ueyama A, Imura K, Kasai-Yamamoto E, Tai N, Nagira M, Shichijo M, et al. Kv1.3 blockers ameliorate allergic contact dermatitis by preferentially suppressing effector memory T cells in a rat model. Clin Exp Dermatol. 2013 Dec 1;38(8):897–903.

94. Fomina AF, Fanger CM, Kozak JA, Cahalan MD. Single channel properties and regulated expression of Ca(2+) release-activated Ca(2+) (CRAC) channels in human T cells. J Cell Biol. 2000 Sep 18;150(6):1435–44.

95. Serrano-Albarrás A, Cirera-Rocosa S, Sastre D, Estadella I, Felipe A. Fighting rheumatoid arthritis: Kv1.3 as a therapeutic target. Biochem Pharmacol. 2019 Jul 1;165:214–20.

96. Koni PA, Khanna R, Chang MC, Tang MD, Kaczmarek LK, Schlichter LC, et al. Compensatory Anion Currents in Kv1.3 Channel-deficient Thymocytes*. J Biol Chem. 2003 Oct 10;278(41):39443–51.

97. Grishkan IV, Tosi DM, Bowman MD, Harary M, Calabresi PA, Gocke AR. Antigenic Stimulation of Kv1.3-Deficient Th Cells Gives Rise to a Population of Foxp3-Independent T Cells with Suppressive Properties. J Immunol. 2015 Aug 15;195(4):1399–407.

98. Safety and pharmacodynamics of dalazatide, a Kv1.3 channel inhibitor, in the treatment of plaque psoriasis: A randomized phase 1b trial | PLOS ONE [Internet]. [cited 2023 Mar 22]. Available from: https://journals.plos.org/plosone/article?id=10.1371/journal.pone.0180762

99. Beeton C, Wulff H, Barbaria J, Clot-Faybesse O, Pennington M, Bernard D, et al. Selective blockade of T lymphocyte K+ channels ameliorates experimental autoimmune encephalomyelitis, a model for multiple sclerosis. Proc Natl Acad Sci U S A. 2001;98(24):13942–7.

100. Lewis RS, Cahalan MD. Subset-specific expression of potassium channels in developing murine T lymphocytes. Science. 1988 Feb 12;239(4841 Pt 1):771–5.

101. Mitogen induction of ion channels in murine T lymphocytes. J Gen Physiol. 1987 Mar 1;89(3):405–20.

102. Reich EP, Cui L, Yang L, Pugliese-Sivo C, Golovko A, Petro M, et al. Blocking ion channel KCNN4 alleviates the symptoms of experimental autoimmune encephalomyelitis in mice. Eur J Immunol. 2005 Apr;35(4):1027–36.

103. DI Felice F, Micheli G, Camilloni G. Restriction enzymes and their use in molecular biology: An overview. J Biosci. 2019 Jun;44(2):38.

104. Capecchi MR. Altering the genome by homologous recombination. Science. 1989 Jun 16;244(4910):1288–92.

105. Smithies O, Gregg RG, Boggs SS, Koralewski MA, Kucherlapati RS. Insertion of DNA sequences into the human chromosomal beta-globin locus by homologous recombination. Nature. 1985 Sep 19;317(6034):230–4.

106. Rouet P, Smih F, Jasin M. Introduction of double-strand breaks into the genome of mouse cells by expression of a rare-cutting endonuclease. Mol Cell Biol. 1994 Dec;14(12):8096–106.

107. Honma M, Sakuraba M, Koizumi T, Takashima Y, Sakamoto H, Hayashi M. Non-homologous end-joining for repairing I-SceI-induced DNA double strand breaks in human cells. DNA Repair. 2007 Jun 1;6(6):781–8.

108. Porteus MH, Carroll D. Gene targeting using zinc finger nucleases. Nat Biotechnol. 2005 Aug;23(8):967–73.

109. Urnov FD, Rebar EJ, Holmes MC, Zhang HS, Gregory PD. Genome editing with engineered zinc finger nucleases. Nat Rev Genet. 2010 Sep;11(9):636–46.

110. Christian M, Cermak T, Doyle EL, Schmidt C, Zhang F, Hummel A, et al. Targeting DNA double-strand breaks with TAL effector nucleases. Genetics. 2010 Oct;186(2):757–61.

111. Li T, Huang S, Zhao X, Wright DA, Carpenter S, Spalding MH, et al. Modularly assembled designer TAL effector nucleases for targeted gene knockout and gene replacement in eukaryotes. Nucleic Acids Res. 2011 Aug;39(14):6315–25.

112. Jinek M, Chylinski K, Fonfara I, Hauer M, Doudna JA, Charpentier E. A programmable dual-RNA-guided DNA endonuclease in adaptive bacterial immunity. Science. 2012 Aug 17;337(6096):816–21.

113. Barrangou R, Fremaux C, Deveau H, Richards M, Boyaval P, Moineau S, et al. CRISPR provides acquired resistance against viruses in prokaryotes. Science. 2007 Mar 23;315(5819):1709–12.

114. Mojica FJM, Díez-Villaseñor C, García-Martínez J, Soria E. Intervening sequences of regularly spaced prokaryotic repeats derive from foreign genetic elements. J Mol Evol. 2005 Feb;60(2):174–82.

115. Biochemical and biological characterization of lymphocyte regulatory molecules. V. Identification of an interleukin 2-producing human leukemia T cell line. | Journal of Experimental Medicine | Rockefeller University Press [Internet]. [cited 2023 Feb 15].

Available from: https://rupress.org/jem/article/152/6/1709/57082/Biochemical-and-biological-characterization-of

116. Panyi G, Deutsch C. Assembly and suppression of endogenous Kv1.3 channels in human T cells. J Gen Physiol. 1996 Mar;107(3):409–20.

117. Aurnhammer C, Haase M, Muether N, Hausl M, Rauschhuber C, Huber I, et al. Universal real-time PCR for the detection and quantification of adeno-associated virus serotype 2-derived inverted terminal repeat sequences. Hum Gene Ther Methods. 2012 Feb;23(1):18–28.

118. Schneider CA, Rasband WS, Eliceiri KW. NIH Image to ImageJ: 25 years of image analysis. Nat Methods. 2012 Jul;9(7):671–5.

119. Cidad P, Alonso E, Arévalo-Martínez M, Calvo E, de la Fuente MA, Pérez-García MT, et al. Voltage-dependent conformational changes of Kv1.3 channels activate cell proliferation. J Cell Physiol. 2021 Jun;236(6):4330–47.

120. Kochetov AV. Alternative translation start sites and hidden coding potential of eukaryotic mRNAs. BioEssays News Rev Mol Cell Dev Biol. 2008 Jul;30(7):683–91.

121. Desai PN, Zhang X, Wu S, Janoshazi A, Bolimuntha S, Putney JW, et al. Multiple types of calcium channels arising from alternative translation initiation of the Orai1 message. Sci Signal. 2015 Jul 28;8(387):ra74.

122. Markakis I, Charitakis I, Beeton C, Galani M, Repousi E, Aggeloglou S, et al. Kv1.3 Channel Up-Regulation in Peripheral Blood T Lymphocytes of Patients With Multiple Sclerosis. Front Pharmacol. 2021;12:714841.

123. Roberts KM, Rosen A, Casciola-Rosen LA. Methods for inducing apoptosis. Methods Mol Med. 2004;102:115–28.

124. Panyi G, Vamosi G, Bacso Z, Bagdany M, Bodnar A, Varga Z, et al. Kv1.3 potassium channels are localized in the immunological synapse formed between cytotoxic and target cells. Proc Natl Acad Sci. 2004 Feb 3;101(5):1285–90.

125. Macian F. NFAT proteins: key regulators of T-cell development and function. Nat Rev Immunol. 2005 Jun;5(6):472–84.

126. Koni PA, Khanna R, Chang MC, Tang MD, Kaczmarek LK, Schlichter LC, et al. Compensatory anion currents in Kv1.3 channel-deficient thymocytes. J Biol Chem. 2003 Oct 10;278(41):39443–51.

127. Cai J, Huang Y, Li F, Li Y. Alteration of protein subcellular location and domain formation by alternative translational initiation. Proteins Struct Funct Bioinforma. 2006 Feb 15;62(3):793–9.

128. Kisselbach J, Seyler C, Schweizer PA, Gerstberger R, Becker R, Katus HA, et al. Modulation of K2P2.1 and K2P10.1 K+ channel sensitivity to carvedilol by alternative mRNA translation initiation. Br J Pharmacol. 2014 Dec 1;171(23):5182–94.

129. Desai PN, Zhang X, Wu S, Janoshazi A, Bolimuntha S, Putney JW, et al. Multiple types of calcium channels arising from alternative translation initiation of the Orai1 message. Sci Signal. 2015 Jul 28;8(387).

130. Touriol C, Bornes S, Bonnal S, Audigier S, Prats H, Prats AC, et al. Generation of protein isoform diversity by alternative initiation of translation at non-AUG codons. Biol Cell. 2003;95(3–4):169–78.

131. Szabò I, Bock J, Jekle A, Soddemann M, Adams C, Lang F, et al. A novel potassium channel in lymphocyte mitochondria. J Biol Chem. 2005;280(13):12790–8.

132. Szabò I, Bock J, Grassmé H, Soddemann M, Wilker B, Lang F, et al. Mitochondrial potassium channel Kv1.3 mediates Bax-induced apoptosis in lymphocytes. Proc Natl Acad Sci U S A. 2008;105(39):14861–6.

133. Cidad P, Moreno-Domínguez A, Novensá L, Roqué M, Barquín L, Heras M, et al. Characterization of ion channels involved in the proliferative response of femoral artery smooth muscle cells. Arterioscler Thromb Vasc Biol. 2010 Jun;30(6):1203–11.

134. Lin CS, Boltz RC, Blake JT, Nguyen M, Talento A, Fischer PA, et al. Voltage-gated potassium channels regulate calcium-dependent pathways involved in human T lymphocyte activation. J Exp Med. 1993 Mar 1;177(3):637–45.

135. Beeton C, Wulff H, Standifer NE, Azam P, Mullen KM, Pennington MW, et al. Kv1.3 channels are a therapeutic target for T cell-mediated autoimmune diseases. Proc Natl Acad Sci U S A. 2006 Nov 14;103(46):17414–9.

136. Zhao N, Dong Q, Du LL, Fu XX, Du YM, Liao YH. Potent Suppression of Kv1.3 Potassium Channel and IL-2 Secretion by Diphenyl Phosphine Oxide-1 in Human T Cells. PLOS ONE. 2013 May 22;8(5):e64629.

137. Handbook of Cell Signaling - 2nd Edition [Internet]. [cited 2023 Mar 7]. Available from: https://www.elsevier.com/books/handbook-of-cell-signaling/bradshaw/978-0-12-374145-5

138. Wulff H, Christophersen P, Colussi P, Chandy KG, Yarov-Yarovoy V. Antibodies and venom peptides: new modalities for ion channels. Vol. 18, Nature Reviews Drug Discovery. Nature Publishing Group; 2019. p. 339–57.

139. Carter PJ, Lazar GA. Next generation antibody drugs: pursuit of the “high-hanging fruit.” Nat Rev Drug Discov 2017 173. 2017 Dec 1;17(3):197–223.

140. Cidad P, Jiménez-Pérez L, García-Arribas D, Miguel-Velado E, Tajada S, Ruiz-Mcdavitt C, et al. Kv1.3 channels can modulate cell proliferation during phenotypic switch by an ion-flux independent mechanism. Arterioscler Thromb Vasc Biol. 2012;32(5).

141. Valle-Reyes S, Valencia-Cruz G, Liñan-Rico L, Pottosin I, Dobrovinskaya O. Differential Activity of Voltage- and Ca2+-Dependent Potassium Channels in Leukemic T Cell Lines: Jurkat Cells Represent an Exceptional Case. Front Physiol. 2018;9:499.

142. Pupo A, Fernández A, Low SH, François A, Suárez-Amarán L, Samulski RJ. AAV vectors: The Rubik’s cube of human gene therapy. Mol Ther. 2022 Dec 7;30(12):3515–41.

143. Highly Efficient One-Step Tagging of Endogenous Genes in Primary Cells Using CRISPR-Cas Ribonucleoproteins | The CRISPR Journal [Internet]. [cited 2023 Jun 13]. Available from: https://www.liebertpub.com/doi/abs/10.1089/crispr.2022.0046

144. Sonenberg N, Hinnebusch AG. Regulation of Translation Initiation in Eukaryotes: Mechanisms and Biological Targets. Cell. 2009 Feb 20;136(4):731–45.

145. eIF1 modulates the recognition of suboptimal translation initiation sites and steers gene expression via uORFs - PubMed [Internet]. [cited 2023 Jun 13]. Available from: https://pubmed.ncbi.nlm.nih.gov/28541577/

146. Fritsch C, Herrmann A, Nothnagel M, Szafranski K, Huse K, Schumann F, et al. Genome-wide search for novel human uORFs and N-terminal protein extensions using ribosomal footprinting. Genome Res. 2012 Jan 11;22(11):2208–18.

147. Kearse MG, Wilusz JE. Non-AUG translation: a new start for protein synthesis in eukaryotes. Genes Dev. 2017 Jan 9;31(17):1717–31.

148. Hinnebusch AG, Ivanov IP, Sonenberg N. Translational control by 5′-untranslated regions of eukaryotic mRNAs. Science. 2016 Jun 17;352(6292):1413–6.

149. Barbosa C, Peixeiro I, Romão L. Gene Expression Regulation by Upstream Open Reading Frames and Human Disease. PLOS Genet. 2013 Aug 8;9(8):e1003529.

150. Spriggs KA, Bushell M, Willis AE. Translational Regulation of Gene Expression during Conditions of Cell Stress. Mol Cell. 2010 Oct 22;40(2):228–37.

151. Kochetov A V. Alternative translation start sites and hidden coding potential of eukaryotic mRNAs. BioEssays News Rev Mol Cell Dev Biol. 2008 Jul;30(7):683–91.

152. Trulley P, Snieckute G, Bekker-Jensen D, Menon MB, Freund R, Kotlyarov A, et al. Alternative Translation Initiation Generates a Functionally Distinct Isoform of the Stress-Activated Protein Kinase MK2. Cell Rep. 2019 Jun 4;27(10):2859-2870.e6.

153. Hopkins BD, Fine B, Steinbach N, Dendy M, Rapp Z, Shaw J, et al. A Secreted PTEN Phosphatase That Enters Cells to Alter Signaling and Survival. Science. 2013 Jul 26;341(6144):399–402.

154. McNally BA, Pendon ZD, Trudeau MC. hERG1a and hERG1b potassium channel subunits directly interact and preferentially form heteromeric channels. J Biol Chem. 2017 Dec 29;292(52):21548–57.

155. M PV, J C, R MM, M C, N C, Mm T, et al. Caveolin interaction governs Kv1.3 lipid raft targeting. Sci Rep [Internet]. 2016 Feb 3 [cited 2023 Apr 10];6. Available from: https://pubmed.ncbi.nlm.nih.gov/26931497/

156. Capera J, Serrano-Novillo C, Navarro-Pérez M, Cassinelli S, Felipe A. The Potassium Channel Odyssey: Mechanisms of Traffic and Membrane Arrangement. Int J Mol Sci. 2019 Feb 9;20(3):734.

157. Jang SH, Byun JK, Jeon WI, Choi SY, Park J, Lee BH, et al. Nuclear localization and functional characteristics of voltage-gated potassium channel Kv1.3. J Biol Chem. 2015 May 15;290(20):12547–57.

158. Friedl P, Wolf K, Lammerding J. Nuclear mechanics during cell migration. Curr Opin Cell Biol. 2011 Feb;23(1):55–64.

159. Calero-Cuenca FJ, Janota CS, Gomes ER. Dealing with the nucleus during cell migration. Curr Opin Cell Biol. 2018 Feb 1;50:35–41.

160. Manley HR, Keightley MC, Lieschke GJ. The Neutrophil Nucleus: An Important Influence on Neutrophil Migration and Function. Front Immunol [Internet]. 2018 [cited 2023 Jun 13];9. Available from: https://www.frontiersin.org/articles/10.3389/fimmu.2018.02867

161. Selezneva A, Gibb AJ, Willis D. The Nuclear Envelope as a Regulator of Immune Cell Function. Front Immunol [Internet]. 2022 [cited 2023 Apr 10];13. Available from: https://www.frontiersin.org/articles/10.3389/fimmu.2022.840069

162. Kent LN, Li Y, Wakle-Prabagaran M, Naqvi MZ, Weil SG, England SK. Blocking the BKCa channel induces NF-κB nuclear translocation by increasing nuclear calcium concentration†. Biol Reprod. 2022 Mar 1;106(3):441–8.

163. Nuclear Envelope Lamin-A Couples Actin Dynamics with Immunological Synapse Architecture and T Cell Activation | Science Signaling [Internet]. [cited 2023 Apr 10]. Available from: https://www.science.org/doi/10.1126/scisignal.2004872

164. Franco-Obregón A, Wang H wei, Clapham DE. Distinct Ion Channel Classes Are Expressed on the Outer Nuclear Envelope of T- and B-Lymphocyte Cell Lines. Biophys J. 2000 Jul 1;79(1):202–14.

165. Selezneva A, Yoshida M, Gibb A, Willis D. Nuclear BK channels regulate CREB phosphorylation in RAW264.7 macrophages. Pharmacol Rep. 2021 Jun 1;73(3):881–90.

166. Lytton J, Westlin M, Hanley MR. Thapsigargin inhibits the sarcoplasmic or endoplasmic reticulum Ca-ATPase family of calcium pumps. J Biol Chem. 1991 Sep 15;266(26):17067–71.

167. Arensdorf A, Diedrichs D, Rutkowski T. Regulation of the transcriptome by ER stress: non-canonical mechanisms and physiological consequences. Front Genet [Internet]. 2013 [cited 2023 Jun 13];4. Available from: https://www.frontiersin.org/articles/10.3389/fgene.2013.00256

168. Vattem KM, Wek RC. Reinitiation involving upstream ORFs regulates ATF4 mRNA translation in mammalian cells. Proc Natl Acad Sci. 2004 Aug 3;101(31):11269–74.

169. Futami T, Miyagishi M, Taira K. Identification of a Network Involved in Thapsigargin-induced Apoptosis Using a Library of Small Interfering RNA Expression Vectors*, [boxs]. J Biol Chem. 2005 Jan 7;280(1):826–31.

170. Chidawanyika T, Sergison E, Cole M, Mark K, Supattapone S. SEC24A identified as an essential mediator of thapsigargin-induced cell death in a genome-wide CRISPR/Cas9 screen. Cell Death Discov. 2018 Dec 18;4(1):1–13.

171. Seidler NW, Jona I, Vegh M, Martonosi A. Cyclopiazonic acid is a specific inhibitor of the Ca2+-ATPase of sarcoplasmic reticulum. J Biol Chem. 1989 Oct 25;264(30):17816–23.

172. Hou P, Zhang R, Liu Y, Feng J, Wang W, Wu Y, et al. Physiological role of Kv1.3 channel in T lymphocyte cell investigated quantitatively by kinetic modeling. PloS One. 2014 Mar 3;9(3).

173. Sebestyén V, Nagy É, Mocsár G, Volkó J, Szilágyi O, Kenesei Á, et al. Role of C-Terminal Domain and Membrane Potential in the Mobility of Kv1.3 Channels in Immune Synapse Forming T Cells. Int J Mol Sci. 2022 Mar 1;23(6).

174. Nicolaou SA, Neumeier L, Steckly A, Kucher V, Takimoto K, Conforti L. Localization of Kv1.3 channels in the immunological synapse modulates the calcium response to antigen stimulation in T lymphocytes. J Immunol Baltim Md 1950. 2009 Nov 15;183(10):6296–302.

175. Artym V V., Petty HR. Molecular Proximity of Kv1.3 Voltage-gated Potassium Channels and β1-Integrins on the Plasma Membrane of Melanoma Cells. J Gen Physiol. 2002;120(1).

176. Levite BM, Cahalon L, Peretz A, Hershkoviz R, Sobko A, Ariel A, et al. Extracellular K ƨ and Opening of Voltage-gated Potassium Channels Activate T Cell Integrin Function : Physical and Functional Association between Kv1 . 3 Channels and ␎ 1 Integrins. 2000;191(7).

177. Hajdu P, Martin G V., Chimote A a., Szilagyi O, Takimoto K, Conforti L. The C-terminus SH3-binding domain of Kv1.3 is required for the actin-mediated immobilization of the channel via cortactin. Mol Biol Cell. 2015 May 1;26(9):1640–51.

178. Chandy KG, Wulff H, Beeton C, Pennington M, Gutman GA, Cahalan MD. K+ channels as targets for specific immunomodulation. Trends Pharmacol Sci. 2004;25(5):280–9.

179. Eil R, Vodnala SK, Clever D, Klebanoff CA, Sukumar M, Pan JH, et al. Ionic immune suppression within the tumour microenvironment limits T cell effector function. Nature. 2016;537(7621):539–43.

180. Edwards W, Fung-Leung WP, Huang C, Chi E, Wu N, Liu Y, et al. Targeting the ion channel Kv1.3 with scorpion venom peptides engineered for potency, selectivity, and half-life. J Biol Chem. 2014 Aug 15;289(33):22704–14.

181. Schmitz A, Sankaranarayanan A, Azam P, Schmidt-Lassen K, Homerick D, Hansel W, et al. Design of PAP-1, a selective small molecule Kv1.3 blocker, for the suppression of effector memory T cells in autoimmune diseases. Mol Pharmacol. 2005 Nov;68(5):1254–70.

182. Liu QH, Fleischmann BK, Hondowicz B, Maier CC, Turka LA, Yui K, et al. Modulation of Kv Channel Expression and Function by TCR and Costimulatory Signals during Peripheral CD4+ Lymphocyte Differentiation. J Exp Med. 2002 Oct 10;196(7):897.

183. Chiang EY, Li T, Jeet S, Peng I, Zhang J, Lee WP, et al. Potassium channels Kv1.3 and KCa3.1 cooperatively and compensatorily regulate antigen-specific memory T cell functions. Nat Commun. 2017 Mar 1;8.

184. Bertin S, Aoki-Nonaka Y, De Jong PR, Nohara LL, Xu H, Stanwood SR, et al. The ion channel TRPV1 regulates the activation and proinflammatory properties of $CD4^+$ T cells. Nat Immunol. 2014 Oct 25;15(11):1055–63.

185. Launay P, Cheng H, Srivatsan S, Penner R, Fleig A, Kinet JP. TRPM4 regulates calcium oscillations after T cell activation. Science. 2004 Nov 19;306(5700):1374–7.

186. Chen G, Panicker S, Lau KY, Apparsundaram S, Patel VA, Chen SL, et al. Characterization of a novel CRAC inhibitor that potently blocks human T cell activation and effector functions. Mol Immunol. 2013 Jul 1;54(3–4):355–67.

187. Jordan MS, Singer AL, Koretzky GA. Adaptors as central mediators of signal transduction in immune cells. Nat Immunol 2003 42. 2003 Feb 1;4(2):110–6.

188. Saveanu L, Zucchetti AE, Evnouchidou I, Ardouin L, Hivroz C. Is there a place and role for endocytic TCR signaling? Immunol Rev. 2019;291(1):57–74.

189. Nguyen K, Sylvain NR, Bunnell SC. T Cell Costimulation via the Integrin VLA-4 Inhibits the Actin-Dependent Centralization of Signaling Microclusters Containing the Adaptor SLP-76. Immunity. 2008 Jun 13;28(6):810–21.

190. Varanita T, Angi B, Scattolini V, Szabo I. Kv1.3 K + channel physiology assessed by genetic and pharmacological modulation . Physiology. 2022 Jan 1;

191. Capera J, Pérez-Verdaguer M, Navarro-Pérez M, Felipe A. Kv1.3 Controls Mitochondrial Dynamics during Cell Cycle Progression. Cancers. 2021 Sep 4;13(17):4457.

192. Lam J, Wulff H. The Lymphocyte Potassium Channels Kv1.3 and KCa3.1 as Targets for Immunosuppression. Drug Dev Res. 2011 Nov;72(7):573–84.

193. Rangaraju S, Chi V, Pennington MW, Chandy KG. Kv1.3 potassium channels as a therapeutic target in multiple sclerosis. Expert Opin Ther Targets. 2009 Aug;13(8):909–24.

194. Comes N, Bielanska J, Vallejo-Gracia A, Serrano-Albarrás A, Marruecos L, Gómez D, et al. The voltage-dependent K+ channels Kv1.3 and Kv1.5 in human cancer. Front Physiol. 2013 Oct 10;4:283.

195. Patel SH, Bachmann M, Kadow S, Wilson GC, Abdel-Salam MML, Xu K, et al. Simultaneous targeting of mitochondrial Kv1.3 and lysosomal acid sphingomyelinase amplifies killing of pancreatic ductal adenocarcinoma cells in vitro and in vivo. J Mol Med Berl Ger. 2023 Mar;101(3):295–310.